

Copyright

by

Guillermo Emilio Aldana

2002

The Dissertation Committee for Guillermo Emilio Aldana
certifies that this is the approved version of the following dissertation:

**The design and simulation of a broadband
directional array in a cylindrical waveguide**

Committee:

Mark Hamilton, Supervisor

Elmer Hixson, co-supervisor

Anthony Bedford

Douglas Drumheller

Raul Longoria

Glenn Masada

The design and simulation of a broadband directional array in a cylindrical waveguide

by

Guillermo Emilio Aldana, B.S., M.S.

Dissertation

Presented to the Faculty of the Graduate School of

The University of Texas at Austin

in Partial Fulfillment

of the Requirements

for the Degree of

Doctor of Philosophy

The University of Texas at Austin

August 2002

♡ This work is dedicated to my family. Silvia “Irene” Calderon Trigueros, my mother; for the many sacrifices she had to endure in uncertain times both at home and abroad, and somehow managing to take the next step forward. I am also very grateful to have been partially raised by my grandmother and aunt Catalina Henriquez and Alba Violeta Aldana, during very difficult times. They provided love, discipline and most important my spiritual background. To “El tío Meco”, for taking me into his house as one of his own, and preparing “pan con seasons” for consumption at “Flor Blanca” Stadium in sunny San Salvador. To my beloved sister; who gave me my first shaved head at a tender age of 5. My haircut launched me 20 years ahead of the fashion industry. Teddy Savalas and Michael Jordan where not leaders of their generation, merely followers of a great visionary. To “Nanny” and Phil Neib for some of the best advice I have ever received. To Tio Aldo and tia Mimi who throughout the years provided extraordinary support to their beloved, and sometimes difficult sister: my mother. Last but not least in the memory of my father, Guillemot Antonio Aldana. It has been a long road for all of us, now you must set aside a place for me at the Thanksgiving and Christmas dinner table. ♡

Acknowledgments

I would like to acknowledge the *rôle* of my advisor Elmer Hixson. His guidance, patience, vision, unstinting support and counselling has made this work possible. I feel privileged to have been one of his students. I still remember having a small chat with John Post, after an Acoustic Seminar, regarding the experimental aspects of his work. John made mentioned Dr. Hixson's experimental prowess. It was not until of late, that I saw it with my own two eyes. I am thankful for having been witness to his elegant experimental techniques.

My most sincere gratitude is extended to my committee members: Dr. D. Drumheller for providing valuable advice and technical guidance throughout my doctoral tenure. I thank Dr. A. Bedford, Dr. G. Y. Masada, Dr. R. Longoria, Dr. M. Hamilton for guiding my work as members of my dissertation committee.

A substantial portion of the work described in this dissertation was done under the sponsorships of the Acoustical Society of America. I wish to thank the people who made this funding possible. I am also indebted to Dr. D. T. Blackstock, Dr. A. Bedford and Dr. E. Hixson for writing a strong letter of recommendation on my behalf to the Acoustical Society of America. Their

sponsorship is gratefully acknowledged.

Several colleagues and associates deserve special thanks. I thank my friend Suman “ we will see” Das for being a great friend, and keeping me focused, and energized. “Chitown” Allan “todavia no” -“no me mires” Parker, whom I remind him that “funny is funny” and he reminds me that “my people were not at the Alamo”. George “The Hairy One” Castle, for telling it how it is and being a cruel, but true friend. Suzanne Richardson who has made me look at my self through a different mirror, for the better (at least lets hope so).

Lastly, to “Little” Amy “Charlie Brown” Engleman, and Elissa “Mighty Mouse”, “I’ll be there in five minutes” Burrall. For their silent, and unparallel support. I am very fortunate to have met you both, you gave with out asking and welcomed me into your family with open arms.

They say it’s all who you work for. I would also like to acknowledge the support of Devin Sheridan and Mark Brock for allowing a compressed schedule in the final stage of my dissertation. It allowed me to pursue my academic interest in parallel with a great career at Motorola.

A second thank you to Dr. Glen Masada who has always been very supportive of my work, despite my lack of focus early on in my academic career.

Do I sound like Holly Berry at the Academy Awards yet?

Salud, dinero y amor.

GUILLERMO EMILIO ALDANA

The University of Texas at Austin

August 2002

The design and simulation of a broadband directional array in a cylindrical waveguide

Publication No. _____

Guillermo Emilio Aldana, Ph.D.

The University of Texas at Austin, 2002

Supervisor: Mark Hamilton

Exploration of deep subterranean wells is accomplished using what is known in the oil industry as a “drill string”. A drill string is a set of long hollow steel pipe joined together by large diameter couplings; with a drill bit attached to the end. Modern oil wells reach depths of two to five miles. For over 50 years, the scientific community has been trying to develop an economical and reliable solution to the problem of acoustic telemetry using the drill string as the information carrier. Acoustic telemetry is the process by which intelligence can be transmitted from the bottom of the drilling operations to the surface, using the drill string as an (acoustic) waveguide. The drill string geometry is responsible for the dispersive and filtering properties of the structure. These two properties, make the transmission of information from one end of the drill string to the other very challenging. Two aspects of the ongoing research

is the development of a repeater and a termination impedance. An acoustic repeater could be used to rebroadcast signals that have attenuated along the drill string, due to inherent attenuating mechanisms in the data carrier, and its interactions with the harsh environment. Current repeaters lack directionality and transmit information in both directions; clearly an undesirable feature. The terminating impedance concept is an “acoustic black body”. The terminating impedance absorbs all of the incoming acoustic energy at the top of the drill string, once it has been analyzed for decision making. Cancelling the echoes from the top of the structure may allow faster data telemetry, as the reflected energy does not interfere with incoming information. The focus of this dissertation is on the design and simulation of both the repeater and the terminating impedance. This work is unique in that it addresses a method to rebroadcast and cancel broadband signals, using an active, feed-forward adaptive algorithm, coupled with a properly spaced and phased array of sources (piezoelectric transducers). Both the repeater and terminating impedance are capable of reproducing complex transient wave forms. The terminating impedance and repeater designed are directional, robust to frequency content, drill string length and geometry.

Contents

Acknowledgments	v
Abstract	viii
List of Tables	xiv
List of Figures	xv
Chapter 1 Application and Historical Background	1
1.1 Application	1
1.2 Historical Background	3
1.3 Floquet Theory	6
1.4 Periodic Waveguide of Interest	7
1.5 Organization of the Dissertation	10
Chapter 2 Previous Work	12
2.1 Introduction	12
2.2 Previous Work in Acoustics	14
2.3 Harmonic Shear and Longitudinal Waves: Theoretical Work .	15

2.4	Torsional Waves	17
2.5	Flexural Waves in Periodic Structures	18
2.6	Literature Survey - Summary	22
Chapter 3	Acoustic Properties of a Drill String	24
3.1	Introduction	24
3.2	Acoustic Telemetry: Previous Work	26
3.3	Acoustic Model	29
3.4	Transient Analysis	34
3.5	Broadband Simulations	37
3.6	Attenuation and Mode Coupling	51
3.7	Summary of the Work to Date	53
3.8	Vision	54
3.9	Focus of the Dissertation	55
Chapter 4	The Design of a Broadband Directional Acoustic Ar-	
	ray	57
4.1	Introduction	57
4.2	Chapter Organization	61
4.3	Section I - Noise Control - Literature Survey	62
4.4	Section II-Transducer Characteristics	77
4.5	Section III - Transient Wave Generation	87
4.6	Incorporating Directionality	96
Chapter 5	Directional Array Performance	109

5.1	Introduction	109
5.2	Evaluation Tone and Performance Indices	110
5.2.1	Evaluation Tone	110
5.2.2	Performance Indices	112
5.3	Results	117
5.3.1	Signal Suppression - Parametric Curves	117
5.3.2	Frequency Domain	122
5.3.3	Directionality	127
5.4	Closing Comments	128
Chapter 6	Directional Array - Numerical Simulations	130
6.1	Introduction	130
6.2	Terminating Impedance Design	135
6.3	Sinusoidal Pulse Train - 2^{nd} Pass band	136
6.4	Sinusoidal Train Pulse in the 3^{rd} Pass band	144
6.5	Hammer Pulse	152
6.6	Double Hammer pulse - One Sinusoidal Cycle in the Middle of the 3^{rd} Pass Band	163
6.7	Concluding Remarks	169
6.8	Suggestions for Further Study	172
Appendix A	Experimental Set up	174
A.1	Introduction	174
A.2	Experimental Set Up	174
A.3	Directional Array	176

A.4	Directional Sensing Array	179
A.5	Experimental Set Up: Conclusions	180
Appendix B	Algorithm Description	182
B.1	Algorithm Description	182
B.1.1	Introduction	182
B.1.2	Subsection I - Defining Array Inputs	183
B.1.3	Subsection II - Directional Array Definition	185
Bibliography		192
Vita		207

List of Tables

3.1	Model dimensions	35
4.1	Waveguide dimensions for Impulse response	82
6.1	Model dimensions	132
A.1	Experimental results - array Directionality	178

List of Figures

1.1	Newton's one-dimensional lattice model	4
1.2	Schematic representation of a drill string	8
1.3	Dispersion relationship of $\frac{1}{20}^{th}$ scale model of a drill string . .	9
2.1	Dispersion relationship for a scaled model of a drill string . . .	13
2.2	Literature survey	14
2.3	Periodic structure analyzed by Lindsay, Thomson et al.	15
3.1	Schematic of a 1-D periodic waveguide for acoustic telemetry .	29
3.2	One-dimensional model used to derive the dispersion relationship	30
3.3	Outline of derivation of dispersion relation	31
3.4	Dispersion relation for a $\frac{1}{20}^{th}$ scale model of a drill string . . .	32
3.5	Transient signals along the scaled model of the drill string . .	36
3.6	Hammer input to the drill string	37
3.7	Output signal - after 5 unit cells	38
3.8	Output signal - 4 inches from the bottom	39
3.9	Input signal - middle of the third pass band	40
3.10	Signal 2.5 units into the structure	41

3.11	Signal as seen halfway through the nine unit cell scaled model	42
3.12	Narrow band signal as seen at the end of the drill string . . .	43
3.13	Narrow stop band input in a stop band	44
3.14	Narrow stop-band signal - one quarter into the drill string . .	45
3.15	Narrow stop band signal - half of the way into the drill string	46
3.16	Narrow stop-band signal - bottom of the drill string	47
3.17	Phase velocity for a long and short drill string	50
3.18	Extensional and flexural mode coupling	51
4.1	Active broadband terminating impedance concept	59
4.2	Typical adaptive acoustic noise cancellation system	64
4.3	Special coordinate system	79
4.4	Velocity algorithm	80
4.5	Displacement algorithm	81
4.6	Waveguide dimensions used to derive the impulse response func- tion	83
4.7	Impulse response velocity field infinite boundary conditions .	84
4.8	Attenuating-differentiating properties of PZT transducers . . .	85
4.9	Lumped element model of a PZT transducer	86
4.10	Electrical to PZT to synthesize transient acoustical signals . .	91
4.11	Electrical inputs to a single PZT transducer	92
4.12	Non directional wave generation from a single transducer . . .	93
4.13	Algorithm flow and logistics	94
4.14	Directional narrow-band acoustic array	97

4.15	Two transducer pairs synthesizing a broadband signal	98
4.16	Next of kin-common array design	99
4.17	Harmonically spaced transducer pairs-one common transducer	100
4.18	Common transducer design -geometric spacing	101
4.19	Forbidden zones may compromise signal integrity	103
4.20	Perfectly tuned transducer pair	105
4.21	Mistuned transducer emitting signals in the forbidden zone . .	106
4.22	Transducer pair two generating signals in the forbidden Zone	107
5.1	Pulse with $T = 3\text{ ms}$, $m = 1$, $n = 1$	111
5.2	Pulse with $T = 3\text{ ms}$, $m = 5$, $n = 50$	112
5.3	Evaluation signals for the directional array	113
5.4	Full strength array: 200 harmonics, 48 transducers	115
5.5	Fourier coefficients at 80% and 50%	116
5.6	Array performance for $T = 3\text{ ms}$, $m = 1$	118
5.7	Array performance $T = 3\text{ ms}$, $m = 5$	119
5.8	Array Performance $T = 1\text{ ms}$, $m = 1$	120
5.9	Array Performance $T = 1\text{ ms}$, $m = 5$	121
5.10	Original and residual spectra $T = 3\text{ ms}$, $m = 1$ and $n = 30$. .	122
5.11	Original and residual spectra $T = 3\text{ ms}$, $m = 5$ and $n = 30$. .	123
5.12	Original and residual spectra $T = 1\text{ ms}$, $m = 1$ and $n = 30$. .	124
5.13	Original and residual spectra $T = 1\text{ ms}$, $m = 5$ and $n = 30$. .	125
5.14	Single transducer pair $T = 1\text{ ms}$, $m = 5$ and $n = 30$	126
5.15	Forward and backward traveling wave	127

6.1	Hammer response of periodic structure	133
6.2	Two-stage terminating impedance	135
6.3	Sinusoidal pulse train - 2^{nd} pass band	136
6.4	Fourier domain output signal 2^{nd} pass band	137
6.5	Half range expansion coefficients	138
6.6	Drill string output and windowed signal 2nd pass band	139
6.7	First stage array output vs. exiting signal 2^{nd} pass band . . .	140
6.8	First stage cancellation of incoming transient 2^{nd} pass band .	141
6.9	Residual from the first stage 2nd pass band	142
6.10	Array output vs. residual signal 2^{nd} pass band - 2^{nd} stage . . .	143
6.11	Second stage output vs. original signal 2^{nd} pass band 2^{nd} stage	144
6.12	Sinusoidal pulse train - 3^{rd} pass band	145
6.13	Fourier coefficients of output signal	146
6.14	Drill string output and windowed signal 3^{rd} Pass band	147
6.15	First stage array output vs. original signal	148
6.16	Original and residual signal	149
6.17	Input to second stage and array output	150
6.18	Fourier coefficients residual signal	150
6.19	Incoming signal and directional array output after two stages .	151
6.20	Hammer input and output of twenty five periodic structures .	152
6.21	Drill String response to hammer input and windowed output .	153
6.22	Half range expansion - coefficients and firing sequence	154
6.23	Original and generated signal - First stage	155

6.24	Hammer pulse with dead zone	156
6.25	Injecting a dead zone for improved convergence	157
6.26	Signal synthesis as a function of distance along the array . . .	158
6.27	Original and reduced hammer pulse - first stage	159
6.28	Extended dead zone into the hammer pulse	160
6.29	Original, first and second stage signals	161
6.30	Windowed signal and residual signal after second stage dead zone used	162
6.31	Double hammer input and drill string response	163
6.32	Double hammer input and windowed signal	164
6.33	Half range expansion coefficient and harmonic frequency content	165
6.34	First stage output vs. windowed signal double hammer	166
6.35	Residual after 1st stage vs. windowed Signal	167
6.36	Residual fed to the second stage & HRFE frequency content .	168
6.37	Second stage residual vs. windowed signal	169
A.1	N-fire directional array	175
A.2	Directional sensor - experimental set up	179
B.1	Windowed drill string output incoming to directional array . .	185
B.2	Directional array design space	186
B.3	Windowed drill string output incoming to directional array . .	187
B.4	Transducer gains algorithm	188
B.5	Signal synthesis	189
B.6	Dual stage directional canceller	190

B.7	Flow diagram of Subroutine IV	191
-----	---	-----

Chapter 1

Application and Historical Background

1.1 Application

For over 50 years, oil companies have been trying to develop an economical and reliable solution to the problem of acoustic telemetry using the drill string as the data carrier. Acoustic telemetry is the process by which intelligence can be transmitted from the bottom of the drilling operations to the surface, using the drilling tool (commonly known as a “drill string” in the oil and gas industry) as an acoustic waveguide.

The inputs to the waveguide originate near the drill bit via a set of actuators, which send crucial information (deviation from vertical, torque, temperature, etc.) to the surface. An example of how acoustic telemetry could be used to transmit downhole information such as the torque load on

the drill bit to the surface is described below:

- Hardwire a torque sensor to the drill bit.
- Convert the sensor's signal to binary output, using some encoding algorithm. A possible method would be to transmit two sinusoidal train pulses of different frequency, each representing the "1" and "0" in the sequence.
- Feed the encoded information to an electro-mechanical transducer array housed within the drill pipe.
- Gather intelligence at the top of the drill string and subsequently cancel redundant (reflected) information.

The focus of this dissertation is the design of a directional broadband acoustic repeater and a terminating impedance for a scaled model of a drill string. The repeater is used to amplify signals that have decayed over the length of the drill pipe, and the terminating impedance cancels the echoes from the receiving end.

The motivation for the study is the author's own interest in the complex dispersive properties of layered media; as well active noise cancellation techniques and algorithm development. A $\frac{1}{20}^{th}$ model of the drill string was chosen because at least in principle, it could be used in a laboratory setting to feed signals to the directional array for cancellation. A periodic medium is arguably the ideal structure (due to its complex dispersive nature), for testing the robustness of the proposed directional array . The incoming signal to the

directional array, emerging from the layered medium can be changed both in magnitude, frequency content and duration by changing the length of the drill string, varying the acoustic impedance of the drill collar (or drill pipe element) and sending information in different frequency domains.

The original intent was to build a scale model of the directional array designed in this dissertation. However, during the construction and testing process, it became obvious to the author's advisor (Elmer L. Hixson) that the Electro-Acoustics Laboratory at the University of Texas was not equipped to handle the high voltages needed to drive a (compact version) of the directional array. The analysis presented here is therefore confined to numerical simulations.

The contribution of this dissertation to the general field of acoustics is the generation of directional complex transient acoustic signals in isotropic solids.

The remainder of this introductory chapter provides the reader with a brief historical background on the general topic of Wave Propagation in Periodic Structures (WPIPS), as well as introducing some of the key issues that must be addressed in the design and implementation of the an acoustic data telemetry system.

1.2 Historical Background

The study of WPIPS is nearly three centuries young. The first documented analysis of wave phenomena propagating through a periodic medium is at-

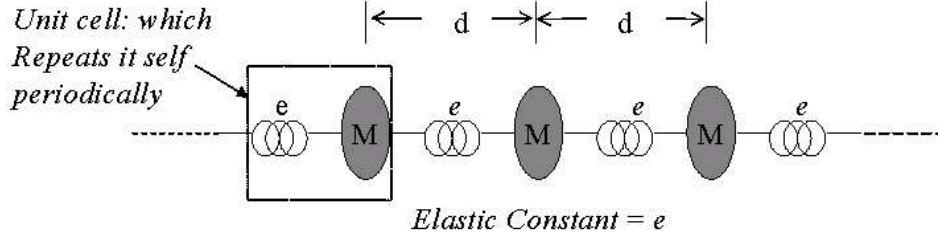


Figure 1.1: Newton's one-dimensional lattice model

tributed to Sir Isaac Newton.

Attempting to estimate the speed of sound, Newton modelled air as a one-dimensional lattice composed of equally spaced point masses, separated by an elastic element. Each mass is assumed to interact solely with its nearest neighbor by means of an elastic element between them. Figure 1.1 shows the *spring-mass* system Newton used to estimate the speed of sound.

Using this model, the velocity of sound was estimated to be:

$$V = \sqrt{\frac{ed}{\rho}} \quad (1.1)$$

V is the velocity of propagation, e is the elastic constant, ρ is the density of air, and d is the length of the unit cell. Newton assumed ed to be the isothermal bulk modulus. Newton designed experiments to verify his theoretical model. Newton's measured and theoretical values were off by about 16 percent. In 1822, Laplace showed that if e is assumed to be the adiabatic elastic constant, the theoretical and measured values are in very good agreement¹.

This one-dimensional model evolved into more complicated lattice structures, allowing interactions with point masses other than the nearest neigh-

¹The concept of adiabatic did not exists when Newton postulated his theory[1],[2].

bors, as well as variations in the spatial mass density. These models provided the foundation for the study of waves propagating through crystalline solids. Electrical analogs of some of the lattice models used by the physics community were independently duplicated by engineers when solving electrical transmission problems in the late 1930's. Although unknown to the engineers, the models needed to solve current transmission challenges had already been developed and were well understood long before electricity was widely available.

As the reader will discover, history repeats itself for the periodic structure discussed in this dissertation. The theoretical model which describes the fundamental properties of acoustic telemetry has been well known for over 40 years, but not consulted until 32 years after they were developed by the physics community.

The interest in WPIPS in the academic community has lead to the publication of books entirely devoted to the subject. The manuscript by Brillouin [2] is arguably the best reference. The classical textbook by Brekhovskikh [3] treats WPIPS in optical, mechanical and electro-magnetic media. Bedford's and Drumheller's textbooks [4] [5] provide an elegant introduction to WPIPS in elastic solids.

WPIPS finds applications ranging from the linear accelerometer to thin reflective films and acoustics waveguides. Elachi [6] provides an excellent historical and modern bibliography of the many applications of WPIPS.

1.3 Floquet Theory

Waves travelling through periodic structures are named Bloch waves after the Nobel Prize Laureate F.X. Bloch ², who solved Schrodinger's equation in a periodic potential.

Floquet theory treats second order differential equations with periodic coefficients $p_n(z)$ of period d . Specifically, Floquet theory describes systems which can be modelled by the following ODE:

$$\frac{d^n \varphi(z)}{dz^n} + p_1(z) \frac{d^{n-1} \varphi(z)}{dz^{n-1}} + p_2(z) \frac{d^{n-2} \varphi(z)}{dz^{n-2}} + \cdots + p_n(z) \varphi(z) = 0 \quad (1.2)$$

Floquet's theorem asserts solutions of the form:

$$\varphi_n(z) = \Theta_n(z) e^{iqz} \quad (1.3)$$

$\Theta_n(z)$ is a periodic function whose period is equal to the length of the *unit cell* d , and the “pseudo wavelength” q is commonly known as Floquet's number. $\Theta_n(z)$ describes the local behavior of the displacement function for all cells while q is responsible for the transfer of information from one cell to the next. The details leading to the solution can be found in Whittaker's book [7] and books by Morse and Feshbach [8] and Ince [9].

Clearly if harmonic solutions of the one-dimensional wave equation in a periodic media are sought, separation of variables reduces the spatial com-

²Other common names are Floquet waves and “backward travelling” waves. Bloch is accredited with the application of Floquet theory to the field of partial differential equations. It is interesting to note that Bloch makes no reference to Floquet's work, which was published some 80 years earlier. It appears as if Bloch derived the relationship independently.

ponent to an ODE with periodic coefficients. When n independent solutions of Equation 1.2 exists, and a transformation can be found that renders the waveguide symmetric with respect to a given axis, Floquet theory can be used to obtain a closed form solution. In the case of a progressive harmonic wave travelling through an infinite periodic structure, the solution to a 1-D wave equation is given by:

$$\varphi_n(z, t) = \Theta_n(z)e^{i(qz - \omega t)} \quad (1.4)$$

The solution for transient waves travelling in a periodic medium is also a Bloch wave. The seminal work by Odeh [10] provides a rigorous treatment of PDE's with periodic coefficients and shows uniqueness and existence of a Bloch wave solution for broadband signals.

1.4 Periodic Waveguide of Interest

Figure 1.2 shows a schematic of the structure of interest. It represents a tool used in the drilling industry, commonly known as a *Drill String*. It is composed of a set of hollow tubular pipes threaded by “tool joints” which repeat periodically in space. The tool joints are used to couple the drill pipes and introduce discontinuities in the acoustic impedance. The periodicity of the tool joints make the drill string a highly dispersive and filtering waveguide. The waveguide of interest throughout the dissertation is a $\frac{1}{20}^{th}$ scaled model of the drill string.

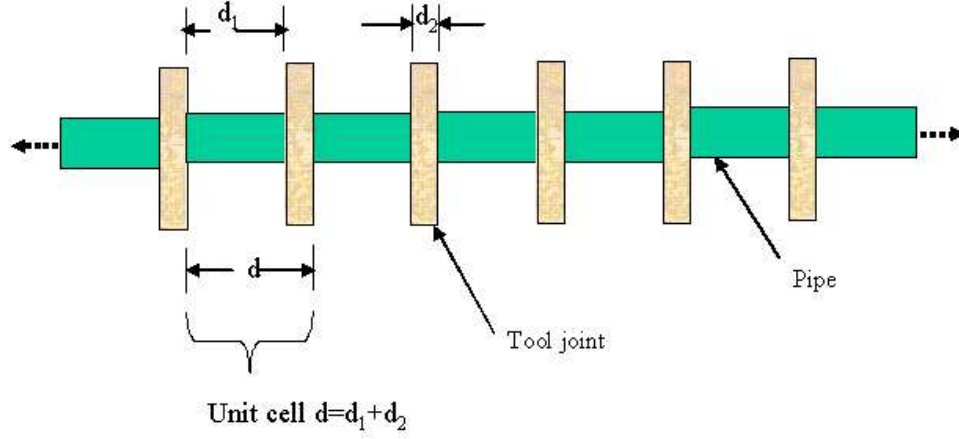


Figure 1.2: Schematic representation of a drill string

The filtering and dispersive phenomena are clearly illustrated by the dispersion curve of a $\frac{1}{20}^{th}$ model drill string shown in Figure 1.2. An outline of the derivation of the dispersion relationship is provided in Chapter 3 of this dissertation³. The discontinuities in the dispersion relationship occur at frequency ranges in which the Floquet number q , is complex. From equation 1.4, it is seen that this will correspond to an exponentially decaying solution. When q is complex the drill string acts as a mechanical filter, trapping all signals with frequencies that lie within the stop bands at the early stages of the structure.

³A complete derivation of the dispersion relationship can be found in Chapter 3 of Bedford's book [4].

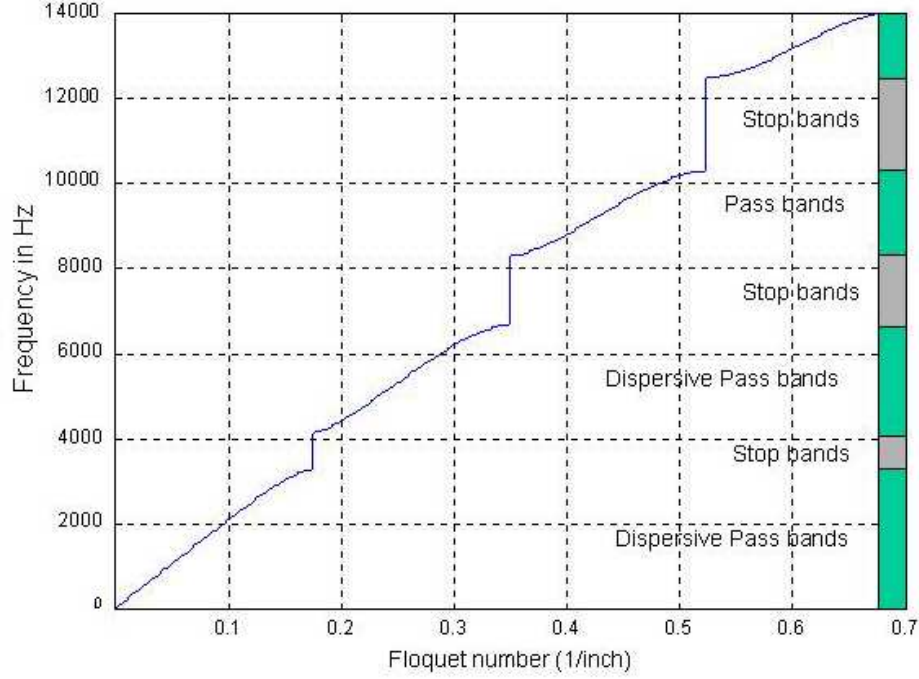


Figure 1.3: Dispersion relationship of $\frac{1}{20}^{th}$ scale model of a drill string

Furthermore, the pass bands are non-linear functions of q , and all frequencies allowed to propagate are dispersed in space. An input signal (i.e. a stress wave) to the drill string undergoes dramatic changes, and if left to propagate without any modifications, is un-recognizable to the receiver. The filtering properties of the drill string should not be confused with attenuation. The model used to derive the dispersion graph presented above does not include any attenuating mechanisms. There are other mechanisms that cause signal attenuation in a drill string, such as mode coupling, pipe ordering, changes in geometry etc., which must be addressed independently.

The challenge in acoustic telemetry is to eliminate the significant signal

distortion due to dispersion, minimize the attenuation and filtering properties of the waveguide, amplify the signal as needed along the waveguide, and cancel the signal once the information has been used for decision making. The dissertation focuses on the later two parts of this challenge: developing an active, directional terminating impedance and a repeater for broadband signals for a scaled model of a drill string.

1.5 Organization of the Dissertation

The dissertation is organized as follows:

- Chapter 2 discusses the underlying assumptions of the scaled model of the drill string and discusses the characteristics of the dispersion relationship. The main focus of the chapter will be the previous work done in the field of wave propagation in periodic structures as it pertains to acoustics in solids. The literature search includes both harmonic and transient inputs, as well as all modes of propagation: longitudinal, torsional, shear and transverse.
- Chapter 3 reviews the work to date on acoustic telemetry, followed by the state-of-the-art systems being developed by Drumheller in Sandia National Labs [11]. The chapter will focus on the transient behavior of broadband signals in a scaled model of a drill string. The numerical models used were developed at Sandia National Labs, and have been field tested. The acoustic model does not incorporate any loss functions, thus

the simulations represent the intrinsic behavior of a periodic structure under transient loading.

- Chapter 4 focuses on the design of both the directional repeater and the active terminating impedance. The chapter describes the algorithm used to model the acoustic transmission across a periodic waveguide, and exposes the behavior of the Piezo Electric Transducers (PZT) in the small frequency domain. The design of the electrical inputs to command a single transducer to send transient signals is developed. The shortcomings of such a design is the lack of directionality, which can be achieved by designing a set of optimized transducer arrays.
- Chapter 5 evaluates the performance of the broadband directional array using a Super Gaussian pulse. The performance indexes evaluated are directionality and signal attenuation.
- Chapter 6 evaluates the performance of the broadband directional array when cancelling incoming disturbance from a scaled model of the drill string. The performance of the two-stage terminating impedance is presented.
- Appendix A describes the experimental set up used to quantify the directionality of a set of speakers embedded in an air filled waveguide.
- Appendix B provides a block diagram description of the algorithm written to synthesize directional transient waves. All of the code is written in MATLAB and available upon request.

Chapter 2

Previous Work

2.1 Introduction

The dispersion relationship for plane wave propagation in a drill string is shown in Figure 2.1. Embedded in the dispersion relationship are some underlying assumptions. They are presented below without proof:

- The model used to derive the dispersion equation is linear, lossless, homogeneous, isotropic, one-dimensional and models a propagation medium infinite in both directions.
- Wave propagation is restricted to plane waves in an isotropic cylinder. This implies $(ka) \ll 1$, where $k = \frac{\omega}{c}$, k is the wave number, ω is the radial frequency, a is the largest radial dimension in the waveguide, and c is speed of sound. This relationship is derived from an expansion of Pochhammer's equation in ka , which enforces the restriction state above

yields a constant propagation speed c . The details of the derivation can be found in both of the classic textbooks by Kolsky [12] and Achenbach [13].

- All other modes of propagation resulting from reflections due to the large change of cross-sectional area are assumed to decay exponentially in the neighborhood of the tool joint¹

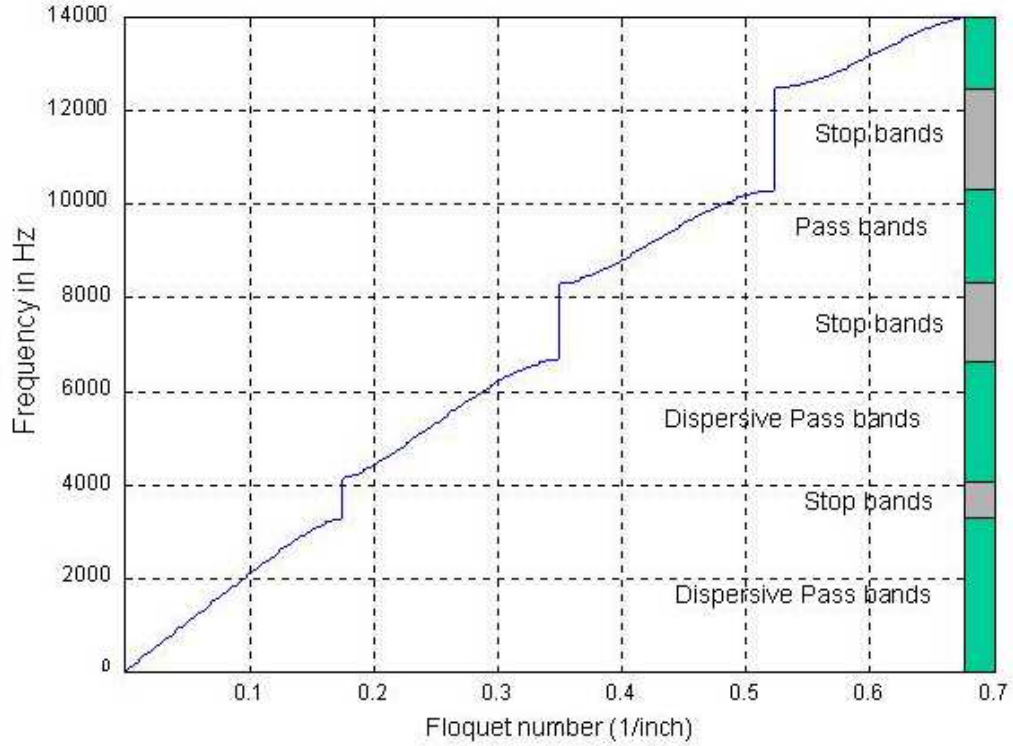


Figure 2.1: Dispersion relationship for a scaled model of a drill string

¹It has been shown that an abrupt change in the acoustical impedance can have significant effects on the dispersion relationship [14]. In fact, the classical Brillouin diagram is severely distorted.

2.2 Previous Work in Acoustics

This section will provide a survey of the relevant work in the area of wave propagation in periodic wave guides as it pertains acoustics of both solids and ideal fluids. The tree diagram shown in Figure 2.2 shows the focus of the literature search. Most of the literature encountered falls under the left-most tree branch shown in Figure 2.2. With the exception of Drumheller[15], [11] very few authors have attempted to treat transient wave propagation in a periodic structure, much less verify the results experimentally.

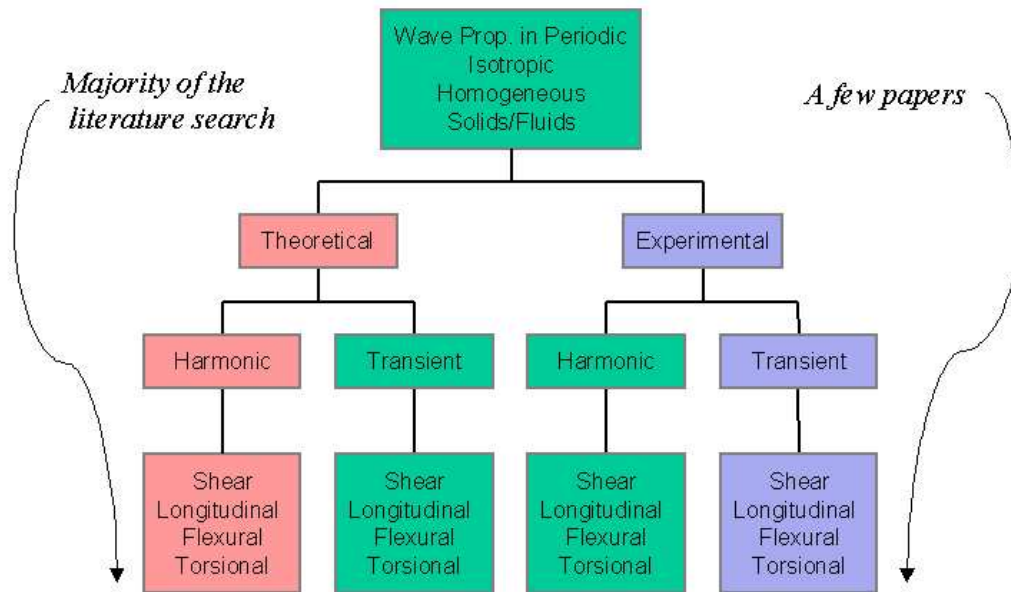


Figure 2.2: Literature survey

2.3 Harmonic Shear and Longitudinal Waves: Theoretical Work

One of the earliest published works in WPIPS is that of Lindsay [16] who treats harmonic, longitudinal waves at normal incidence to a infinite periodic structure. A schematic representation of Lindsay's model is shown in Figure 2.3.

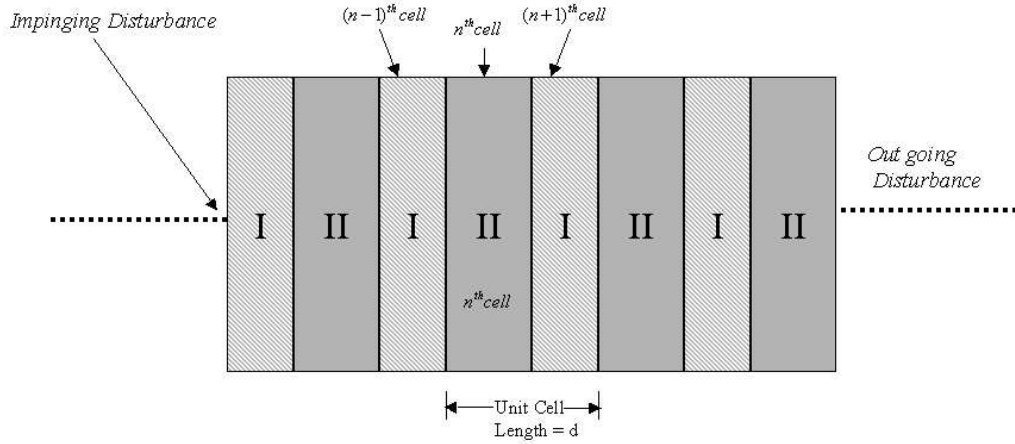


Figure 2.3: Periodic structure analyzed by Lindsay, Thomson et al.

In his work, Lindsay does not make use of Floquet's theorem, but rather derives it indirectly using appropriate boundary conditions at the interfaces of each of the layers and exploiting the infinite medium. Lindsay derives the acoustic (Bloch) impedance and an expression for the dispersion relationship from fundamental principles.

Lindsay expands his work by analyzing unit cells composed of fluid-

to-fluid and solid-to-fluid interfaces, with the wave impinging at an oblique angle [17]. The dispersion relationship is shown to be a function of the angle of incidence. Because the fluid is assumed to be ideal, the shear stresses generated in the solid vanish at the solid-fluid interface, thus limiting shear waves to exist only in the solid structure.

Lindsay's work was expanded by Thomson [18], who treated the two-dimensional solid-solid interface with a plane wave incident at an oblique angle. This complicates matters significantly, since shear waves are now allowed to propagate from one solid structure to the other. Unfortunately, Thomson's final results are valid only for a very special class of solids: those which have identical shear modulus. Extensions to Thomson's work can be found in Folds and Loggins publication [19], in which they treat a unit cell composed of an arbitrary number of layers, with arbitrary compression and shear bulk moduli.

More recent work in the field of WPIPS at oblique incidence is that of Rosusseau [20], who treats the same problem as Lindsay [17], but makes use of Floquet theory to arrive at a pseudo-critical angle of incidence.

Perhaps the most complete work to date of WPIPS in solids at oblique incidence is that of Sastry and Mujal [21] who treat the three dimensional, oblique incident case.

Other often-quoted works in the acoustics community deal with the treatment of Harmonic shear plane waves [22] and anti-plane waves in an infinite solid [23] by Delph et. al. These two papers show the true complexity of the dispersion relationship which due to the two-dimensional motion, forms a surface in

the space-frequency domain. Several properties of the dispersion relationship, including the un-coupling at the ends of the Brillouin zones, and its asymptotic behavior are discussed.

Delph's work is complemented by Sun [24], who treats wave propagation in the direction of the layering and E.H. Lee [25] and Lee et al. [26], who treat the problem at normal incidence in composites.

The majority of the work encountered treats WPIPS via Floquet theory, classical matrix methods or a combination of the two. However, Ma and Huang [27], [28] solve the harmonic and transient solution using integral transforms, which are inverted using the Cagniard-de Hoop method. Further literature using modal analysis to treat wave motion in layered media is also available to the interested reader [29], [30] and [31].

2.4 Torsional Waves

One of the first published papers in the area of torsional waves in periodic structures is that of Barnes and Kirkwood [32], who make use of Lindsay's work [16] to solve the dispersion relationship for one dimensional wave propagation in an idealized drill string. The dispersion relationships for both the torsional and longitudinal plane wave were derived, and the widths of the passbands/stopbands are compared. It is concluded that due to the large ratio of the rotational impedance, the dispersion curve for the torsional mode has wider stop bands than its longitudinal counterpart. This analysis shows that longitudinal waves are preferred over torsional waves for telemetry purposes.

Kaul and Lee [33] and Kaul and Herrmann [34], treat the same problem as Barnes and Kirkwood, in a solid and hollow cylindrical pipe, respectively. Both works start with a three-dimensional model, assuming stress-free boundary conditions on all surfaces of the structure. Kaul and Herrmann's work is unique because it lifts the plane wave restriction imposed by many other authors and derives the dispersion relationships for the 0^{th} and 1^{st} mode. The analysis also reveals the effect of the boundary conditions on the dispersion relationship.

2.5 Flexural Waves in Periodic Structures

The topic of flexural waves² in periodic structures gained a substantial amount of interest in the acoustic community early on (1930's). This is attributed to the many practical structures (ships, airplane wings, etc.) that can be modelled as matrix of periodically spaced beams, which under the appropriate dynamic loading will flex and propagate waves in all directions.

Heckl [35] investigates WPIPS in the bending of a rectangular plate system with a periodic array of beams. Heckl's results bring insight to the root cause of the dispersion curve in periodic structures. Heckl's finds the contributions to the acoustic field in the center of the ν unit cell due to waves incoming from the $(\nu - 1)$ and $(\nu + 1)$ cells in an infinite structure. The total

²Some authors have refused to apply Floquet's theorem to the solution of flexural waves in periodic structures, because the model used to describe the underlying phenomena is a fourth order PDE. The work of Brillouin implies (but never restricts) that only second order ODE's can be addressed with Floquet's theorem. Ince [9], Odeh [10] and Morse and Feshbach[8] assures the reader otherwise.

contribution is given by:

$$v_{\nu}^{+} = v_{\nu-1}^{+} T \frac{e^{-ikl}}{1 - R^2 e^{-2ikl}} + v_{\nu+1}^{-} T R \frac{e^{-i2kl}}{1 - R^2 e^{-i2kl}} \quad (2.1)$$

$$v_{\nu}^{-} = v_{\nu-1}^{+} T R \frac{e^{-2ikl}}{1 - R^2 e^{-2ikl}} + v_{\nu+1}^{-} T \frac{e^{-ikl}}{1 - R^2 e^{-2ikl}} \quad (2.2)$$

Where v_{ν}^{+} and v_{ν}^{-} are the $+ve$ and $-ve$ components of the wave in the ν cell, respectively.

Heckl introduces the notion of a propagation constant³ gl and determines the solutions from one cell to the next must be related as:

$$v_{\nu}^{+} = e^{gl} v_{\nu+1}^{+} \quad (2.3)$$

$$v_{\nu}^{-} = e^{-gl} v_{\nu-1}^{-} \quad (2.4)$$

Equation the equation pairs 2.1 and 2.3, 2.2 and 2.4, he forms a homogeneous set of linear equations, whose determinant is forced to vanish in order to avoid a trivial solution. This yields the following dispersion relationship:

$$\cosh gl = \frac{e^{ikl}}{2T} (1 - R^2 e^{-2ikl} + T^2 e^{-2ikl}) \quad (2.5)$$

The behavior of the dispersion relationship is clearly seen to be a nonlinear function of the reflection and transmission coefficients R and T , respectively. Thus, it is the multiple reflections and transmissions at each discontinuity which are responsible for the dispersion and filtering properties of the structure. The methodology used by Heckl is general and applies to any type of

³Same as Floquet's theorem, which ironically Heckl did not think was applicable to this problem.

plane wave propagation (longitudinal, torsional etc.); only the reflection and transmission coefficients need to be modified.

Heckl's work was followed by Ungar [36], who treated the Bernoulli-Euler beam with periodically spaced impedances. The impedances are treated as point discontinuities and allow for damping. The results obtained are identical to those derived by Heckl.

Mead [37] treats an infinite beam supported by mechanical impedances which are spaced periodically in space. Mead analyzes three type of boundary conditions and loading mechanisms: simply-supported, torsional and an elastic spring. The concept of propagation constants is used to obtain various dispersion relationships. Mead's paper also presents a thorough explanation on the peculiar nature of a Bloch wave, termed *backward travelling waves*.

At the same institute⁴, Gupta [38] treats the same problem as Mead [37], except the beam is of finite length. Various boundary conditions at each end are incorporated. Gupta develops a novel technique for graphically extracting the natural frequencies of a structure composed of n periodically supported beams from the dispersion relationship. He shows how the number of natural frequencies in a pass band are related to the number of elements in the structure.

Lee [39], [40] treats a periodically inhomogeneous beam with piecewise constant and space-variable coefficients, respectively. Combining transfer matrix and Floquet theory, the authors show that the dispersion characteristics for a flexural beam are identical in shape to its torsional and longitudinal

⁴Institute of Sound and Vibration Research University of Southampton, England.

counterparts.

Other theoretical work includes that of Nayfeh [41], Nusayr [42] and Salant [43], who addressed perturbations in the acoustic field due to a small periodic grating in the walls of an air filled wave guide.

The amount of literature which treats transient wave propagation in periodic structures is at least one order of magnitude less than its harmonic counterpart. Experimental verification of the theoretical analysis is even more rare. Experimental verification of the dispersion relationship in composites is treated by Drumheller and Sutherland [44], who experimentally verify the dispersive characteristics of an aluminum matrix filled by periodically spaced rows of tungsten rods. This work was soon followed by Robinson [45], who in a steel copper composite, propagate shear and plane waves and duplicate the theoretical dispersion curve using experimental data.

In a series of papers, El-Raheb [46], [47] develops one and two-dimensional models for the propagation of transient waves using transfer matrix theory and modal analysis expansion. His work focuses on weakly coupled structures (hard brittle ceramics periodically separated by a polymer). Experimental verification of the models developed by El-Raheb in his first two papers is published by the same author in [48]. Raheb concludes that the one-dimensional model is inadequate. It is unable to predict the dispersive properties of a periodic structure, and the experimental data deviates tremendously from the one-dimensional model. After modifications, the two-dimensional model (which accounts for flexural bending) is capable of predicting the general transient

behavior of the stress pulse. This work provides an insight into the *mode coupling* mechanism which is known to cause longitudinal signal strength loss in acoustic telemetry.

Almost in parallel with El-Raheb, Gazanhes [49] attempted to verify the filtering properties, as well as the phase and group velocities of a periodic test bed (metal plates submerged in a fish tank, separated by water) for plane waves. The results published were in very good agreement with his theoretical model.

As will be discussed in detail in Chapter 3, Drumheller [15] experimentally verified the dispersive and filtering properties of a drill string.

Other experimental work in the field of WPIPS includes that of Bradley [14] who modifies Achenbachs' [50] work in the scattering of sound in three dimensions for his one-dimensional, air filled waveguide. Bradley experimentally verifies the dispersion relationship generated by a shunt scattering impedance.

2.6 Literature Survey - Summary

The literature provided here is a brief account on the general subject. In the field of acoustics in homogeneous, isotropic media, however, it provides a good summary of the work addressed to date.

It is clear from the literature search that wave propagation in a periodic structure, whether it is torsional, flexural, longitudinal or shear can be described in terms of Floquet theory. All four types of motion share a common denominator: the filtering, and the nonlinear behavior of the dispersion

relationship.

In selecting the type of disturbance for acoustic telemetry, longitudinal waves are the clear choice over torsional, flexural and shear modes. Longitudinal waves propagate faster than either torsional or shear disturbances. Shear waves may give rise to flexural waves which are not only dispersive in uniform rods, but would also radiate sound and lose energy. Torsional waves have the added disadvantage that the dispersion relationship has wider stop bands than its longitudinal counterpart. It is no coincidence that the focus of acoustic telemetry has been the transmission of axial plane waves.

Chapter 3

Acoustic Properties of a Drill String

3.1 Introduction

Exploration of deep subterranean wells is accomplished using what is known in the oil industry as a “drill string”. Modern oil wells reach depths of two to five miles. It is impossible to manufacture a continuous drilling pipe of that length. The drill string is created by coupling segments of hollow steel pipe, usually on the order of 30 to 32 feet long and five inches in diameter, through a threaded “tool joint” as the drill bit advances.

The material removed by the drill bit finds a path to the surface through the annular space between the drill string and the recently drilled hole. The inner annular gap is filled with mud to carry the cuttings to the surface.

Telemetry of intelligence from the drill bit to the surface is of paramount

importance. Feedback to the operator of downhole conditions, such as pressure, torque, drill bit temperature, deviation from vertical, etc., can be used to control the drilling operation. The operator can use this information for navigational purposes, to control the drill bit torque, or to abort the mission, if necessary. Obtaining this capability translates to increased efficiency and substantial reductions in operating cost.

There is a need for a system to accurately capture the information and transmit it upstream to the drilling platform. The development of an economically feasible telemetry system has been a challenge for the oil industry for over fifty years. Many downhole communication systems have been attempted. Most of them are too complicated and interfere with the drilling operation.

Sending the information directly via a wire is the most obvious solution. However, the harsh downhole environment makes it impossible for most wire telemetry systems to survive. This type of feedback system would also interfere with daily operations and is therefore not economically feasible.

Other telemetry methods that have been attempted include: electromagnetic radiation through rock formation, which is too lossy [51]; acoustic telemetry, which until recently was thought unfeasible; and finally the current industry standard, acoustic *mud pulse* telemetry.

Mud pulse telemetry makes use of the pressurized mud injected in the inner annulus of the drill pipe. Sensor data is converted into binary format, which is subsequently translated to *binary mud pulses* by choking the mud emerging from the inner annulus using a valve inside the drill string just above

the drill bit [52]. Pressure changes are sensed at the top of the rig, and the transmitted information can be used for decision making. The primary drawback to this method is the low rate of transmission, which is in the range of 10-14 bits/second [53]. The oil and drilling industry is demanding rates at least five to six times larger than is currently possible with this method. Also, mud pulse telemetry is a one-way communication system: from the drill bit to the upstream operator. Acoustic telemetry has the potential of increasing the transmission rate and establishing a two-way communication channel between the operator and the machinery. It is therefore not surprising that efforts in this area have been ongoing since the early 1940's. Unfortunately, previous attempts did not make use of the available modelling techniques, and until recently, acoustic telemetry was not thought to be a viable solution.

3.2 Acoustic Telemetry: Previous Work

Sun Oil Company attempted to design an acoustic telemetry system in 1948 [54]. The theoretical work on periodic structures by Lindsay [16] was well known, but was not used for predictive purposes. The results obtained from the first experimental attempts were fruitless. Barnes and Kirkwood [32] make use of Lindsay's work to model the drill string as a periodic acoustic structure and predict frequency domains in which information should be transmitted through the drill string with minimal distortion. Barne's publication resurrected the interest in acoustic telemetry, and was the basis of a second experimental investigation in the late 1970's by Sun Oil Company. Multiple attempts by

the Sun Oil Company concluded that the experimental data did not correlate well to the theoretical predictions. It was concluded that signal attenuation was prohibitive, and that the downhole environment was too noisy to make acoustic telemetry feasible [15].

Transmission of intelligence across the drill string for navigational purposes has been attempted by many. Most of the efforts have been documented through patents. A few of them are listed below chronologically:

Hixson [55] developed a mechanical system which transmits a sonic pulse, using the drill string as a wave guide when deviations from the vertical are detected downstream. In his patent, Hixson addresses the theoretical implication of using long wavelengths to minimize signal attenuation. Hixson conceptually outlines a quarter wavelength transformer, which is used by Drumheller [56] 36 years later to optimize impedance matching between the drill bit and the drill collar.

Petersen et al. [57] discussed a downhole system to transmit longitudinal waves along the drill string. His patent addressed the need for a portable “in house” (i.e. embedded within the drill string) transducer system.

Shawhan [58] attempted to overcome the inherent attenuation encountered over long distances by placing repeaters along the drill string. The specifics of the repeaters are not provided - the repeater is placed along the drill string to transmit signals upstream without regard for directionality.

Sharp [59], aware of the filtering properties and the behavior of the signal within a pass band, develops a phase shifted mechanism which transmits

data at frequencies which coincide with the natural frequencies of the drill string. Sharp contends this will avoid transmitting a signal in one of the “pit falls” within a pass band¹.

Unfortunately, none of the methods mentioned above have gained wide commercial use. The lack of an accurate predictive model of the waveguide - e.g. the drill string, technology (such as the computing and signal processing techniques widely available today), and the complexity of some of the designs, have kept the patents from becoming reality.

In a series of papers Drumheller [15], [11], [60] and [52] successfully modelled and experimentally verified the steady state and transient behavior of the drill string. Drumheller was able to explain several phenomena observed by the Sun Oil company when attempting to use the drill string as a telemetry system. The model, which was successfully used by Sandia National Labs to obtain an accurate description of the acoustical properties of the drill string, is essentially the same as that of Lindsay’s [16]. However, the numerical methods developed to find the behavior of the drill string as an acoustic telemetry system is novel. The algorithm will be discussed in greater detail in the next chapter. The remainder of this chapter is devoted to describing the behavior of the drill string when used as a waveguide for transmitting information.

¹The “pit falls” within a pass band turn out to be zones in between the “fine structure” reported by Cox [54]. However, the fine structure changes with length and boundary conditions, thus Sharp’s approach would not work.

3.3 Acoustic Model

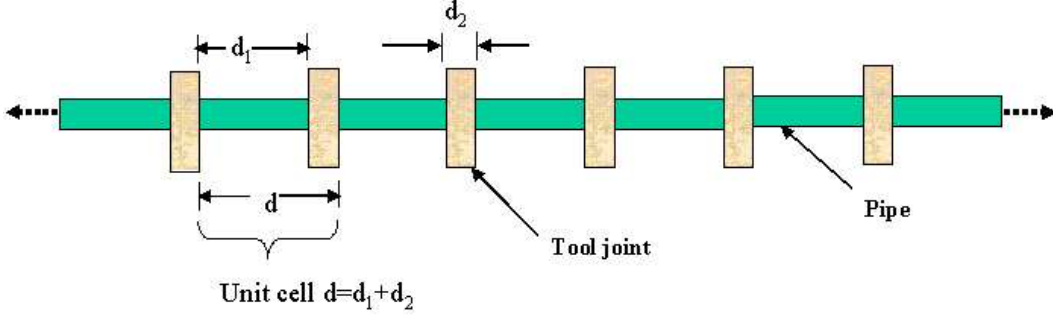


Figure 3.1: Schematic of a 1-D periodic waveguide for acoustic telemetry

Figure 3.1 shows a one-dimensional, periodic acoustic waveguide, along with the one-dimensional wave equation that models the propagation of information through the structure. The unforced one-dimensional linear wave equation which describes the dynamics of each of the layers in the structure is given in Equation 3.1:

$$\frac{\partial^2 U}{\partial t^2} = \beta(z) \frac{\partial^2 U}{\partial x^2} \quad (3.1)$$

Here $\beta(z)$ is a piecewise constant, periodic function, with period equal to that of a unit cell d ; U is the displacement field; and t and x are the temporal and spatial coordinates, respectively.

The one-dimensional, lossless dispersion relationship that describes the propagation of plane waves through a periodic structure can be obtained using various techniques. The derivation outlined in this section uses the continuity of displacement and stress at the interface between unit cell components.

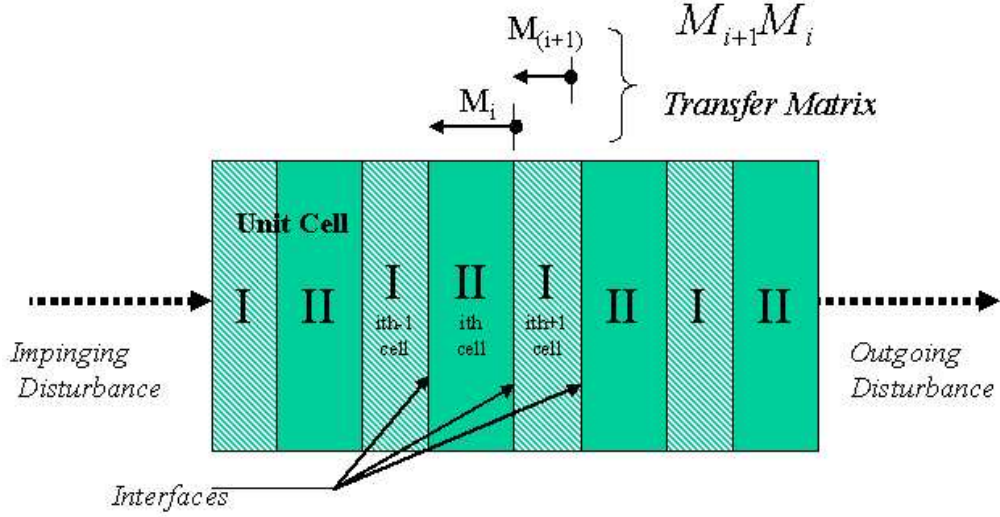


Figure 3.2: One-dimensional model used to derive the dispersion relationship

Figure 3.2 shows the one-dimensional model used to derive the dispersion relationship of the drill string.

An outline of the derivation of the dispersion equation is given in Figure 3.3. The details of the derivation can be found in [61] and [17]. A slight variation of the technique used herein can be found in Chapter 3 of Bedford's book [4]. Continuity of the velocity ν and stress σ field across the I cell couple the two field variables across the $(i-1)^{th}$ and $(i)^{th}$ interfaces of the transfer matrix M_i . Likewise the matrix M_{i+1} relates the velocity and stress fields at the interface between the $(i)^{th}$ and $(i+1)^{th}$ interfaces on cell II . The product of matrices $M_{i+1} M_i$ therefore relate the stress and field velocities from the left-most boundary of the I cell to the right most boundary of the II cell. Due to the periodicity of the structure, Floquet theory demands these two interfaces vary only by a phase shift through the matrix F . This demand is a

$$\left. \begin{aligned}
\begin{Bmatrix} v \\ \sigma \end{Bmatrix}_{i+1} &= \overbrace{\begin{bmatrix} M_{i+1} & M_i \end{bmatrix}}^M \begin{Bmatrix} v \\ \sigma \end{Bmatrix}_i \\
\begin{Bmatrix} v \\ \sigma \end{Bmatrix}_{i+1} &= \underbrace{\begin{bmatrix} 1 & 0 \\ 0 & 1 \end{bmatrix}}_F \begin{pmatrix} e^{iqd} \end{pmatrix} \begin{Bmatrix} v \\ \sigma \end{Bmatrix}_i
\end{aligned} \right\} \begin{aligned}
&\overbrace{\begin{bmatrix} M - Ie^{iqd} \end{bmatrix}}^A \begin{Bmatrix} v \\ \sigma \end{Bmatrix}_i = \begin{Bmatrix} 0 \\ 0 \end{Bmatrix} \\
&\text{Demand consistency of solution.} \\
&\text{To avoid trivial solution (eigenvalue problem)} \\
&Det[A] = \begin{Bmatrix} 0 \\ 0 \end{Bmatrix}
\end{aligned}$$

Figure 3.3: Outline of derivation of dispersion relation

direct result of $\beta(z)$ being a piecewise constant, periodic function.

Since the solution must be unique, the transfer matrix and Floquet theory form an eigenvalue problem, which has a non-trivial solution only if the determinant of A is forced to vanish. The solution to the eigenvalue problem $Det[A] = 0$, yields the dispersion relationship given in Equation 3.2, where $[A] = [M - Ie^{iqd}]$ and $[M] = [M_{i+1}][M_i]$.

$$\cos(qd) = \cos\left(\frac{\omega d_1}{c_1}\right) \cos\left(\frac{\omega d_2}{c_2}\right) - 0.5\left(\frac{Z_1}{Z_2} + \frac{Z_2}{Z_1}\right) \sin\left(\frac{\omega d_1}{c_1}\right) \sin\left(\frac{\omega d_2}{c_2}\right) \quad (3.2)$$

Here ω is the circular frequency, c_i the speed of the wave in the i^{th} cell, Z_1 and Z_2 are the characteristic impedance of the drill pipe and tool joint, respectively and d_1 and d_2 are the length of the drill pipe and tool joint, respectively. The plot of the dispersion relationship is shown in Figure 3.4.

The dispersion relationship is an even function with respect to Floquet's

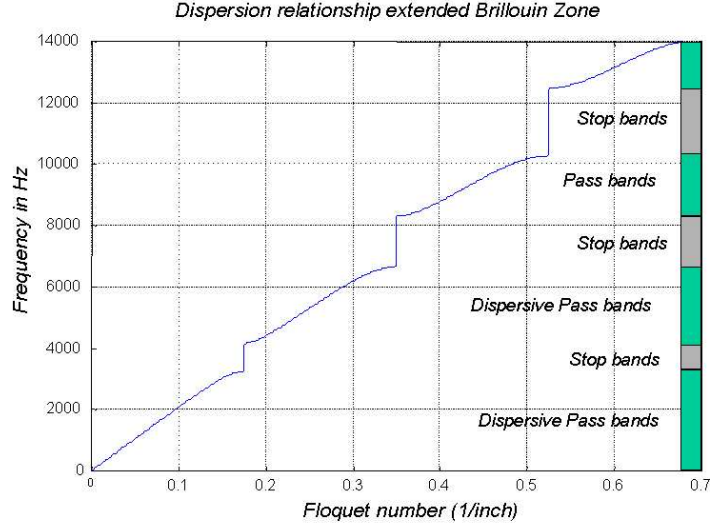


Figure 3.4: Dispersion relation for a $\frac{1}{20}^{th}$ scale model of a drill string

number², and therefore it is sufficient to limit all of the analysis to the positive half of the Floquet domain. Although derived for an infinite waveguide, the characteristic behavior of harmonic wave propagation in periodic finite structures has been shown in fact to be a Bloch wave [14].

The published literature in WPIPS is extensive and the properties of one-dimensional linear Bloch waves are well known. The following references provide a detailed analysis of the behavior of harmonic wave propagation in periodic solids. It should be noted that the literature provides a rich theoretical background in the steady frequency state domain, but relatively few papers on the transient behavior of Bloch waves.

²Only because of the symmetry of the wave guide.

- Characteristic impedance of a two cell periodic structure: Lindsay [16] [17], Esquivel [62] and Shenderov [63].
- Behavior of harmonic waves in the pass bands and stop bands: Delph [22], Lee [25] and Kaul's work [33].
- Reflection and Transmission Coefficients: Brekhovskikh [64], Thomson [18], Loggins [19] and Aislie [65].
- Experimental verification of the dispersion relationship/phase velocity: Bradley [14], Robinson [45] and Gaznahes [49].
- Graphical representation of the behavior of Bloch waves in the pass band and stop band: Bradley [14].
- Backward wave properties of Bloch wave propagation: Mead [37].

Acoustic data telemetry involves sending, receiving and deciphering signals which travel through a highly dispersive, filtering and lossy medium. Broadband signals are heavily penalized in these types of environments, but also have the biggest potential for increasing transmission rate since a *bit train* could be transmitted across the structure, sending bulks of data at a time. Transient stress waves designed to represent a binary bit may be capable of transmitting accurate information upstream at baud rates an order of magnitude larger than is currently possible. Thus the transient analysis of the wave guide is of paramount importance.

3.4 Transient Analysis

The simulations that follow re-create by Drumheller's [15] work. The intent of this section is to provide with a clear understanding of acoustic wave propagation in periodic waveguides.

One of the most powerful methods of solving the one-dimensional wave equation (both linear and non-linear) is the method of characteristics. By properly selecting the discretization scheme in the time-space domain, the method of characteristics can be easily adapted to treat problems in layered media. The method of characteristics is an exact solution, not an approximation. Thus the numerical solutions obtained for the velocity field (ignoring round off error) are essentially samples of the closed analytical solution at different space and time intervals.

The algorithm developed by Drumheller [15] was used to simulate the propagation of a transient pulse in a scaled model of the drill string. It solves for the velocity, stress and displacement fields as a function of space and time.

Perhaps the most important question answered by closely examining the behavior of transient waves in a periodic structure is its *filtering* properties. The numerical model presented does not include any loss functions, but spectral analysis clearly shows that the energy at the receiving end of the drill string is orders of magnitude less than the original transmitted signal. The dispersive nature of the drill string accounts for some of the energy which reaches slowly to the top of the drill string, however it can not account for the bulk of it. The question begs: Where does the energy of signals with frequencies

contained within the stop bands go? Simulations show that the *filtering* properties of the drill string are in reality a *trapping mechanism*; signals centered in a *stop band* get *trapped* in the early stages of the structure.

The numerical simulation presented in this chapter uses a $1/20^{th}$ scale model of a copper drill string, and nine unit cells (a unit cell is composed of a drill pipe followed by a tool joint). Stress free boundary conditions are used on both ends.

The dimensions of the scaled model are listed in Table 3.1

Section	Length	Cross-sectional Area	Speed of Sound
Pipe	$d_1 = 17in$	$a_1 = 0.0185in^2$	$3840\frac{m}{s}$
Tool Joint	$d_2 = 1in$	$a_2 = 0.0968in^2$	$3840\frac{m}{s}$

Table 3.1: Model dimensions

A transient signal was injected at the bottom of the waveguide (i.e. where the drill bit is located), and downstream information was (numerically) sampled at various locations along, to capture the effect of the periodic structure on the input signal as it travels downstream. Numerical gauges were placed at 2.5, 4.5 unit cells into the structure, and four inches from the top of the scaled model. Figure 3.5 shows a graphical representation of the sampling scheme.

The type of input signals used are as follows:

- Hammer Input: Ideally this would be a *delta* function. However, this type of stress impulse response is physically unrealizable. Instead, the

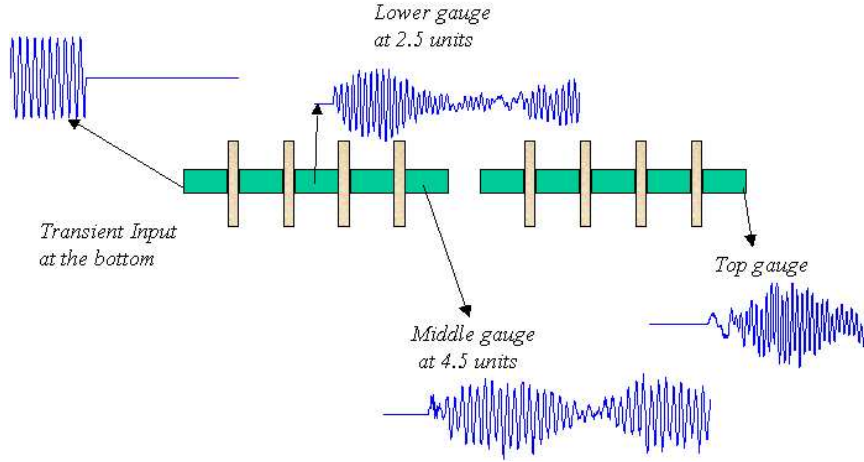


Figure 3.5: Transient signals along the scaled model of the drill string

δ function is modelled as half a cycle of a sine wave of $60\mu s$ in duration and unit amplitude. The broadband signal will illustrate the filtering and dispersive properties of the periodic structure.

- The input spectrum is subsequently narrowed by increasing the duration of the pulse³. Two transient pulses are considered:
 - A finite wave train of fixed frequency whose dominant lobe lies in the middle of a pass band. This type of signal minimizes dispersion and maximizes the transmission of the energy.
 - A narrow band signal whose dominant lobe lies in the middle of a stop band.

³The uncertainty principle [66]

3.5 Broadband Simulations

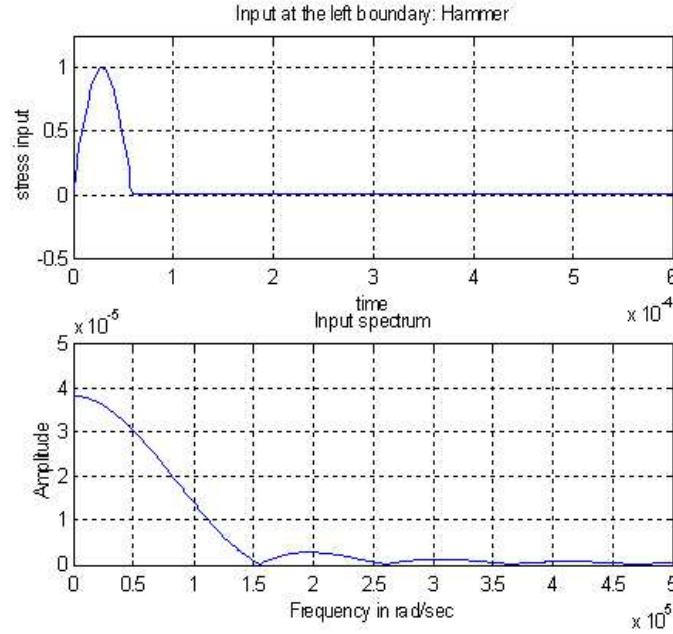


Figure 3.6: Hammer input to the drill string

Figures 3.6 and 3.7 show the numerical results for a broadband input at the *bottom* of the drill string. The top portion of each figure shows the transient response, with its respective spectrum directly underneath. Figure 3.6 shows the broadband input to the periodic structure. The numerical output halfway through the periodic structure is shown in Figure 3.7. Two important features of the general behavior of waves in finite periodic structures can be observed. First and foremost, note the distortion of the original pulse due to the filtering and dispersive properties of the waveguide. Midway through the waveguide, an observer would have a difficult time extracting the information sent from the bottom of the drill string.

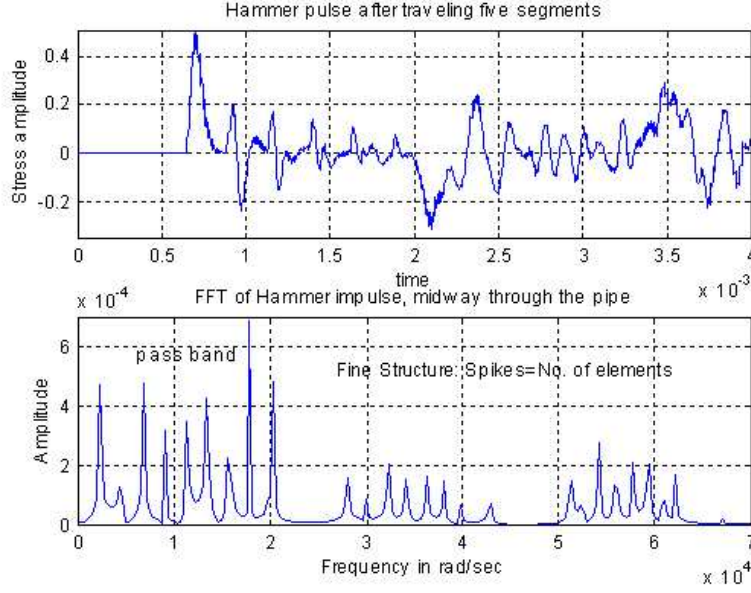


Figure 3.7: Output signal - after 5 unit cells

Secondly, the spectrum is clearly segmented into pass and stop bands. The first three pass bands are shown. The spikes predicted by the algorithm within each pass bands are the “fine structure” as coined by Cox [54]. The number of spikes correspond to the number of unit cells in the structure. In this example nine unit cells were used for the numerical simulation, thus there are nine “spikes” in each of the pass bands. Physically the spikes correspond to the natural frequencies of the structure, which are excited by the broadband input signal. As the number of unit cells increases (i.e for longer drill strings), the number of spikes increase proportionally, eventually “filling” the pass band until fine structure is finally smoothed. Structural damping also plays a role in smoothing out the comb structure [15].

Figure 3.8 shows the signal four inches away from the tip of the periodic

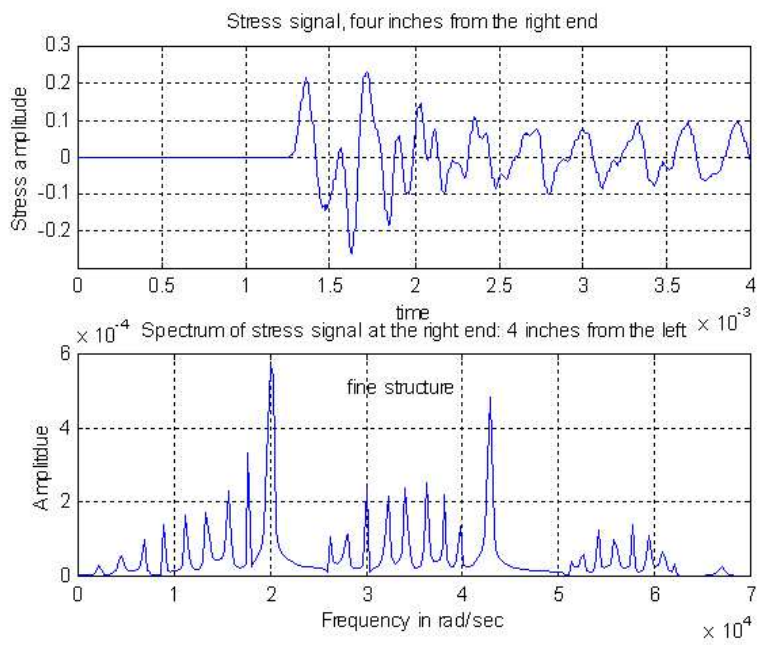


Figure 3.8: Output signal - 4 inches from the bottom

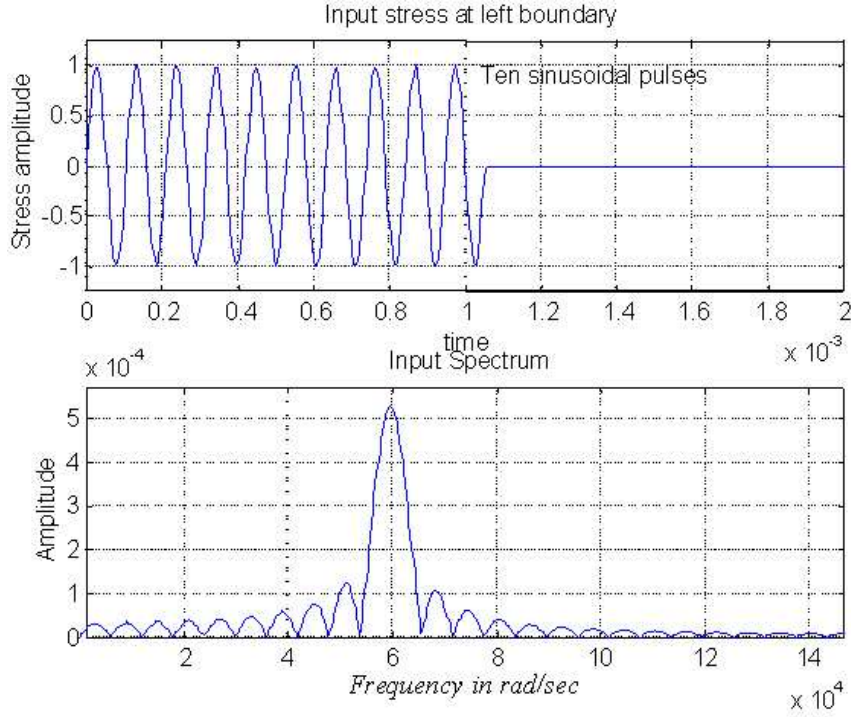


Figure 3.9: Input signal - middle of the third pass band

structure. Once the signal travels all the way to the top of the drill string, the output has a noise-like appearance. The complex wave shape is due, in part, to the reflections emitted from the top of the drill string caused by the reflections from a stress free boundary. This type of boundary condition was kept to emphasize the effect of not properly terminating the drill string - reflected signals interfere with incoming information.

The numerical results from a narrow band signal, whose dominant lobe is located in the middle of the third pass band, as shown in Figure 3.9, are given in Figure 3.10. The output signal was sampled roughly at one quarter of the length of the waveguide. Clearly the signal has been dispersed, but note

the bulk of energy content remains concentrated in the original main lobe⁴.

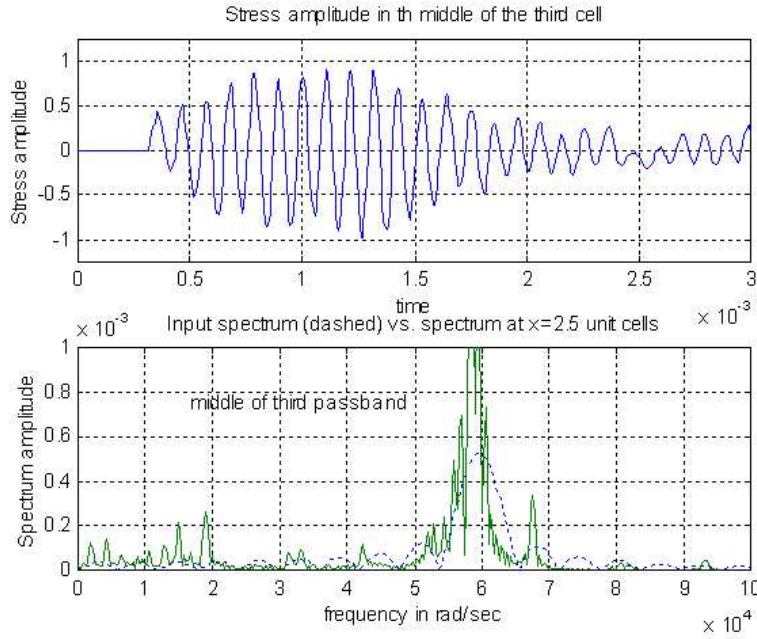


Figure 3.10: Signal 2.5 units into the structure

Figure 3.11 shows the same signal at the middle of the waveguide. The strength of the signal in the pass band has clearly decreased, and the stop bands are clearly marked. Note how the filtering properties of the structure have begun taking a toll on the input wave. The periodic structure filters the signal by trapping frequency components that lie in a stop band early into the drill string.

Finally, the signal (and its energy content), as seen by the receiver, is shown in Figure 3.12. As expected, the signal is highly dispersed, as seen by the decrease in amplitude and the filtered energy spectrum.

⁴The energy of the signal is larger than the input. This is because the fixed gauge measures not only the incoming signal, but also all subsequent reflections.

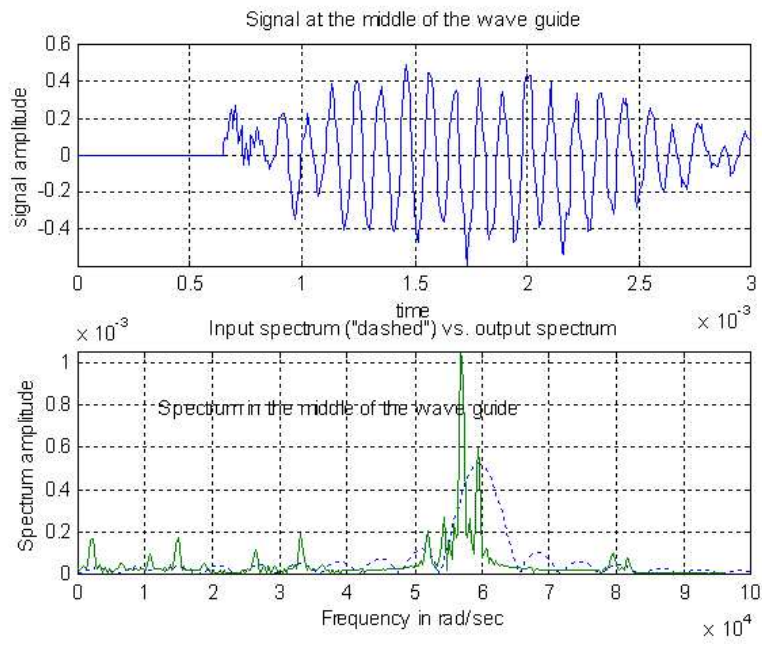


Figure 3.11: Signal as seen halfway through the nine unit cell scaled model

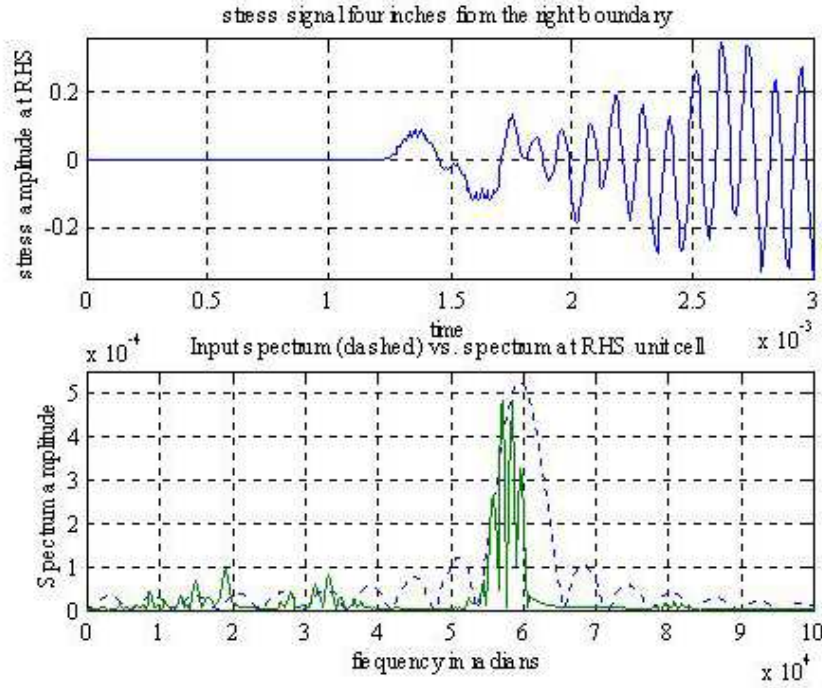


Figure 3.12: Narrow band signal as seen at the end of the drill string

As mentioned in Section 3.4, periodic structures behave as a mechanical filter; trapping the energy of signals which lie in the stop bands. This “trapping” mechanism is described by examining what happens to a signal whose dominant frequency lies in one of the stop bands.

Figure 3.13 shows a pulse train with a dominant lobe in the middle of the fourth stop band.

Figure 3.14 shows the signal after travelling only 2.5 unit cells. The peak amplitude of the signal and spectrum are decreased nearly 80 percent. Note also how the periodic structure has begun to filter out frequencies in the dominant lobe.

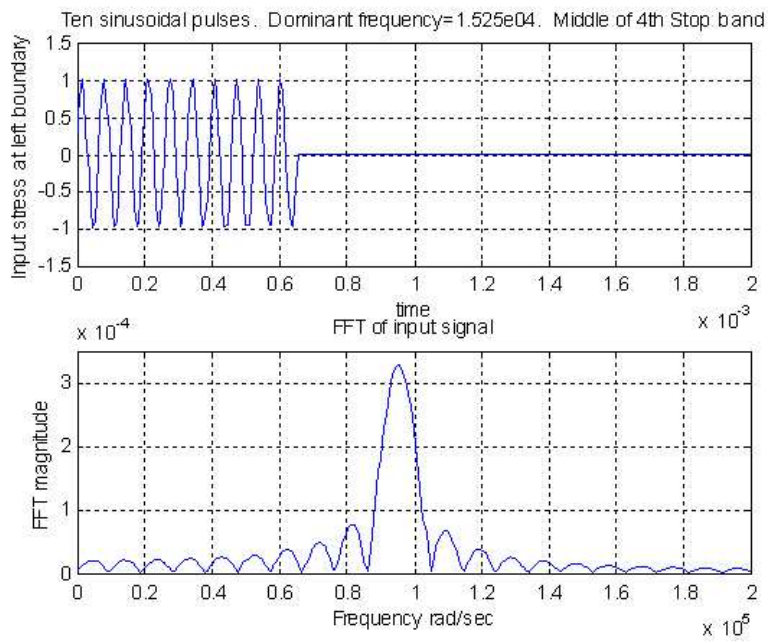


Figure 3.13: Narrow stop band input in a stop band

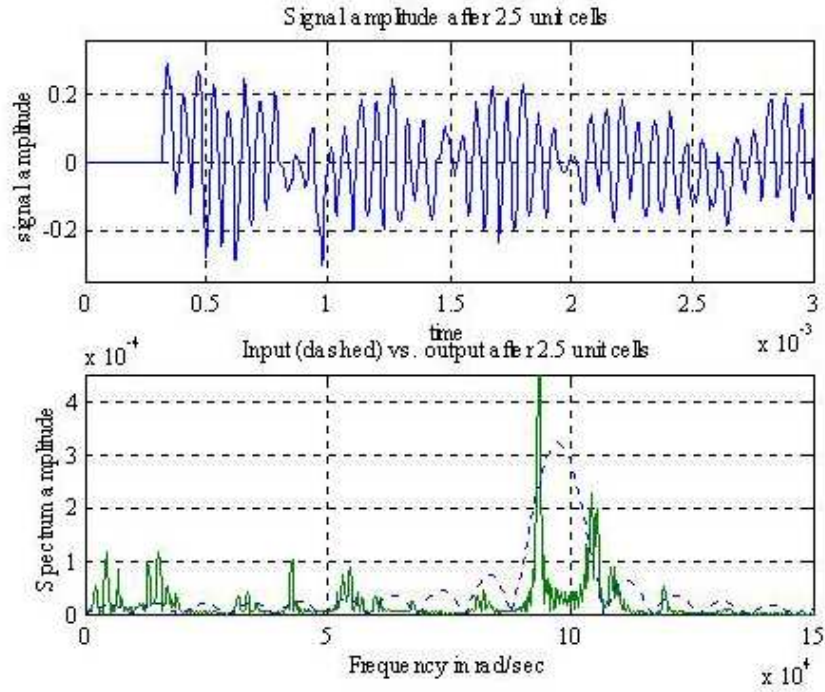


Figure 3.14: Narrow stop-band signal - one quarter into the drill string

As the signal travels downward, the energy inside the dominant lobe decreases. Figure 3.15 shows that the amplitude of the signal has decayed substantially after travelling only half-way through the periodic structure.

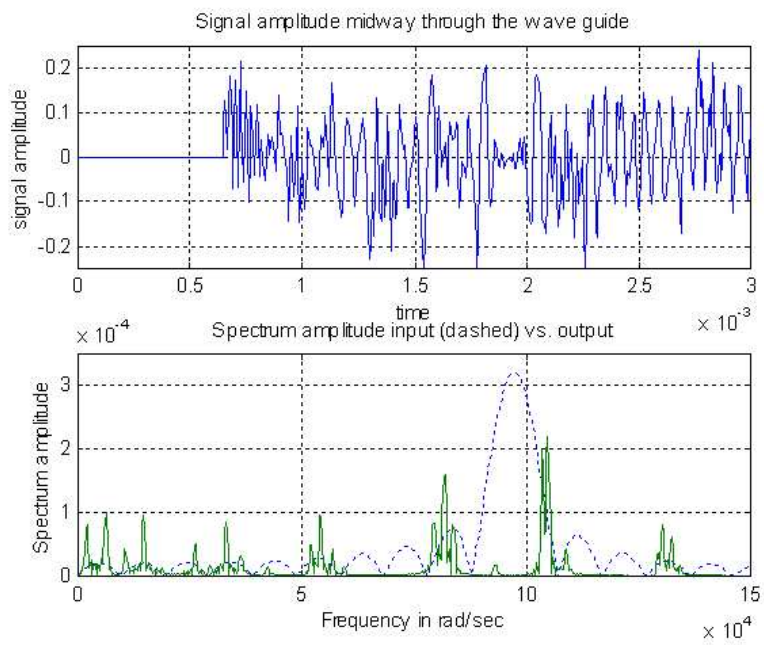


Figure 3.15: Narrow stop band signal - half of the way into the drill string

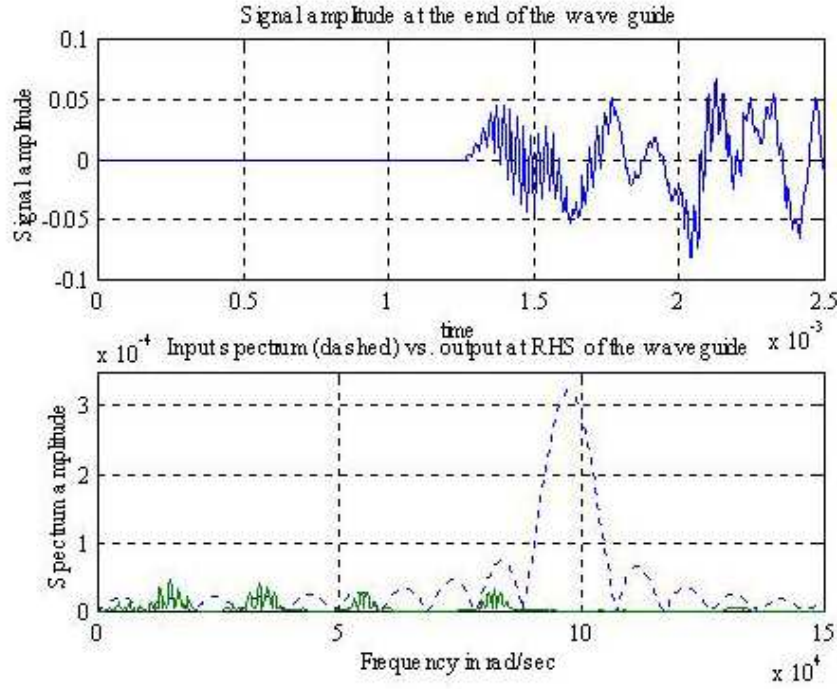


Figure 3.16: Narrow stop-band signal - bottom of the drill string

Figure 3.16 is the signal with its corresponding spectrum sampled four inches from the top of the waveguide. The energy contained in the dominant lobe of the signal has all but disappeared. Following the spectra on the broadband signal, which lies in the middle of a stop band, clearly shows the *trapping* phenomena of the drill string. The spectrum clearly shows energy at this frequency present early in the drill string. As the depth increases, the energy in the main lobe decreases substantially. Thus the drill string is a mechanical filter whose acoustic impedance which is a strong function of frequency and position.

The general behavior of a drill string used in the field has been shown

to correlate very well with the results obtained in the scaled model. Data from previous field experiments by the Sun Oil Company were re-analyzed by Drumheller [15] and found to be in good agreement with his model.

Drumheller’s finite difference model was able to predict the transient behavior of the a periodic structure; the boundaries of the pass bands and stop bands, and the “fine structure” (i.e. resonant frequencies) within each of the pass bands.

Both the laboratory and field experiments revived the interest in acoustic data telemetry, and other field experiments soon followed. The main focus of the experiments that followed was to quantify the attenuation as a function of drill string length. The transient characteristics of the drill string were studied by experimentally detonating explosives at specific locations downhole and examining the signal upstream.

Interactions between the drill string and its environment, specifically the signal transmitted through the surrounding mud upstream was examined in detail. The results of the first Long Valley [60] experiment are summarized as follows:

- Upon detonation, a mud pulse is generated in the annular portion of the hole, in conjunction with the acoustic signal in the drill string.
- Attenuation of the acoustic signal was measured empirically as a function of distance and pass bands. It was shown that attenuation increased linearly with distance (drill string length) and with pass bands, $10.9dB/km$ in the first pass band, compared with $30.6dB/km$ in the fourth pass

band.

- The attenuation mechanism was modelled using a modified Maxwell Damping [12] constitutive relationship. The parameters were modified until the experimental results matched the predictive model.
- The fine structure within the pass bands was attributed to the variation in lengths of the unit cell within the drill string. Thus a random ordered drill string causes interference patterns.

This last point is not obvious until the phase velocity of a drill string with varying pipe lengths is closely examined. Figure 3.17 shows two overlapping phase velocity plots of a drill string composed of different drill pipe length. The simplest case is one in which half of the drill string is composed of *short* unit cells, followed by the second half of the drill string which is composed of *long* unit cells. Both halves of the drill string will have their own dispersion and phase velocity functions. The signal generated from the bottom of the drill string must travel through both halves of the drill string, which implies that only signals whose frequency lie in the intersection of the pass bands within the phase velocity plots will be allowed to exit the drill string. Based on the arguments discussed above, the attenuation of the signal was hypothesized to be caused by the randomness of the pipe lengths. This was verified by a second Long Valley experiment in which a drill string was assembled to minimize the standard deviation between adjacent pipe elements [52].

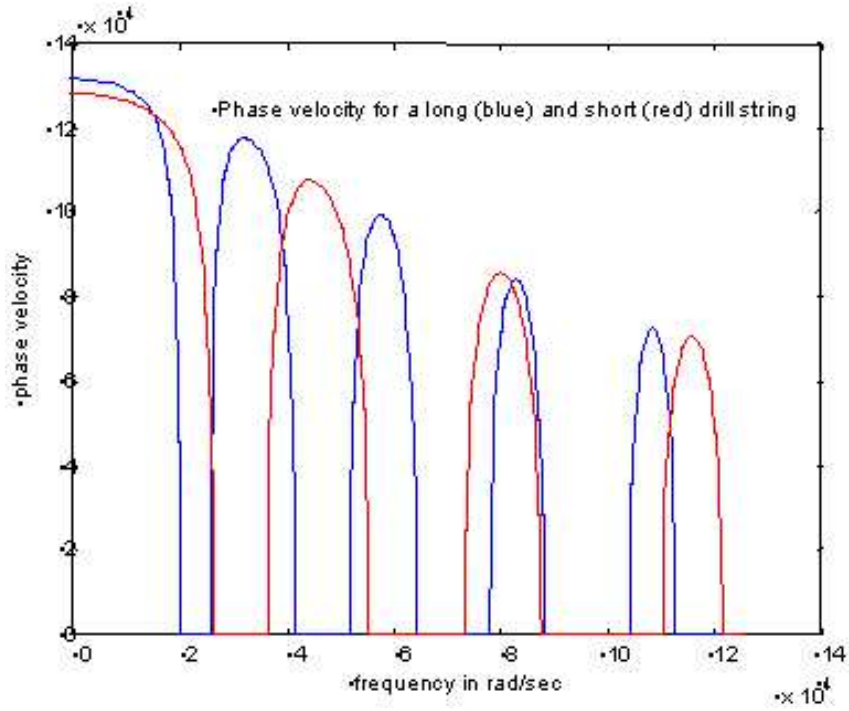


Figure 3.17: Phase velocity for a long and short drill string

The drill string was assembled by placing the shortest drill pipes at the beginning of the drill string and the longest at the end, while minimizing the change in length from one pipe to another. The results are summarized below:

- The experimental results showed the fine structure had disappeared within the pass bands.
- Attenuation was still present, but substantially reduced (by a factor of two).
- Drill string rotation did adversely affect the mud pulse generated outside the waveguide, but the stress wave propagating through the drill string

remained unchanged.

- Environmental noise is present, but is significant only in the second pass band.

3.6 Attenuation and Mode Coupling

The attenuation mechanism in the drill string is not well understood, but it is thought to be due to the coupling between the longitudinal and flexural wave motion inherent to the drilling operation.

Coupling between flexural, torsional and longitudinal modes while drilling is a well documented phenomena, both experimentally and theoretically. Figure 3.18 shows a schematic representing the coupling between extensional and flexural modes.

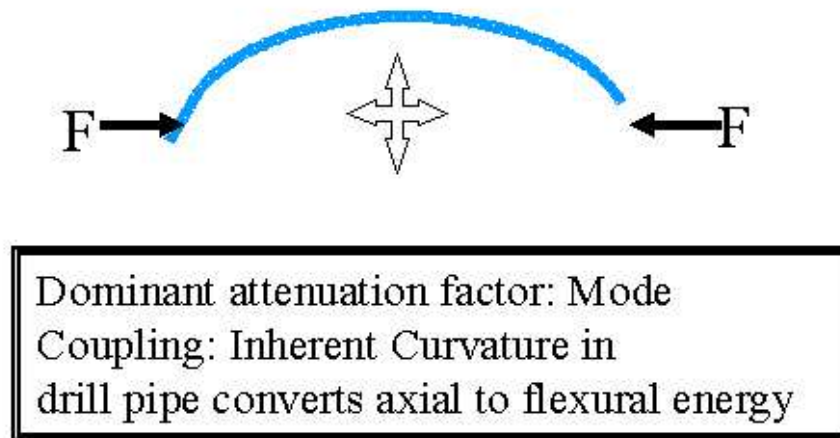


Figure 3.18: Extensional and flexural mode coupling

Vandiver et. al. [67] showed the existence of coupling between axial and bending vibrations due to curvature in the drill collar.

Aarrestad [68] investigated the coupling mechanism between torsional and longitudinal waves in a drill string. The investigation was able to predict the distortion due to rotation on a longitudinal wave travelling through the drill string.

Wu and Lundberg [69] have shown theoretically that a longitudinal wave impinging on a bent bar is transmitted as a flexural wave, and vice versa (with the curvature of the bend playing an important role).

More related to the problem at hand: Drumheller has verified the transfer of energy between flexural and longitudinal wave in an uniform bent bar [70]. The proposed hypothesis in [11], which claimed part of the attenuation in the drill string was caused by mode coupling due to inherent curvature in the drill pipe, was verified experimentally. Attenuation was found to be present even in absence of fluids and was independent of frequency.

When the proposed (coupled) model was used to simulate the steady state behavior in the drill string, the calculated attenuation was of the same order of magnitude as that measured in the field $\simeq \frac{13.9dB}{km}$. Friction between the drill string and the casing is another suspected cause of attenuation in the drill string, as the geometry of the drill string changes - thus changing its dispersion characteristics.

Other attenuation mechanisms exist but are very hard to quantify, and can be modelled empirically at best [71].

3.7 Summary of the Work to Date

- The work to date on the drill string has been composed of a one-dimensional model, which is able to predict the underlying phenomena of transient wave propagation in a drill strings.
- The available frequency bands for transmission are well understood.
- The effect of environmental noise, drill string rotation and the influence of the surroundings have been quantified, and while all contribute to the deterioration of the signal, they are not crippling [11].
- Attenuation has been modelled empirically, and the root cause for one half of the loss in signal strength has been found. A portion of the remaining attenuation within the drill string has been shown to be caused by mode conversion.
- The effects of signal dispersion can be minimized either by sending a narrow band signal in the middle of a pass band or by correcting the incoming signal to account for dispersion [15].

The only other work found which addresses transient wave propagation in a drill string is that of Neils [72], who models the drill string using Markov chains. Neils' statistical model is able to reproduce the band structure of the drill string when excited by a Dirac delta function. Neils is also able to model the loss of energy due to changes in lengths and diameter of the drill pipe and

tool joint. His model proposes a uniform distribution of energy throughout the drill string (for a signal lying in a pass band) at steady state conditions.

3.8 Vision

Ideally, an acoustic telemetry system would transmit a signal upstream (unidirectional), amplifying it along the way to account for the attenuation, compensate for dispersion (if needed), interpreting the information for decision making, and absorb all of the information at the top of the drill string to avoid reflections which might interfere with incoming signals.

Some of the desired components of an ideal acoustic telemetry system have already been addressed:

- Repeaters have been proposed [59] to amplify the signal in an effort to compensate for the inherent attenuation of the drill string - unfortunately, the repeaters are not optimized to transmit information in one direction.
- Adaptive noise cancellation has been proposed to avoid echos from the bottom of the drill string, and to transmit monochromatic signals only in one direction [73]
- In-situ telemetry systems have been designed and tested in the field [74].
- Transducers specific for the acoustic telemetry in a drill pipe have been designed, analyzed and field tested [71].

- Analog Circuit for Controlling Acoustic Transducer Arrays proposes a simplified version of a delay and inversion scheme for active noise cancellation [75].
- Acoustic Transducer, a patent which proposes an alternate model of and acoustic transducer for acoustic data telemetry. [76].
- Electro-mechanical Transducer for Acoustic Telemetry System discusses the design of a modern in-situ transducer for drill strings. [74].
- Downhole Pipe Selection for Acoustic Telemetry discusses the ordering of the pipes to minimize attenuation [77]
- Acoustic Data Transmission Through a Drill String a patent which describes the hardware and techniques used for data telemetry [78].
- Circuit for echo and noise suppression of acoustic signals transmitted through a drill string has been designed [73]

3.9 Focus of the Dissertation

The work presented herein addresses the design and simulation of a directional array for broad band signals. It can be used as both a terminating impedance and a repeater. The design and simulation is numerical in nature. The capabilities of the directional array are restricted to cancelling incoming signals from a scaled model of a drill string. The dissertation does not address stability issues that may occur due to the possible feedback to the sensing element.

This later may be a crippling factor in the implementation of the open loop system described herein.

Chapter 4

The Design of a Broadband Directional Acoustic Array

4.1 Introduction

This chapter focuses on the two major aspects of this dissertation: the design of an active termination impedance and a directional repeater for broadband signals. The design of both systems is accomplished by a properly phased directional array. A directional array as defined here is composed of a set of transducers, embedded in a uniform waveguide, properly spaced and phased to generate signals in one direction.

There are two main aspects to the design of such systems: the design of the electrical inputs to a single transducer to generate a fixed but arbitrary broadband acoustical signal and the algorithm necessary to provide directionality. The main challenge is to generate directional broadband acoustic wave

forms with a finite set of transducers. Directionality is achieved by synthesizing the desired signal into its Fourier half range expansion and properly distributing the components amongst the available transducers.

This chapter defines the electrical inputs to the transducer array necessary to generate arbitrary transient signals of a pre-determined length, the transducer layout, firing sequence, selection and phase delay necessary to provide directionality. The design of a directional repeater has been a focus of research and development in the area of acoustic telemetry. The filtering and dispersive properties of the drill string are only two of the hurdles in the area of acoustic telemetry. Even if it becomes feasible to successfully inject transient signals at a high rate, signal attenuation is inherent and unavoidable for large drilling depths. A method for boosting the signal strength as it travels along the drill string could help overcome the inherent attenuation of the medium. The strategic placement of the repeaters has already been defined: Drumheller has found optimal locations along the drill string to amplify the incoming signal strength [56], which would enhance the operation of the directional array discussed in this dissertation.

Once the signal is injected at the tip of the drill string and transmitted to the top of the structure, information must be extracted and compiled for decision making. Ideally, reflections from the top of the drill string should be avoided (i.e. terminated or cancelled), as they would interfere with incoming information.

What is needed therefore, is a *terminating impedance* attached at the

top of the drill string, that perfectly matches the impedance of the drill string at all times.

A passive terminating impedance design is not a practical solution. Even if the material and geometry could be identified, it would have to be redefined for each drill string and drilling depth¹. Interference with operations alone would make the design prohibitive.

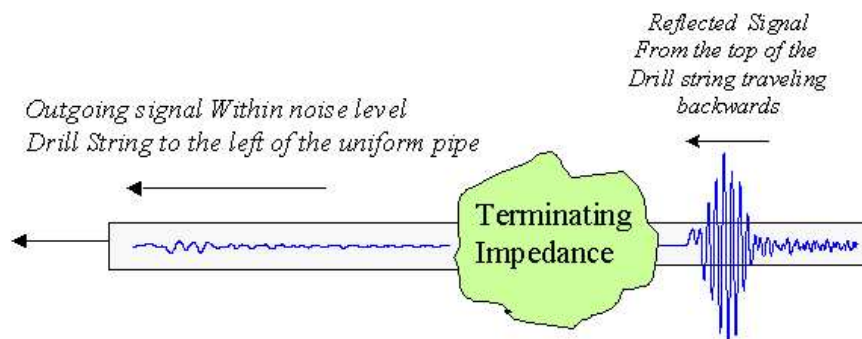


Figure 4.1: Active broadband terminating impedance concept

The word *match* as used here refers not to a physical entity which absorbs all of the incoming sound, but rather a cancellation device capable of eliminating incoming broadband acoustic energy. The goal is thus to design an *active terminating impedance* capable of handling broadband signals of arbitrary dynamic spectrum, and whose design is independent of drill string geometry and targeted drill depths. The concept of an *active terminating impedance* is shown below in Figure 4.1. After some forethought, it becomes clear that the design of a broadband directional repeater and a termination

¹The impedance of a drill string is a function of frequency, and position, as well as drill string dimensions. The acoustical impedance changes as the drill string length's increases, and as tool joints and pipe dimension change due to inherent operational wear and field failure.

impedance system is one and the same. Once the algorithm for the directional repeater has been defined and optimized, it can easily be turned around and used as an active termination impedance by multiplying the input signal to the directional array by -1 . This requires the array to generate a signal equal in magnitude, but opposite in phase of the incoming signal; thus providing cancellation instead of amplification of the signal.

The key point in designing the repeater/terminating impedance is achieving directionality. Any significant leakage in the opposite direction would interfere with incoming information. A repeater that re-broadcasts signals in both directions, not only will reduce the transmission rate, but it may also cause instabilities unless a directional sensor has been incorporated into the feedback loop. The instabilities are caused by the backward travelling wave, which feeds back information to the directional array for amplification. Drumheller has created a directional sensor [56] capable of detecting stress waves travelling in one direction. It is geometrically configured to “ignore” backward travelling waves. This type of sensor configuration may help resolve the feedback problem.

The development presented in this dissertation makes use of the algorithms designed by Drumheller [15], [11], while exploiting the low frequency behavior of the PZT transducers in the vicinity of the origin; and compensating for the dynamics of the PZT sources. The algorithm provided is all numerical in nature and should be viewed as a design tool to define a directional array along with its inputs for broadband signals. It is described in a flow diagram

in the appendix; which also provides the measurements of an experimental proof of concept test bench designed in the Electro-Acoustics Laboratory.

4.2 Chapter Organization

The chapter is organized as follows:

Section I - Noise Control Techniques - Previous Work

This section discusses the results of a literature search on the general topic of active and passive noise cancellation. Several techniques which have been used in the past will be reviewed, including active noise cancellation techniques using adaptive filtering.

Section II-Transducer Characteristics, This section outlines the finite difference model developed by Drumheller [15], [11] used to predict plane wave behavior in an isotropic solid waveguide with complex geometry and sources.

The numerical model is used to predict the frequency response of a *type II source*² which is key to the design of a directional acoustic array.

The behavior of the transducers is also described using a lumped circuit element model of a PZT transducer sandwiched between two isotropic, elastic, acoustically matched wave guides.

Section III - Transient Wave Generation - In this section we defines

²The frequency response or transfer function of a PZT transducer, depends on the transducer dimensions, electrical connections, boundary conditions, acoustical impedance of adjacent waveguide, and stacking configuration. A *type II source* is a PZT transducer thin enough such that $\phi = \frac{\xi}{h}$ holds. Where ϕ is the potential across the electrodes, ξ is the electric field and h is the thickness of the transducer.

the electrical input to a single transducer which generate arbitrary (albeit frequency restricted), omnidirectional transient acoustic signals in an elastic waveguide. It will be shown that a Half Range Fourier Expansion, a solution usually reserved for steady state analysis of periodic signals, can be modified for such purposes.

Section IV - **Incorporating Directionality**

The stress wave generated using electrical inputs to a single transducer by synthesizing the waveform as a Half Range Fourier Expansion is arbitrary in shape, but it lacks directionality. Transducer spacing must be re-defined to prevent information from travelling in all directions.

4.3 Section I - Noise Control - Literature Survey

Acoustic telemetry, by definition, implies that cancellation will be done near the receiver, after the information has been decoded for decision making. To date, the literature provides little insight on active/adaptive directional cancellation of broadband acoustic signals in an isotropic, elastic waveguide. The majority of the focus of the acoustic community has been on the development of adaptive controllers to filter out noise in air ducts, and very little emphasis has been placed on the directional aspect of the cancelling wave.

There are three main noise cancellation techniques: Passive Noise (PNC), Reactive (RNC) and Active Noise Cancellation (ANC). Reactive and Passive

Noise Cancellation require modifications to the path between the source and the receiver, so that acoustic energy either gets reflected, trapped or absorbed before reaching its target. Active Noise Cancellation refers to the technique by which a secondary source generates a wave of equal amplitude and frequency, but opposite in phase as the incoming signal to cancel it. By definition, this technique implies that the system is linear so that the superposition principle applies. Leug [79] is given the credit of inventing the ANC concept.

Active cancellation techniques can be applied either at the source, the receiver or the medium between them. A typical ANC system is usually composed of a source, a microphone or sensor, a primary path, a secondary source (to cancel the incoming wave), an error path, an error microphone, and a feedback loop to provide information to the control algorithm for filter updates.

The secondary source along with an optimized control scheme are responsible for generating the cancelling signal while minimizing the error. Open-loop cancellation techniques have also been designed, in which case the feedback loop from the error microphone to the input filtering schemes can be removed.

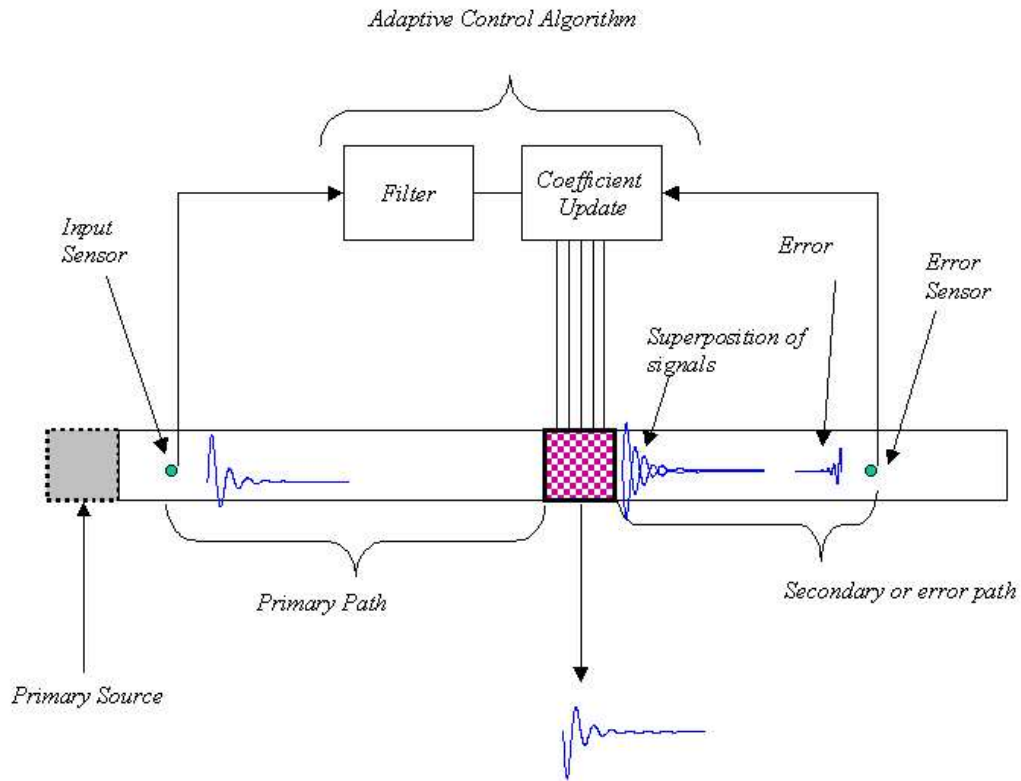


Figure 4.2: Typical adaptive acoustic noise cancellation system

Figure 4.2 shows a typical closed-loop ANC system. To accurately model a noise cancellation system, properties of the source, receiver and the medium between the two must be well known. For the terminating impedance, the source is composed of a set of PZT transducer arrays, the path is the (scaled model) of the drill string and the receiver another set ferroelectric transducers designed to capture the information for decision making.

The concept of ANC is straightforward - the secondary source must simply duplicate the incoming signal, but opposite in phase, and be exactly syn-

chronized in time with the passing unwanted sound wave. In practice however, ANC requires substantial real time signal processing and modelling techniques (Kalman, adaptive and digital filtering, fairly advanced system modelling and computing power) not available until the later part of the previous century. The first reported successful experimental set up was reported by Jessel et al. [80] in 1975 some 36 years after Leug's disclosure. They were able to achieve 23 to 50 dB attenuation at discrete frequencies [81].

A clear drawback of the typical acoustic noise cancellation system shown in Figure 4.2 is that the secondary source emits sound in both directions. Ideally, the secondary source would be directional so that the interference from the backward travelling wave could never disrupt the cancellation efforts.

One of the first documented efforts in designing a directional secondary source is the work proposed by Swimbanks [82]. Swimbanks proposed an open-loop, directional ANC system to cancel noise in an air duct. The secondary source was composed of a set of point sources around the circumference of the waveguide—a *ring* source. Two geometries were considered: a circular duct and a rectangular wave guide. The three-dimensional wave equation with a source density distribution is solved using transform methods, and the expression for the pressure field within the waveguide is obtained. The general solution reveals the restrictions necessary to restrain subsequent analysis to plane waves within the waveguide. The distribution of the point sources around the ring is symmetric (three point sources spaced 120 degrees for the circular duct, and in the center of the four walls for the rectangular waveguide), to avoid gen-

erating transverse modes within the ducts. Having defined which frequencies are allowed to propagate, Swimbanks proposes a two-ring system to generate a directional cancelling wave. The spacing between the two-ring sources is fixed but arbitrary. The delay between the two-ring sources is defined to be the distance between the two-ring sources divided by the speed of sound. The ring source strengths are opposite in phase - thus the combination of rings produces no output in the backward travelling direction. Because the distance between the two-ring sources is *not* restricted to be one quarter wavelength of the intended wave, Swimbanks finds what he calls the *useful* frequency range - the range in which the two source rings can generate a positive travelling wave with amplitude greater than one - with the maximum amplitude possible being reached at the *standard* quarter wavelength spacing. The fundamental interval allowed for a $2\frac{1}{3}$ octave range centered about the quarter wavelength spacing, with subsequently decreasing frequency spectra. Swimbanks seeks to expand the frequency range by using a third ring, spaced again at an arbitrary length d to the right of the two-ring set. The first ring is used to cancel any signals generated by the other two. The source strengths are defined in such a way that the two right most rings are in phase to positively reconstruct a signal. The frequency range is expanded to $4\frac{1}{3}$ octave. That is, over $4\frac{1}{3}$ octave frequency span, the three-ring configuration can transmit directional waves with amplitude greater than one. All of Swimbanks's work is limited to the steady state domain. Swimbanks is able to define a directional wave source, which is not confined to the standard quarter wavelength design, thus Swim-

banks is able to define the useful frequency range of a directional transducer triplets. Swimbanks work has been experimentally verified by Poole and Leventhall [83], who reported 40 dB attenuation at discrete frequencies, but only 10 dB with a 100Hz bandwidth. The focus of the ANC community shifted from developing directional cancelling arrays to eliminating the feedback produced by an omni-directional secondary source. The main reason for this focus is, that for a directional acoustic array to work, the spectra of the incoming signal must be known *a priori* in order to define the spacing between the *ring* sources. This limited the work to a narrow band spectrum. The obvious choice was to allow for the secondary source to emit sound in all directions of arbitrary frequency, and to literally *ignore* the backward travelling sound until it is reflected back from downstream structures. Such an approach must include either a system which ignores backward travelling waves by either strategically placing the appropriate sensors downstream, or to configure a set of arrays to only *accept* forward travelling waves. Swimbanks [82] proposed a ring configuration to ignore backward travelling waves. His configuration is very similar to Drumheller's [56], while Eghtesadi [84] strategically places the input microphone between the two secondary sources to eliminate feedback. Unfortunately all of these systems assume the wavelength of the incoming wave is known *a priori*. The focus of the research community moved towards signal processing schemes to cancel unwanted signals using adaptive systems.

The literature is rich in the area of ANC in ducts without regard to the downstream travelling wave generated by the second source. Adaptive

systems which showed promise of being capable of tackling broadband signals began emerging in the 1980's. Adaptive filtering was not only used to solve the problem of acoustic feedback, but also for system modelling.

Adaptive filtering techniques have been around since the late 1940's. The seminal work done by Wiener [85], Bucy [86] and Kalman [87] describe the basic algorithms behind adaptive noise enhancement/suppression and system modelling. Adaptive filtering techniques expand from MODEM applications to antenna side lobe cancelling, electrocardiography, long distance telephone transmission lines and elimination of periodic interference to name a few. A brief and interesting historic summary is provided by Widrow [88]. In this article Widrow also describes the basic closed-loop feedback used in most noise suppression applications. Wiener filtering techniques for statistical noise cancellation, notch and high pass filter design, adaptive line enhancers, and a self tuning filter are presented. Widrow et al. [88] present the basic Least Mean Squares (LMS) algorithm (which is used to place the adaptive filter constants near the optimal setting of the quadratic performance index). Widrow has also published an entire textbook devoted to subject of adaptive filtering [89]. Widrow's book is perhaps the most complete introductory textbook on the subject³. The signal processing techniques described above are all approached from the same point of view: that operations can be carried out on the train-

³Widrow's book begins with the different applications of adaptive filtering techniques, and walks the reader through the definition of the quadratic performance index, why it was chosen and describes why the Wiener-Hopf algorithm (a closed-form analytical solution) is not always a pragmatic solution to the adaptation process. The lack of information about the incoming signal forces a *suboptimal* solution: the widely-used LMS algorithm. All theoretical aspect of the properties of the class of signals for which the LMS algorithm is applicable are discussed.

ing, and error signal *on demand*, without regard for any possible distortion due to the inability of the *source* to generate the adapted signal.

Although Burgess [90] is attributed as being the first one to apply the concept of adaptive filtering to the process of noise control, it was Sondhi [91] who discussed the possibility of using adaptive filtering to cancel unwanted echos in a telephone line. Sondhi realized that the approach previous taken by Flanagan in an internal Bell Labs memorandum was a working solution, but not robust to line or signal fluctuations. Flanagan's approach was to model the unwanted echo E_1 from an incoming signal S_1 as a digital filter, obtain the filter's impulse response, and feed the filter a copy of the signal S_1 so that echo E_1 could be reproduced and subsequently subtracted from the incoming signal $S_1 + E_1$. Sondhi proposed a transverse digital filter which would automatically adjust the impulse response of the echo signal E_1 to take into account the dynamics of the telephone line communication system. Two years later, Kido and Onada [92] published an adaptive, closed-loop narrow band filter, which cancels a pure tone in the presence of noise. Burgess [90] modifies Sondhi's approach to suppress unwanted noise in an air duct. Burgess deviates from the typical signal processing approach taken by most of the researchers, to adaptive *control* of a plant. Burgess takes into account that physical systems can not respond instantaneously to electrical or mechanical inputs. Burgess argues that if adaptive control is going to be successful, system modelling of the sensors and plants (microphones and speakers, respectively) should be incorporated in the feedback control loop. The sensor and plant

models are assumed to be second order IIR filters, with poles to match the impulse response of typical microphones and loud speakers. The stability criteria for the entire plant is defined, and adaptation time and convergence of the algorithm are discussed for narrow and broadband inputs. It is shown (via computer simulations) that the closed-loop system is capable of suppressing broadband signals in the presence of white noise with various degrees of success depending on the training signal selected, the size of the filter, bandwidth and desired adaptation time.

Prior to Burgess' work, there were significant contributions being made in the area of adaptive signal processing, which appear to have promise in the area of noise cancellation. Morgan [93] describes the software and hardware necessary to implement an adaptive linear predictor which, instead of computing a linear system of equations composed of statistical information of delayed values of the incoming signal to estimate the present signal, uses the Least Mean Square (LMS) recursive algorithm to obtain and adapt filter coefficients. This type of adaptive filtering scheme is also used to cancel a sinusoid in the presence of white noise. It is shown that the larger the filter (i.e. the more coefficients - or *loops*) the better the notch around the desired frequency and the residual noise is mostly *white*. Unfortunately, the filter also suppresses other frequencies due to the constant sampling scheme. Treichler [94] discusses the convergence and transient behavior of the Adaptive Line Enhancer - ALE (a generalization of the Adaptive Linear Predictor). Treichler follows an eigenvalue-eigenvector approach to study the convergence

and transient response of the algorithm. Cases for high and low Signal to Noise Ratio (SNR) are presented. Both convergence and transient behavior are heavily influenced by the ability of the filter to de-correlate the training signal from the input (which is usually done by adding a tapped delay between the lines). Simulations show that using the LMS algorithm to approximate the optimal Wiener-Hopf solution takes anywhere from 300 to 4500 iterations for convergence (assuming the training signal is properly decoupled from the input signal). The algorithm shows exceptional ability to remove a sinusoid (or multiple sinusoids) in white noise. The clear advantage of the ALE is that little, if anything, needs to be known about the incoming signal. The ALE algorithm can also be used to predict the frequency content of dynamic narrow band signals⁴. Griffiths [95] uses an adaptive filter to identify the spectrum of time varying signals. Griffiths's work provides bounds for the adaptive coefficient μ , and bounds for the filter's convergent constant τ , as well as optimal filter length L as a function of Signal to Noise Ratio (SNR). All of the estimates however, are based on the eigenvalues of the correlation matrix, information which may not be known *a priori*, but can nevertheless be used to evaluate filter performance. The proposed filter (both algorithm and hardware) is capable of identifying the frequency content of a signal composed of several frequencies.

Morgan [96] assumes the ALE proposed by Treichler [94] has reached steady state (i.e. all of the coefficients have adapted) and uses a predictive

⁴Dynamic narrow band signals are defined as signals whose narrow band spectrum is constantly in flux

algorithm to design a steady state *notch* filter. Closed-form solutions for the steady state filter (sinusoidal) constants are provided. All of the analysis is done in the steady state domain. The size of the filter and the frequency range for which good SNR is obtained are presented, along with the effect of the filter coefficients on the outgoing noise. It is shown that adaptive filtering techniques increase the output noise power of the signal, but that it is bounded and predictable in the steady state. Morgan's filter again uses a tapped delay to un-correlate the training signal from the incoming corrupted data. Morgan follows up his own work with a second publication [97], in which he addresses the increased power noise spectrum as a function of filter constant μ . Morgan's second work assumes steady state behavior and assumes low variance in the adaptation coefficient matrix. Long follows up on Morgan's work in [98]. The stability characteristics of the tapped delayed coefficients are examined. Bounds for the type of signals which the delayed algorithm can handle are provided.

The stability, convergence and performance of adaptive filtering techniques have been extensively studied, and their mathematical properties are well known. Their use for signal attenuation (i.e notch filter design) in the late 1970's had been limited to the signal processing world with out regard for physical characteristics of the *control* plant. The adaptive properties of the filter were assumed to be constrained only by the statistical properties of the incoming signal, the *hardware*, and the error signal. The *hardware* in the case of acoustic noise cancellation is a sound producing instrument, which

has its own intrinsic characteristics, which do not allow it to exactly duplicate the desired signal with out delays or distortion. Adaptive filtering techniques operate on the incoming signal, with a feedback control loop which instructs the next operation to be performed, not the next sound wave amplitude to be generated. Directionality of the *cancelling* signal is also not considered. Error signals must also pass through a transducer, which also has its own impulse response. Thus up until the 1980's there is a *void* in the control of offending sound: directionality and system modelling needed to be incorporated into the closed-loop system. C. F. Ross [99] begins to use adaptive algorithms to predict the behavior of the control plant for steady state signals. He develops a feedback system which attenuates plane waves in an air conditioned duct. The transfer function of the control plant is obtained using a least-squares system identification scheme. Once the impulse response of the plant are well known, the cancelling properties of the entire system can be estimated. Directionality however, is not considered. The attenuation levels are frequency dependent ranging from $-30dB$ at 65Hz to $0dB$ for frequencies in the 400–425Hz range.

In a series of papers Darlington [100], [101] began including the dynamics of the entire control plant, while using adaptive filtering techniques to continuously update the filter coefficients. Both of Darlington's papers focus on steady state adaptation. Once the plant dynamics (controller, plant and transducers) are incorporated into the transfer function, the stability of the algorithm is no longer dictated only by the statistical properties of the signal but also by the plant dynamics. The plant dynamics thus influence

the behavior of the LMS adaptive algorithm. Frequency bounds for a control loop designed to cancel a monotone steady state system are provided. Darlington follows up his work [101] by incorporating the effects of a delayed coefficient adaptation, the control plant and a transfer function designed to cancel the dynamics of the control plant. The control plant is modelled as a simple delay and the stability of the transfer function is discussed. It is shown that larger delays adversely affect system stability dramatically around the intended notch frequency, but that good cancellation still occurs. The sound cancellation community is slowly moving towards the direction of total plant modelling. However, directionality of the cancelling signal is still not being addressed.

Beringer and Roure [102] begin a new effort in the noise control community by modelling secondary sources (speakers) in a rectangular waveguide (i.e. physical modelling rather than using adaptive methods to obtain a transfer function numerically). They recognize that while the mechanical impedance of the loud speaker is much greater than its acoustic counterpart, it is the latter that becomes the dominant factor in noise cancellation. Their work shows that the presence of multiple secondary sources couple the acoustic impedance of the individuals, and that once a primary source is added into the system, it also changes the acoustic impedance of any embedded secondary sources. Limiting their work to plane waves, they propose an open-loop directional system composed of two loudspeakers for a specific incoming wavelength.

Further modelling work is done by Munjal and Eriksson [103], who use

a lumped element model to describe the propagation of the wave generated by the primary source onto a system composed of an input and error microphone with a secondary source. Munjal and Eriksson’s main objective is to define the correct input to the secondary source. Their approach is to find an analytical form of the transfer function of the entire acoustic system H_o , which can be inverted to define the input to the secondary source for cancellation. Relating the input pressure and velocity fields via transfer matrix methods, they are able to reduce the acoustical circuit to an electrical *Thevenin* equivalent. The transfer function H_o is derived to be a function of the source impedance, the characteristic impedance of the duct, and the distance between the input microphone and the secondary source. The error path and terminating impedance do not play a role in the transfer function. Munjal’s ANC system is omni-directional.

Snyder and Hansen [104] expand on Belingers’s and Munjal’s work by including source strength and volume velocity into the analysis of acoustic radiation in a rectangular wave guide. Once again, it is postulated that the primary and secondary source impedance are coupled, and that noise cancellation is not entirely due to an injection of an *anti-phase* wave by the secondary source, but also due to absorption of sound at the designated *canceller*. Using Morse’s model [105] of the impedance of a single rectangular source in a rectangular waveguide, Snyder and Hansen obtain the acoustic power output for both the primary and the secondary sound sources, accounting for the coupling between them ⁵. Unlike most of the previous work to date, Snyder’s primary

⁵The coupling is modelled using an acoustic circuit with series impedances as seen from

source is mounted at the end of the duct, with the radiating field along the axis of the duct wall as opposed to embedded along the side wall. The analytical model is verified experimentally. It clearly shows that the presence of one active source can influence the radiating impedance of sources around it. The analysis is done for a monopole system and subsequently extended for the general multipole ANC method.

The literature search showed that there has been a trend in the acoustic community towards system modelling and adaptive filtering for ANC. None of the papers addressed provided a clear solution to the problem of generating transient, directional waves in a uniform waveguide. The general idea developed in this dissertation, however, was generated using bits and pieces of the majority of the preceding work. Swimbanks’s ring source used multiple transducers to expand the frequency range of a directional wave. Adaptive feedback systems, although not ruled out, may not learn fast enough to adapt to short transient. However, it is clear that some sort of open-loop adaptive scheme is needed to send information to the cancelling transducers prior to the arrival of the acoustic wave. Plant modelling of the sensors and plant (drill string) have been incorporated into the algorithm developed herein. The process developed to address the problem at hand uses most of the fundamental ideas behind all of the previous work. The general behavior of the “plant” in question, the drill string, was described in Chapter 3. The next section in this chapter discusses the frequency response of the transducers selected for this application.

the primary and secondary sources.

4.4 Section II-Transducer Characteristics

The design proposed in this dissertation uses a series of identical type II sources (transducers), which together form a directional array. Once the frequency response is defined for one, it can be used throughout the algorithm to define the inputs to the entire array.

The equations that model the behavior of one-dimensional plane waves in a cylindrical waveguide in the presence of changing acoustical impedance, viscous damping, internal sources, boundary interactions and changing geometry have been developed by Drumheller [11]. The model is restricted to plane waves; that is $ka \ll 1$ where k is the wave number and a is the largest diameter of the cylindrical waveguide. Roughly speaking, this translates into wavelengths three to five times larger than the largest diameter on the structure.

Drumheller [15] developed algorithms for both the velocity and displacement fields contained within an elastic waveguide of arbitrary geometrical complexity. The velocity algorithm is a closed-form solution which is obtained by solving the wave equation using the method of characteristics within each spatial element in the t-x space. The displacement field is obtained by applying finite difference approximation for the time derivative.

The numerical algorithms are presented without proof below. The algorithms incorporate the coupled, piezo-electrostatic equations with the one-dimensional wave equation. The reader is referred to [106] and [107] for a detail modelling of piezoelectric materials and Drumheller's seminal paper on

the finite difference algorithms for 1-D wave propagation in complex media. Equations 4.1 and 4.2 are the iterative equations of the velocity and displacements fields developed by Drumheller in [11]

$$v_n^{j+1} = -v_n^{j-1} + \frac{z_{n+\frac{1}{2}}}{z_n} v_{n+1}^j + \frac{z_{n-\frac{1}{2}}}{z_n} v_{n-1}^j + \frac{1}{2z_n} [\beta_{n+\frac{1}{2}}^{j+1} - \beta_{n-\frac{1}{2}}^{j-1} - \beta_{n-\frac{1}{2}}^{j+1} + \beta_{n-\frac{1}{2}}^{j-1}] \quad (4.1)$$

$$u_n^{j+1} = -u_n^{j-1} + \frac{z_{n+\frac{1}{2}}}{z_n} u_{n+1}^j + \frac{z_{n-\frac{1}{2}}}{z_n} u_{n-1}^j + \frac{\Delta t}{2z_n} [\beta_{n+\frac{1}{2}}^{j+\frac{1}{2}} + \beta_{n-\frac{1}{2}}^{j-\frac{1}{2}} - \beta_{n-\frac{1}{2}}^{j+\frac{1}{2}} + \beta_{n-\frac{1}{2}}^{j-\frac{1}{2}}] \quad (4.2)$$

Where v is the velocity field, u is the displacement field, z_n is the acoustical impedance of the element Δx given by $\rho c A$ which represents the product of the density, zeroth order wave velocity, and cross sectional area respectively. The spacial and temporal mesh are $x_{n+1} - x_n$ and dt respectively. The subscripts n and j are integers used to discretize the spatial and time coordinates respectively. The function β may be defined across the entire t - x diagram. It has units of force and in the case of the velocity field it is defined as:

$$\beta_{n+\frac{1}{2}}^{j+1} = \Theta A \phi_{n-\frac{1}{2}}^{j+1} \quad (4.3)$$

Θ is a piezo-electric constant of the transducer, A is the cross sectional area of the transducer, and ϕ is the input voltage, which is assumed to be known a priori across the appropriate structures.

Depending on the application, β can incorporate viscous damping, fading memory material, ferroelectric material mechanically coupled in parallel

$$dt = \left(\frac{X_i - X_{i-1}}{c_i} \right) = \left(\frac{X_j - X_{j-1}}{c_j} \right) \quad \forall (i, j) \subseteq X$$

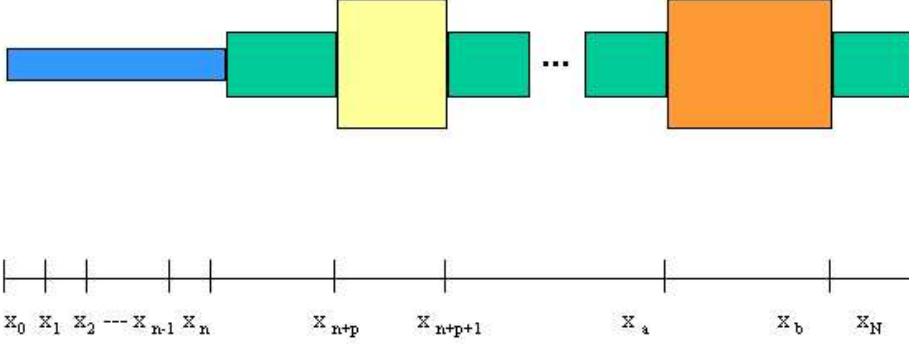


Figure 4.3: Special coordinate system

with an elastic material, and input voltages to the transducers. In the case presented here, β is proportional to the input voltage.

Solving for the velocity and displacement field require a special coordinate system. Figure 4.3 shows the special coordinate system used in the numerical algorithm. The coordinate system is obtained by applying the *von Neumann* stability analysis [108] and imposing the *Courant-Friedrichs-Levy* stability criterion $\frac{|c|\Delta t}{\Delta x} \leq 1$. Here, c , is the speed of sound in the waveguide, Δt is the critical time step⁶, and Δx is step size in the x-direction.

The coordinate system is chosen such that the time step between the mesh points is identical. The t - x diagrams below in Figures 4.4 and 4.5

⁶For a complete explanation of the effect of the critical time step on the stability of the numerical solution, the reader is referred to Chapter 7 of Gershenfeld's book [109] and its original developer Courant [110].

describe how the velocity and displacement field move across the solution space, as well as how the impedance function z and input function β are defined across the spatial and time domains.

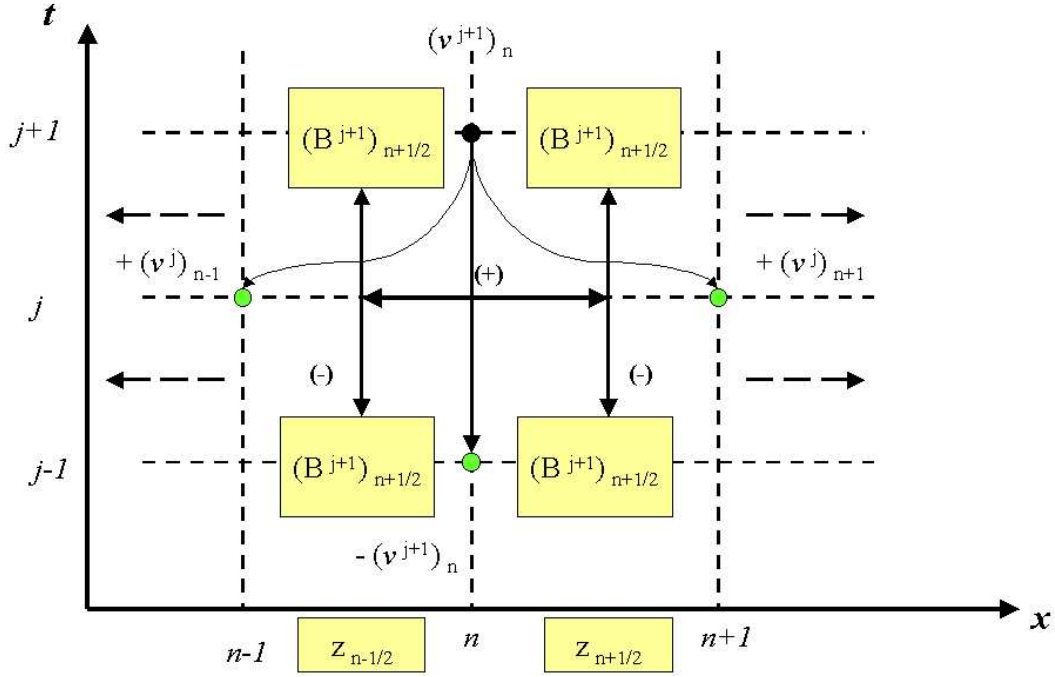


Figure 4.4: Velocity algorithm

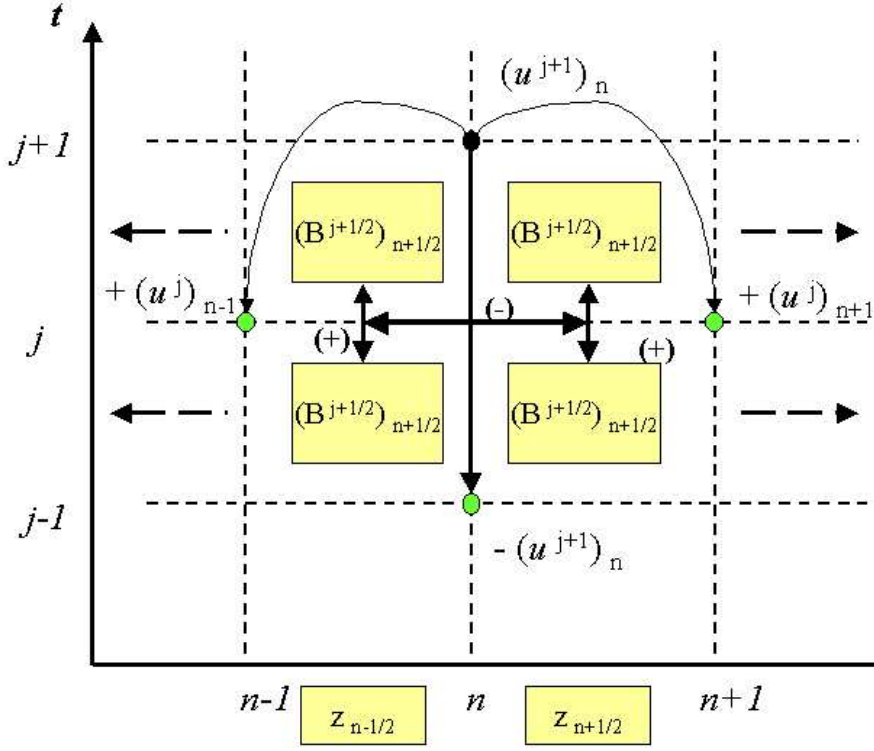


Figure 4.5: Displacement algorithm

It is important to note that Equations 4.1 and 4.2, which describe the velocity and displacement fields, imply that within the ferroelectric ceramic the ceramics behave as a elastic material. Only the electrodes attached to the ends of the piezoelectric material radiate sound. The walls of the PZT transducers behave as point source pistons generating sound in both directions within the waveguide. This is because the field equations demand $\vec{\nabla} \cdot \vec{\mathcal{D}} = 0$, where $\vec{\mathcal{D}}$ is the dielectric displacement vector.

The numerical algorithms presented above provide solutions in time and space for a wide range of materials. Of particular interest is the impulse

response of the PZT transducers used to design the directional array. To maximize the output energy of the sources, the impulse response should be obtained with the transducer acoustically matched to the uniform waveguide of interest.

The PZT transducers used throughout this chapter along with the mechanical properties, geometry and temporal and spatial grid of the waveguide used to obtain the impulse response of the transducer is given in Table 4.1.

<i>Variable</i>	<i>Brass</i>	<i>source</i>	<i>gauge</i>
ρ	$8470 \frac{kg}{m^3}$	$7500 \frac{kg}{m^3}$	$7500 \frac{kg}{m^3}$
s_{33}^ε	<i>na</i>	$20.7 \times 10^{-10} \frac{m^2}{N}$	$20.7 \times 10^{-10} \frac{m^2}{N}$
d_{33}	<i>na</i>	$593 \times 10^{-12} \frac{m}{V}$	$593 \times 10^{-12} \frac{m}{V}$
k_{33}	<i>na</i>	0.75	0.75
l	∞	5mm	5mm
$\Theta = -\frac{d_{33}}{s_{33}^\varepsilon} l$	<i>na</i>	-57.30	-57.30
$\alpha_{n+\frac{1}{2}}$	3576	2616	3041
$x_{n+1} - x_n$	4.6429 mm	5.0 mm	5.0mm
$A_{n+\frac{1}{2}}$	$8.6726 \times 10^{-5} mm^2$	$1.298 \times 10^{-4} mm^2$	$9.0949 \times 10^{-5} mm^2$
dt	1.9701 μs	1.9701 μs	1.9701 μs

Table 4.1: Waveguide dimensions for Impulse response

Here ρ is the density, s_{33}^ε , d_{33} and k_{33} are piezo-electric constants, l is the transducer thickness, Θ is a dimensionless constant of proportionality, and $\alpha_{n+\frac{1}{2}}$ is the speed of sound. The spacial and temporal meshes are $x_{n+1} - x_n$ and dt , respectively. $A_{n+\frac{1}{2}}$ is the cross-sectional area of each element.

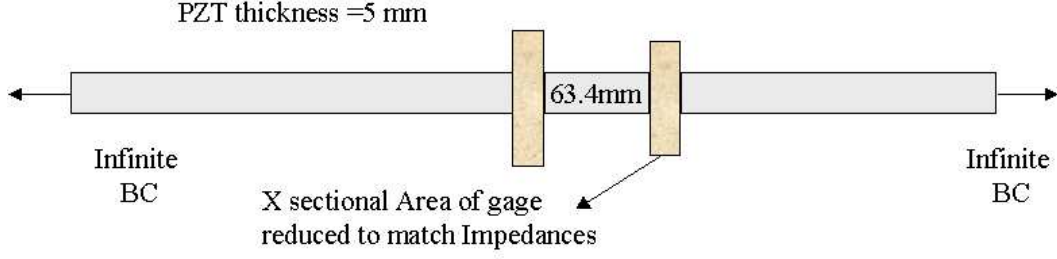


Figure 4.6: Waveguide dimensions used to derive the impulse response function

A schematic of the waveguide used to model the impulse response is shown in Figure 4.6. Infinite boundary conditions are forced on both sides of the structure. The impulse response is obtained by injecting a voltage of amplitude $\frac{1}{dt} \text{ volts}$ to the transducer and sensing the voltage induced across the gauge. The voltage across the gauge is proportional to the strain between the two electrodes. Specifically $\phi = \mathcal{V}[u(x_b) - u(x_a)]$. \mathcal{V} is the proportionality constant, ϕ is the voltage sensed across the gauge, and $u(x_b) - u(x_a)$ is the strain across the . However, the algorithm used to synthesize transient acoustic signals, demands the velocity field impulse response, not the strain impulse response.

The velocity impulse response shown in Figure 4.7. The effect of not matching the impedance to the right and left of the transducer is evident. The performance of the transducer is decreased due to the reflections seen at each mismatched interface. Note that all frequencies have a unique gain, but this is not the general case, as the frequency response varies depending on transducer stacking configuration. Figure 4.7 shows that in the neighborhood

of the origin, the gains are linearly proportional to the frequency. It can be shown that the relationship between the voltage and velocity field is given by:

$$v = \left(\frac{i}{2}\right)\omega l d_{33} x i \quad (4.4)$$

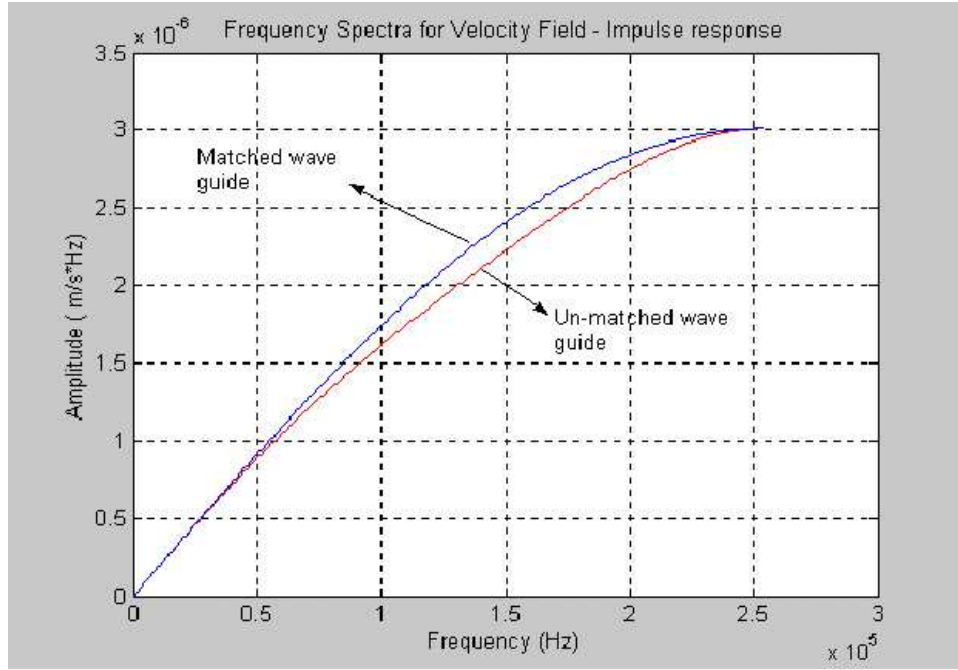


Figure 4.7: Impulse response velocity field infinite boundary conditions

where ω is the angular frequency, l is the thickness of the transducer, d_{33} is a piezo electric constant, and $\vec{\xi}$ is the electric field across the transducer. The expression $\frac{i}{2}\omega$ in the frequency domain is equivalent to time differentiation $\frac{d}{dt}$ in the time domain.

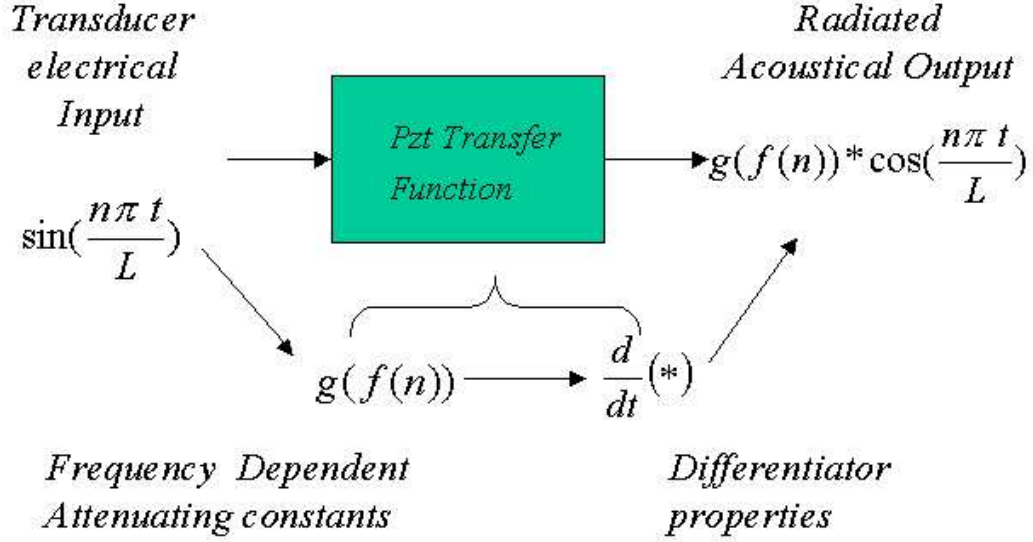


Figure 4.8: Attenuating-differentiating properties of PZT transducers

A graphical description of the (large wavelength) behavior of the ferroelectric ceramic is shown in Figure 4.8.

As mentioned before, the transducer can be modelled by using lumped elements [111], [112], [113], [114]. This type of modelling (although not appropriate for the type of synthesis being considered in this work) does provide some insight on general properties of ferroelectric ceramics; the most appealing property of a lumped element model is its simplicity. The user can quickly determine the frequency response using circuit analysis tools.

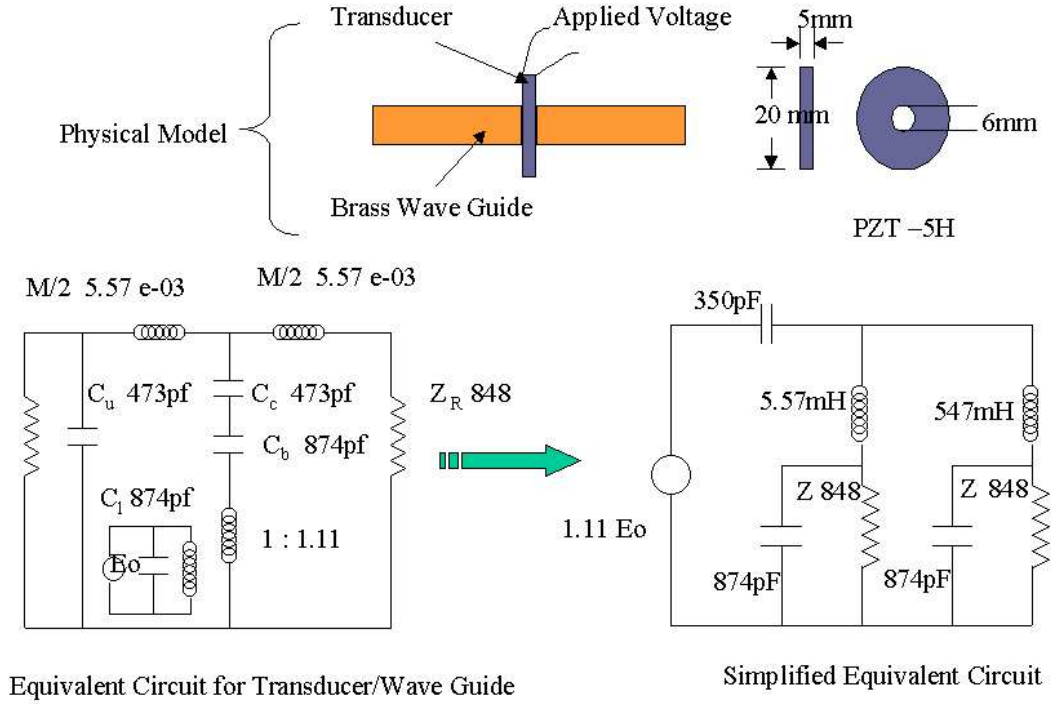


Figure 4.9: Lumped element model of a PZT transducer

A simple model for a PZT transducer sandwiched in between two acoustically matched, isotropic waveguides is shown in Figure 4.9. The symmetry of the model with respect to the transducer can be exploited to simplify the circuit. Hixson [115] modelled and experimentally verified the behavior of a single transducer embedded in an acoustically matched waveguide using a lumped element electrical analog circuit. The transfer function (both magnitude and phase) are consistent with the finite difference model proposed by Drumheller [11]. In the neighborhood of the origin, the transducer behaves like an attenuating differentiator.

4.5 Section III - Transient Wave Generation

This section expands the model developed in section III to incorporate directionality. The shortcomings of the standard $\frac{\lambda}{4}$ spacing, $\frac{\pi}{2}$ phase delay transducer pair, when used as broadband transmitter, are exposed. It is shown that even for a “perfectly tuned” transducer pair, there is a *non-convergent* region and a *leakage* region that expands beyond the intended time domain of the signal.

The use of the standard quarter wavelength configuration is less than optimal in transient applications when used as a stand alone tool, but can effectively be used in concert with other design parameters such as space between transducers, timing delays, and overlapping frequency spectra to approximate transient signals. Thus, an “array of arrays” is used to synthesize the desired information. The transducer array is optimized within the constraint space available to minimize the induced error due to overlapping frequency band widths. Design limitations, such as the balance between signal length and design space, as well as the type of signal which is not well suited for the design, will be discussed.

The algorithm for generating broadband, directional waves in a uniform pipe will be described in a detailed fashion. As it currently stands, the algorithm developed is very robust. It is capable of handling different transducer types, geometries, drill pipe geometry and length, as well as the dispersive properties of the drill string in its first four pass bands. The algorithm should be looked upon as a design tool, which can be used to define the transducer

placement, delay, firing sequence, and inputs to cancel a user defined input.

Once the behavior of a single PZT transducer is well understood, the focus shifts to the design of the electrical inputs to generate an arbitrary acoustical signal in a uniform waveguide. In devising the inputs to the transducer, it is clear that the frequency content of the desired acoustical signal must be known *a priori*, to account for the impulse response of the ferroelectric transducer - on a frequency by frequency basis. Thus some sort of decomposition must be considered.

The mathematical representation of transient signals is usually accomplished by integral transform methods [116]. The most popular is the Fourier Transform, which provides a closed form analytical mapping of the real function in the time domain via integration of a continuous kernel over an infinite frequency range. The approach used here is to synthesize the desired acoustical wave by a Half Range Fourier Series expansion - not the Fourier Integral. An even, periodic signal $f(t)$ of period $2L$, denoted by $f(t)_{2L}$, can be represented by an infinite series:

$$f(t)_{2L} = a_o + \sum_{n=1}^{\infty} a_n \cos\left(\frac{n\pi t}{L}\right) \quad (4.5)$$

Fourier series expansions are usually reserved for periodic functions, however when used as inputs to the type of PZT transducers discussed herein, they can be used to generate broadband acoustic signals. This can be achieved by pulsing the transducer over the length of the desired signal with a (albeit modified) Half Range Fourier Series. Thus, while the input provided to the

transducer represents a periodic signal over time, it never has a chance to repeat, as it's source is shut down. The domain of interest can be restricted to $0 \leq t \leq L$ with a pair of Heaviside functions:

$$f(t) = f(t)_{2L}(H(t) - H(t - L)) \quad (4.6)$$

The electrical input is converted to an acoustical signal which propagates off to the left and right of the transducer. Mathematically, this is equivalent to demanding the convergence of the series over the entire real line, but limiting the analysis to only half a period. The convergence is not a function of the domain of interest⁷.

Using a half range expansion suits the transducer behavior quite nicely, as the superposition principle can be used to synthesize acoustic waves by properly selecting the electrical inputs. The reason for choosing a half range expansion is to ease the computational efforts; however, for the application presented here, there is an ulterior motive: the algorithms used to model the velocity field, show that discontinuous electrical inputs such as $\cos(t)$ introduce a discontinuity at the beginning and end of the acoustical signal⁸. The numerical discontinuities can be easily tracked back to the spatial distribution of the input function β , which may be a discontinuous function. Input functions which smoothly ramp up the input value from zero, do not present an issue. A close examination of figures 4.4 and 4.5, and equations 4.2 and

⁷For a detail analysis of the Fourier Series and the implications of the half range expansion, uniform convergence, etc. the reader is referred to [117].

⁸Personal communication with Dr. Drumheller relay back that these spikes are not simply a numerical perturbation. Transducers of the type presented here have issues with discontinuous electrical inputs

4.1 reveal that a discontinuous input (such as a cosine wave) will give rise to a numerical discontinuity at the beginning and end of the acoustical signal generated within the waveguide.

In order to avoid numerical discontinuities and minimize computation time, the acoustical signal will be synthesized using **electrical** inputs composed of a modified **sine** Fourier Series Expansion.

In order to synthesize an acoustical signal within the waveguide, each of the (harmonic) inputs to the transducer must be modified to compensate for the dynamics of the PZT transducer. The algorithm used to synthesize a bi-directional acoustical waveform in an elastic, isotropic waveguide is shown in Figure B.5. Because the PZT transducers differentiate electrical inputs, the acoustical signal is in reality being synthesized using a **cosine** series.

The algorithm describe above is not without its limitations:

- It is computationally expensive. A large number of computations must be made to obtain the Fourier coefficients.
- It is frequency restricted. Acoustical signals with strong DC components can not be properly synthesized.
- The number of harmonics that can be used to approximate the signal is restricted by the linear domain of the impulse response. That is, for a given transducer thickness l , the restriction $\frac{c}{l} \gg n_{max}f_0$ inherently limits the frequency content of the signal to be synthesized. Where c is the speed of sound of the waveguide, l is the transducer thickness, f_0 is the fundamental frequency defined as: $f_0 = \frac{1}{2L}$, where L is the length of

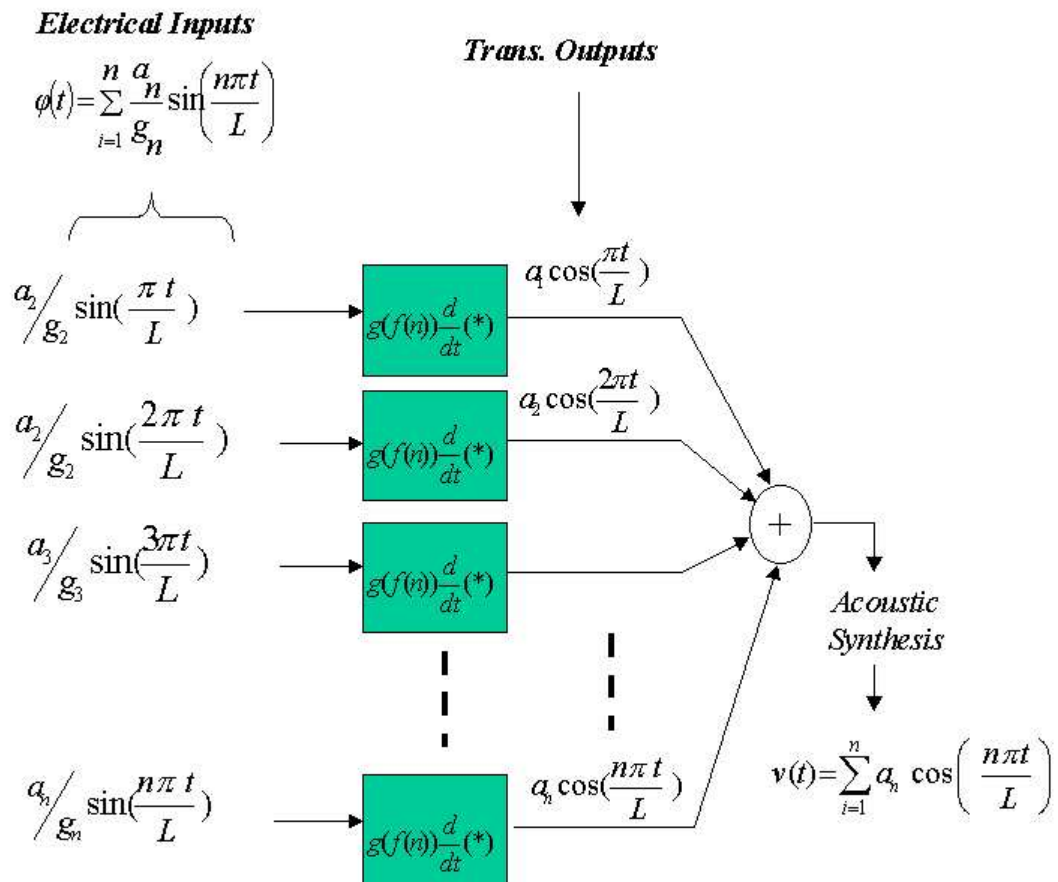


Figure 4.10: Electrical to PZT to synthesize transient acoustical signals

the transient signal, and n_{max} is an integer corresponding to the largest harmonic in the Fourier decomposition.

- The synthesis presented here is defined for a single transducer and is inherently bi-directional. A single PZT transducer will generate acoustic waves in both directions within a waveguide. If directionality is desired, an array of transducers, properly spaced, timed, and delayed relative to each other must be designed. The design of such an array will be discussed in Section 4.6.

Figure 4.11 shows electrical inputs to a single transducer. Figure 4.12 shows the bidirectional output of the waveguide using one transducer.

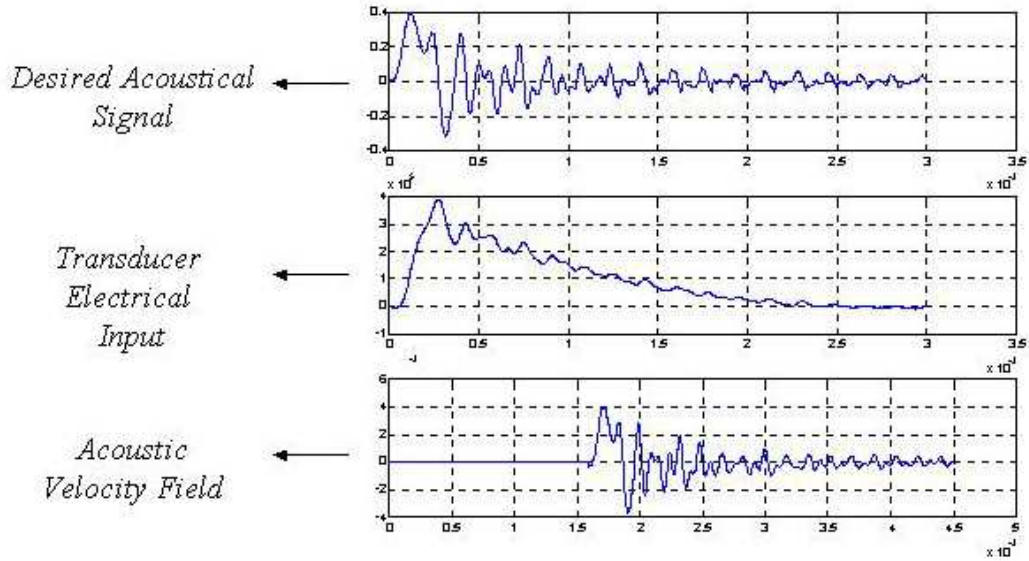


Figure 4.11: Electrical inputs to a single PZT transducer

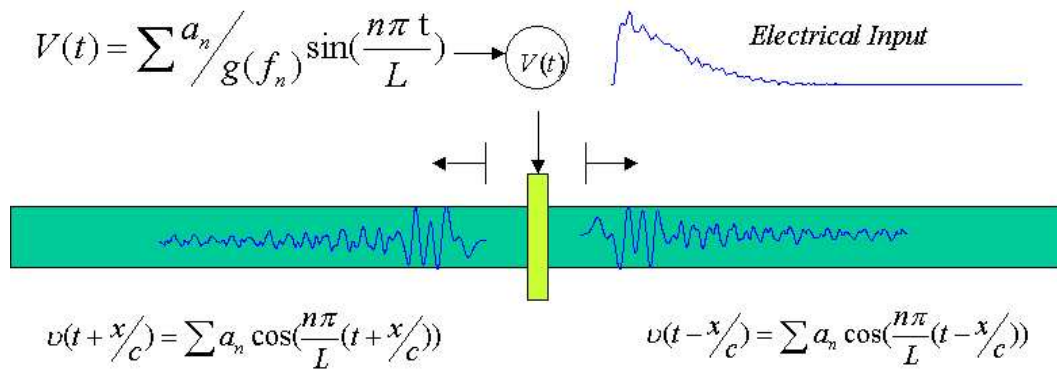


Figure 4.12: Non directional wave generation from a single transducer

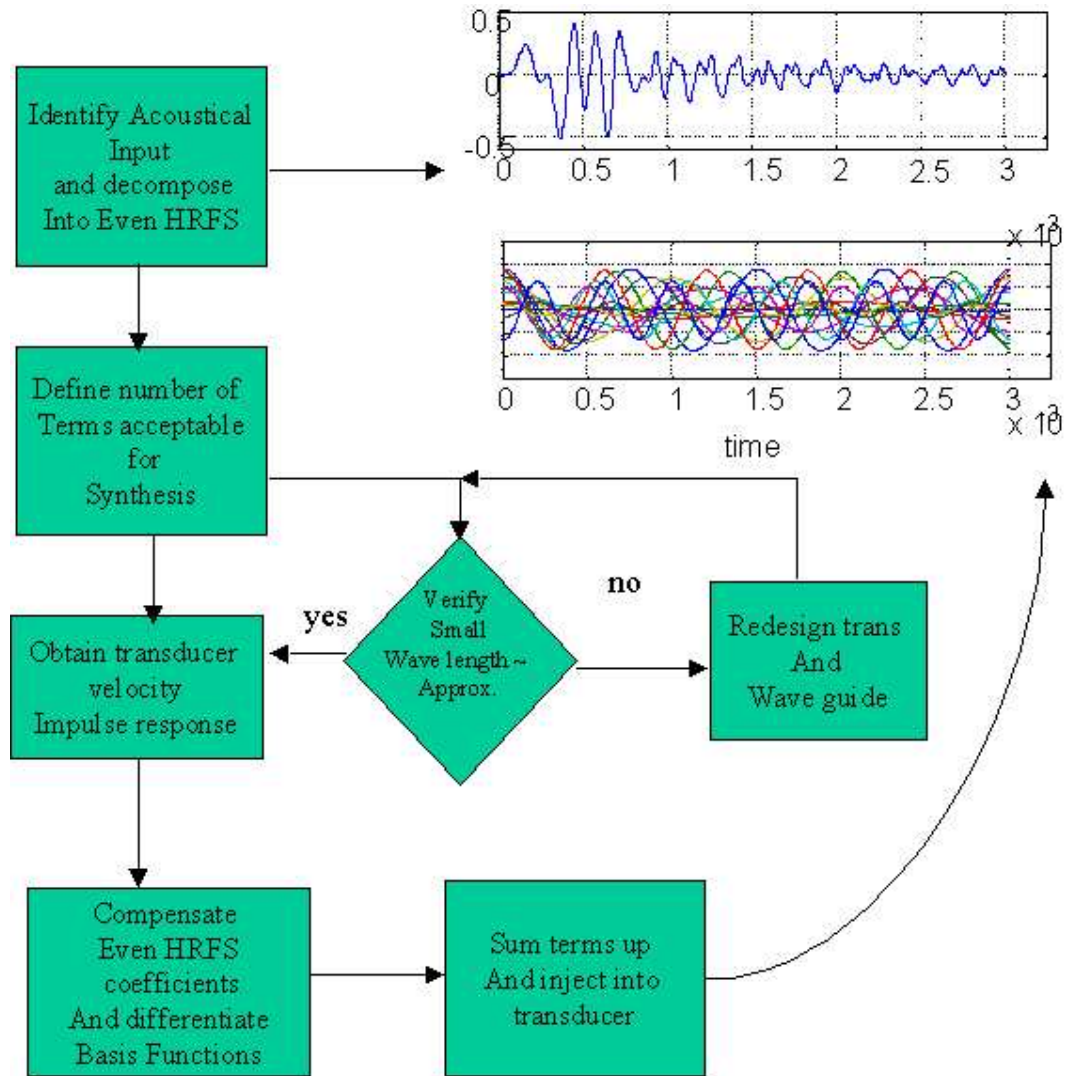


Figure 4.13: Algorithm flow and logistics

Figure 4.13 describe the logistics for generating omni-directional, transient acoustical signals in an isotropic solid with one transducer.

This section will come to closure by emphasizing a few subtle but important points:

1. To synthesize an acoustic wave using the output from a velocity sensor, the output signal from the sensor must be broken down into its Fourier Series Components. If the largest frequency falls within the domain in which the transducer can be modelled as a differentiating attenuator, the algorithm must operate on each kernel and its corresponding coefficient to compensate for the transducer transfer function.
2. Number 1 above implies that a directional sensor array must be placed upstream from the terminating impedance. Combined, they form an *open-loop*, feed forward design.
3. Adaptive closed-loop systems for transient signals have not been investigated. The techniques presented here may not be suitable for a closed-loop adaptive systems since the signal decomposition and the operations necessary to synthesize the transient signal may be too time consuming.
4. The transfer function shown in Equation 4.7 applies to steady state sinusoids, not sinusoidal wave trains. Thus our compensation constants compensate only for the dominant frequency of the sinusoidal kernel, not its entire frequency content.
5. The algorithm designed does not constitute a mathematically pure Half Range Fourier Series Expansion, but rather exploits the general behavior

of the PZT transducers in the small frequency domain. Within the specified range, a PZT transducer is capable of generating approximations to basis functions which can be summed to synthesize a transient wave.

6. For the transducer examined herein, the transient signal has (for all practical purposes) infinite precision. Up to 250 harmonic terms can be used to approximate the transient signal. This is precision holds for $\frac{l}{\lambda} \ll 1$, where l is the transducer thickness.
7. Once directionality is incorporated into the design, the bandwidth of the system may be reduced. This type of bandwidth loss will be discussed in Section 4.6.

4.6 Incorporating Directionality

A well known technique used to generate directional, steady state, monotone signals in an acoustic waveguide is to space two transducers a quarter wavelength apart. Each transducer is powered by equal magnitude, oppositely phased, voltages and ninety degrees out of phase⁹. To obtain a right travelling wave, the right-most transducer is “fired” at $t = 0$. This transducer generates waves in both directions. The left-most transducer, which is spaced $\frac{\lambda}{4}$ to the left, and phased in time by 90 degrees, is given an identical electrical input as the first transducer, except phase shifted by 180 degrees. The delay and phases

⁹Once the spacing between transducers, time delays and input voltages are set as described above, the transducer pair is said to be *tuned* to radiate a monotone steady state signal of wavelength equal to four times the spacing between the transducers: λ_{tuned}

are such that the backward travelling wave generated by the rightmost transducer is exactly cancelled at the left-most transducer interface. The technique is illustrated below in Figure 4.14.

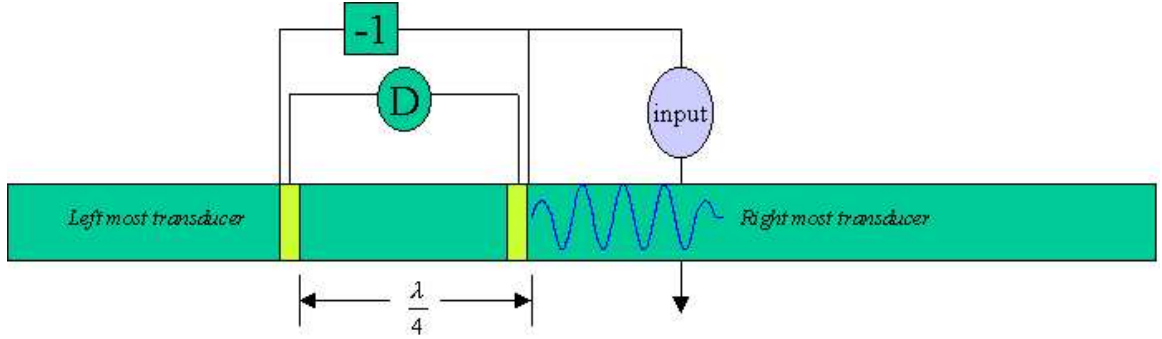


Figure 4.14: Directional narrow-band acoustic array

As mentioned earlier, a transient signal of length $2L$ can be represented by it's half range expansion over the interval $0 \leq t \leq 2L$:

$$f(t) = a_o + \sum_{i=1}^{\infty} a_n \cos\left(\frac{n\pi t}{L}\right) \quad (4.7)$$

Since a transducer pair can be tuned to generate monotone acoustic signals, it seems plausible that the electrical inputs (to several transducer pairs) could be designed to generate each of the acoustic kernels: $\cos(\frac{n\pi t}{L})$ in Equation 4.7. The transducer pairs will no longer be used to generate a steady state monochromatic signal, but rather a transient pulse train of length L , with a dominant frequency $f = \frac{c}{\lambda}$, where c is the speed of sound in the waveguide and λ defines the spacing between the transducers. The idea is to synthesize a directional acoustic signal at a pre-determined location by generating orthog-

onal functions through paired, tuned transducers. Mathematically, Equation 4.7 represents an even, periodic function about the origin of period $2L$. The transducer pairs however, generate acoustical signals of length L since they are only fired for half the of the period of the signal. This avoids rebroadcasting a mirror image of the desired wave.

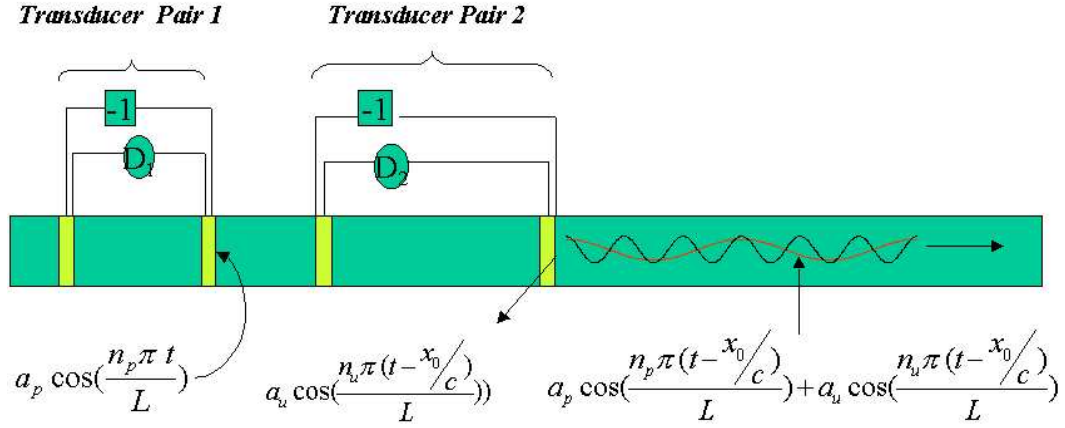


Figure 4.15: Two transducer pairs synthesizing a broadband signal

Complex transient directional signals are generated using several transducer pairs; each generating directional kernels, all timed to add constructively at a predetermined location in space (where cancellation is to occur). Figure 4.15 shows the general concept using two transducer pairs. Using this transducer configuration, a transient wave can be synthesized as follows:

Transducer pair 1 is fired generating a directional transient acoustical kernel, of a specific frequency. The wave is allowed to travel to the rightmost transducer of *transducer pair 2*, which is subsequently fired in such a fashion

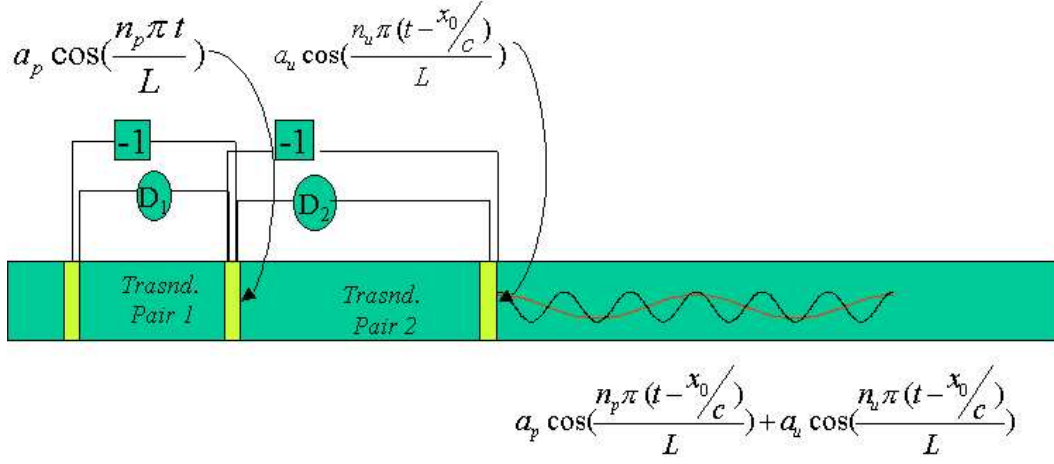


Figure 4.16: Next of kin-common array design

that the signals constructively add up to synthesize the desired acoustic wave.

Note that the transducer pairs are staggered from left to right, each pair spaced $\frac{\lambda_n}{4}$ apart, where λ_n is a harmonic wavelength. The design could be expanded to include as many transducers as allowed by the space limitations.

Figures 4.16 and 4.17, show alternative transducer configurations which minimize the design space, the length of the cylindrical waveguide needed to embed the entire transducer configuration to synthesize the desired transient signal.

Figure 4.16 is a “next of kin” design, in which the transducer of the previous pair is common to both transducer pairs. Figure 4.17 shares a “common” transducer, whose input is a delayed sum of voltages. Since the transient signal will be generated using harmonics the design space is fixed by half the period of the signal, i.e. the fundamental frequency. The largest

distance between transducers becomes: $d_{max} \approx \frac{c}{4f_o}$.

Using a common transducer, followed by harmonically spaced sources which make a transducer pair with the common transducer, allows the design space to shrink significantly from the staggered configuration.

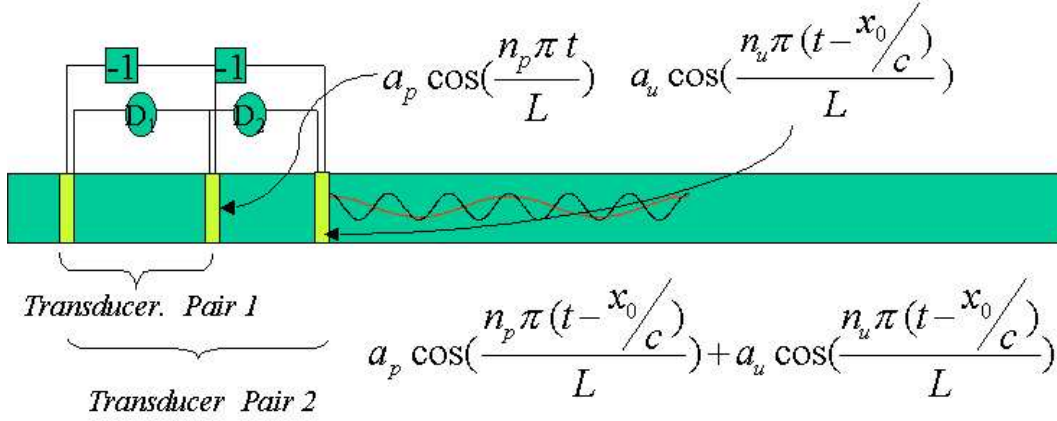


Figure 4.17: Harmonically spaced transducer pairs-one common transducer

The penalty for reducing the array length is signal integrity, as transducer pairs are forced to send signals for which they are not tuned. This is because the spacing between transducers is a geometric sequence. As the transducers are placed between the smallest quarter wavelength pair and the fundamental wavelength, it is physically impossible to fit all of the transducers necessary to incorporate the entire frequency spectrum in the design space available. Thus, there is a potential for gaps in the frequency content of the transmitted signal. Figure 4.18 shows a *harmonically spaced transducer array*.

Manufacturing constraints demand there be a minimum spacing δ_{wg} between transducers. It is easy to show that the spacing constraint between

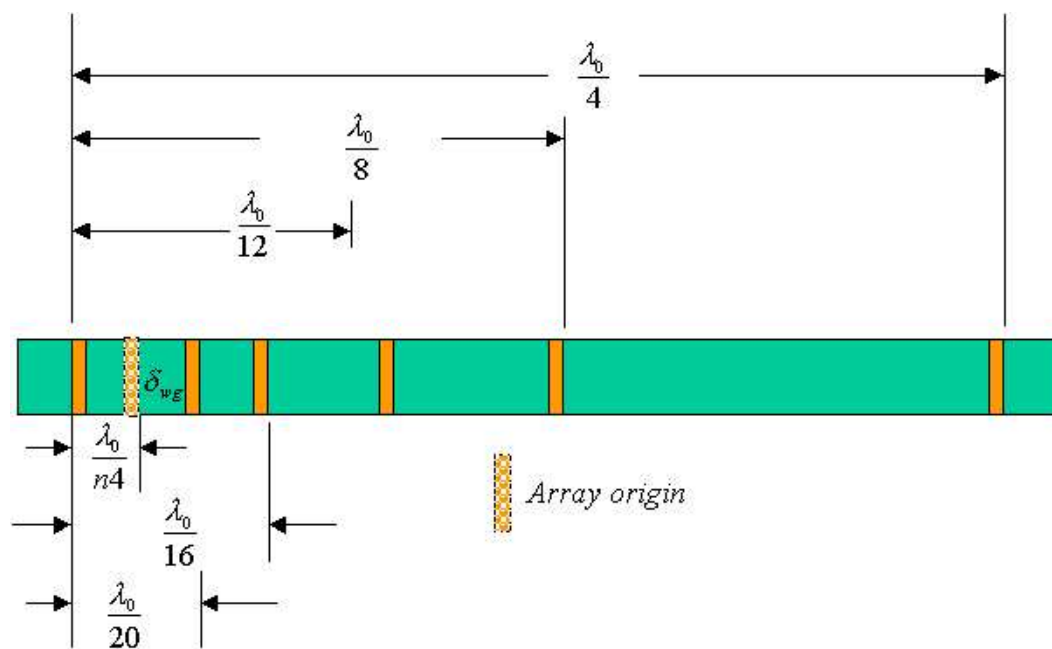


Figure 4.18: Common transducer design -geometric spacing

the $n - 1$ and n transducers is given by Equation 4.8:

$$\frac{1}{n-1} - \frac{1}{n} \geq \frac{4\delta f_0}{c} \quad (4.8)$$

where n represents the n^{th} harmonic wavelength, $\delta = \delta_{wg} + l$, where δ_{wg} is the length of the forbidden zone and l is the transducer thickness. The “origin” of the array is the right-most electrode of the largest harmonic frequency.

The space limitations induce a *forbidden zone* in which no transducer can be placed. Figure 4.19 shows the *forbidden zone* and the transducer configuration around it. If the frequency content of the signal is such that dominant wavelengths fall inside the *forbidden zone*, signal integrity will be compromised. Since the spacing limits the number of transducers we can place onto the waveguide, while the design requires the directional array to be capable of generating broadband signals, it is necessary to distribute the spectrum amongst the transducer pairs available.

Use of the common transducer configuration forces most pairs tuned for higher harmonics to generate “wave packets” of the form:

$$f(t - \frac{x - x_r}{c}) = \sum_{n=r}^p a_n \cos(\frac{n\pi}{L}(t - \frac{x - x_r}{c})) \quad (4.9)$$

Where x_r is the location of the master¹⁰ transducer sending the wave packet relative to the origin of the harmonically spaced array.

For example, if the signal frequency content is such that it is necessary

¹⁰All transducers except the common transducer are referred to as the *master*. The *common transducer* is referred to as the *slave*, since it has to mimic delayed inputs of all of the *master's* demands.

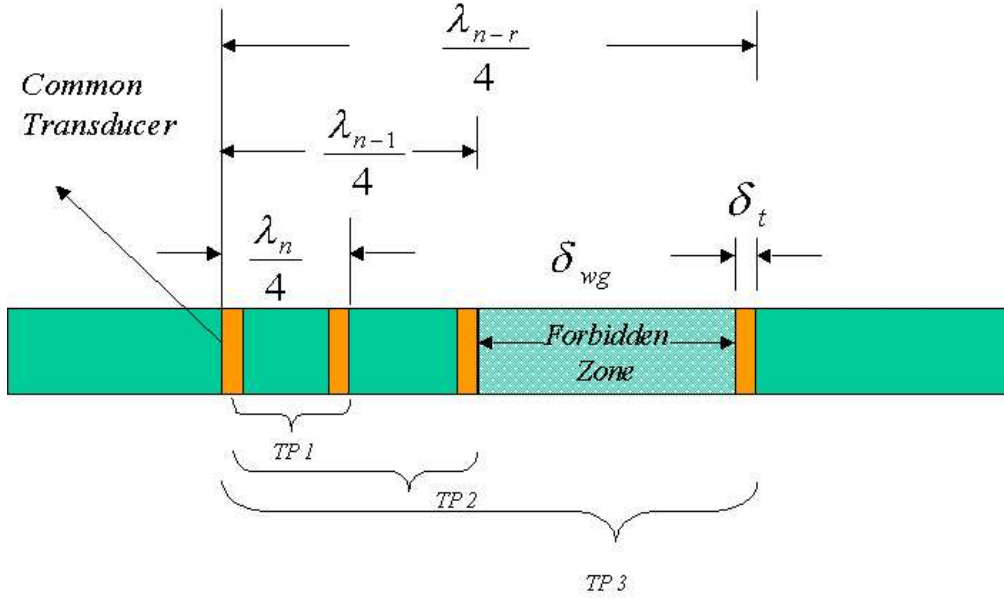


Figure 4.19: Forbidden zones may compromise signal integrity

to generate signals whose wavelengths lie within the *forbidden zone* shown in Figure 4.19, the two transducers pairs *TP2* and *TP3* would share the responsibility. The distribution of the load would be based on the transducer of closest proximity to the *forbidden wavelength*. The phase delay (which determines signal directionality) is always chosen such that the backward travelling waves generated from any master to the slave cancel.

Wave packets generated in this fashion are not optimal, as this type of phase delay will force the signal generated from the *slave* transducer to arrive early or late to it's respective *master*- causing destructive interference. There are inherent limitations in trying to generate ideal orthogonal functions using paired transducers (beyond the frequency limitations already imposed

by the transducer impulse response). Wave packets generated by any given transducer pair will be victims of induced *leakage* and *non-convergent* zones. A closer look at the behavior of tuned transducer pairs, when used for transient sinusoidal pulse generation, is illustrated in Figure 4.20.

Ideally, a perfectly tuned transducer pair as shown in Figure 4.20 would generate a sinusoid train of amplitude two, over the region labelled *Targeted Convergence Region*. The sinusoid train generated by the transducer pair would be a basis function in the Half Range Fourier Expansion. Clearly this is not the case. A perfectly tuned transducer pair generates sound outside of the *Targeted Convergence Region* and fails to converge for one half of the period of the signal. This type of configuration, one which is perfectly spaced and phased to generate a directional “pure tone” over a finite length of time, is only capable of generating a pure tone of a specific frequency over a reduced window. Two undesirable regions emerge: a “*Non-convergent*” region, where only half of the desired signal is obtained, as well as a transducer “*leakage*” region, where half a period of the acoustic wave “*escapes*”, and distorts the intended output.

The sizes of the non-convergent and leaky regions are frequency dependent. The error induced in the signal depends on the ratio $\frac{\lambda}{2cL}$, where L is the duration of the “Targeted Convergent Region” in the time domain and $\frac{\lambda}{2c}$ is the size of the leakage and non convergent zones in the time domain. Clearly, long duration high frequency signals will have minimal error and leakage, while short duration, low frequency signals will be heavily penal-

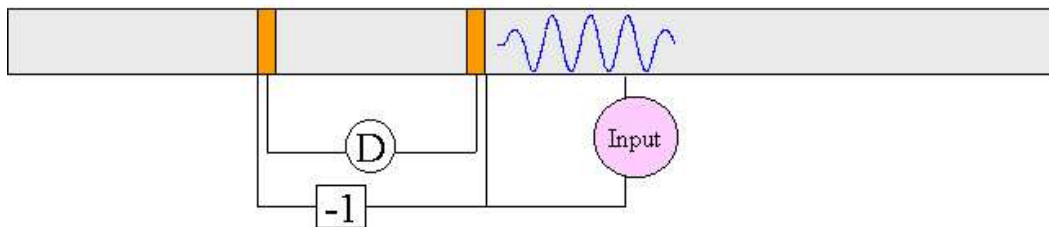
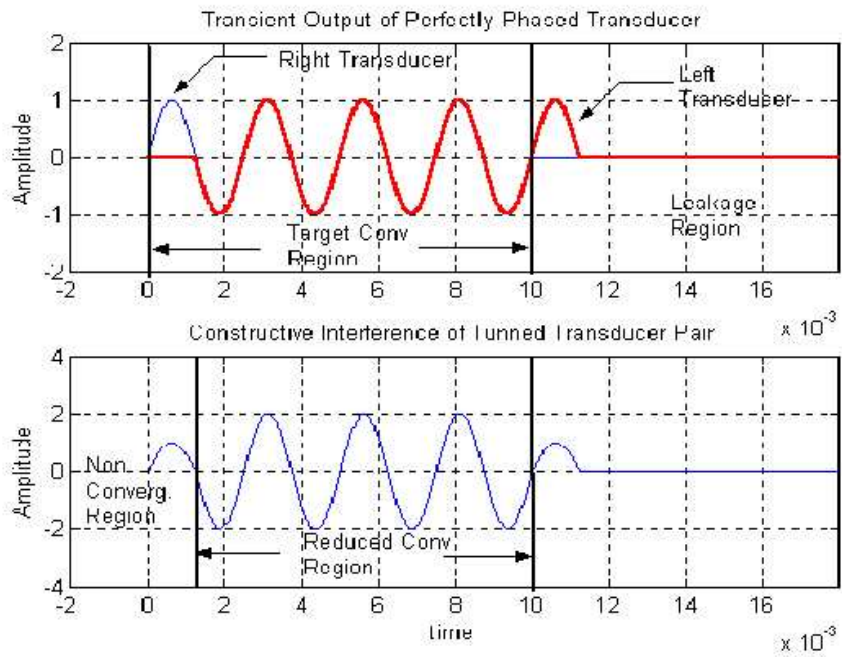


Figure 4.20: Perfectly tuned transducer pair

ized. The leakage and non-convergent zones are the penalties for maintaining directionality. They are inherent and can not be removed or minimized.

When a transducer pair is asked to generate directional signals other than what they are tuned for, in this case frequencies that fall within the forbidden zones the signal radiated in the wave guide will be penalized further. The induced error is defined by the minimum spacing allowed between transducers, the number of dominant frequencies within the desired wave packet and transducer type and geometry. Waves from the left-most transducer arrive either early or late, depending on the transducer spacing relative to desired wavelength. The error in all three zones (non-convergent, convergent and leakage) increases.

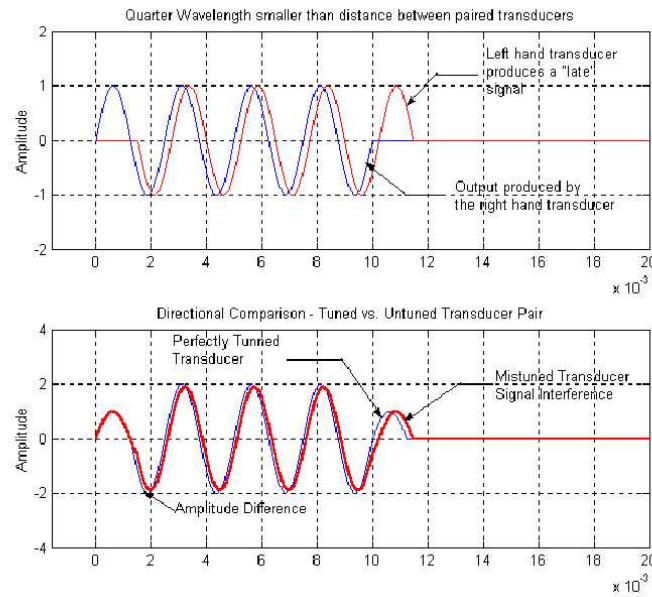


Figure 4.21: Mistuned transducer emitting signals in the forbidden zone

Figure 4.21 and 4.22 show the effect of transmitting signals outside

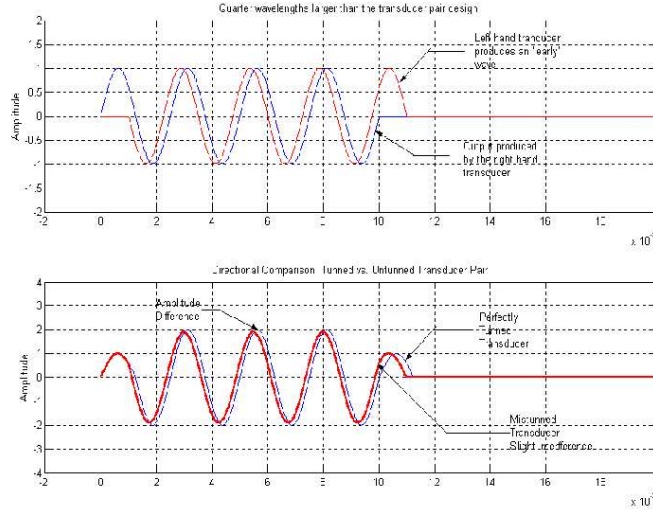


Figure 4.22: Transducer pair two generating signals in the forbidden Zone

the tuned parameter space. Figure 4.21 shows the effect of *transducer pair 1* transmitting signals whose wavelengths fall in the *forbidden zone*. The phase delay between *transducer pair 1* is such that no backward travelling waves are generated. The spacing between the transducers however is slightly smaller than the “forbidden” quarter wavelength. The signal generated by the common transducer is not in phase with the second half period of the wave generated by the right-most transducer. Destructive interference takes place. A similar phenomena occurs when *transducer pair 2* is asked to transmit signals in the *forbidden zone*. Since the desired wavelength is smaller than the transducer pair can optimally generate, the signal generated from the common transducer arrives early causing destructive interference.

Thus, the integrity of any *wave packet* generated by a given pair of

transducers is compromised, not only in the non-convergent zone, but most importantly in the *convergent zone*. Without modifying the voltages to the transducer pair, destructive interference is unavoidable when using a directional “common transducer” design. The input voltages to the transducers all need a “buffer” zone, which eliminates the poor initial convergence and induced leakage at the end of the signal. This will be discussed in greater detail in Chapter 5.

Destructive interference can be completely eliminated at the expense of directionality. The phase can be modified such that the forward travelling waves add up as if the transducer was perfectly tuned to that frequency. The penalty is a backward travelling wave. However, for the array design under investigation, there is no immediate need to sacrifice directionality for the sake of convergence. The common transducer design generates accurate, directional broadband signals. This is because the length of the forbidden zone is small compared to distance between the two transducers surrounding it. The directional array described in this section was simulated in MATLAB. The appendix contains a flow diagram of the entire algorithm as well as detail explanation of all of the submodules and functions which define the entire algorithm. Chapter 5 presents numerical simulations which quantify the performance of the directional array when used as a termination impedance.

Chapter 5

Directional Array Performance

5.1 Introduction

Two transducers, spaced one-quarter wavelength apart, can be used to cancel monotone, steady-state acoustic signals. These systems are designed to cancel incoming steady-state signals whose frequency content is known a priori. The cancelling array proposed in this dissertation makes use of multiple transducer pairs, each pair generating wave packets which synthesize the desired transient acoustic signal via a Fourier series decomposition at a specific location in space. The frequency content of the incoming signal is not assumed to be known a priori, but it is assumed that the energy of the signal is contained within a known time interval.

Use of multiple transducers (i.e.,harmonics) should, in theory, increase the bandwidth of the directional array. This chapter evaluates the performance of the directional array designed in Chapter 4.

5.2 Evaluation Tone and Performance Indices

5.2.1 Evaluation Tone

The performance of the directional array is assessed by quantifying the ability of the array to cancel broadband signals of various durations, frequency content and signal complexity. Various array configurations (i.e., number of harmonics used to generate the cancelling waveform) are tested to quantify the advantages of cancelling transient signals using multiple transducer pairs and a Fourier decomposition.

A tapered tone burst pulse is used as the test signal. This pulse is defined such that one may vary the rise time of the signal (in a smooth fashion) as well as the frequency content. The ability of the directional array to produce a directional signal of equal energy content as that of its input will be the basis of the evaluation. The pulse is defined by Equation 5.1.

$$\Psi(t) = \exp\left[\left(\frac{-2t}{T}\right)^{2m}\right] \sin \omega_0 t \quad (5.1)$$

The rise time is controlled by m . The duration of the pulse, T , is defined by $T = \frac{2\pi n}{\omega_0}$, where n is the number of cycles in the pulse

Figures 5.1 and 5.2 show two tone burst used for the evaluation, and their corresponding frequency spectra.

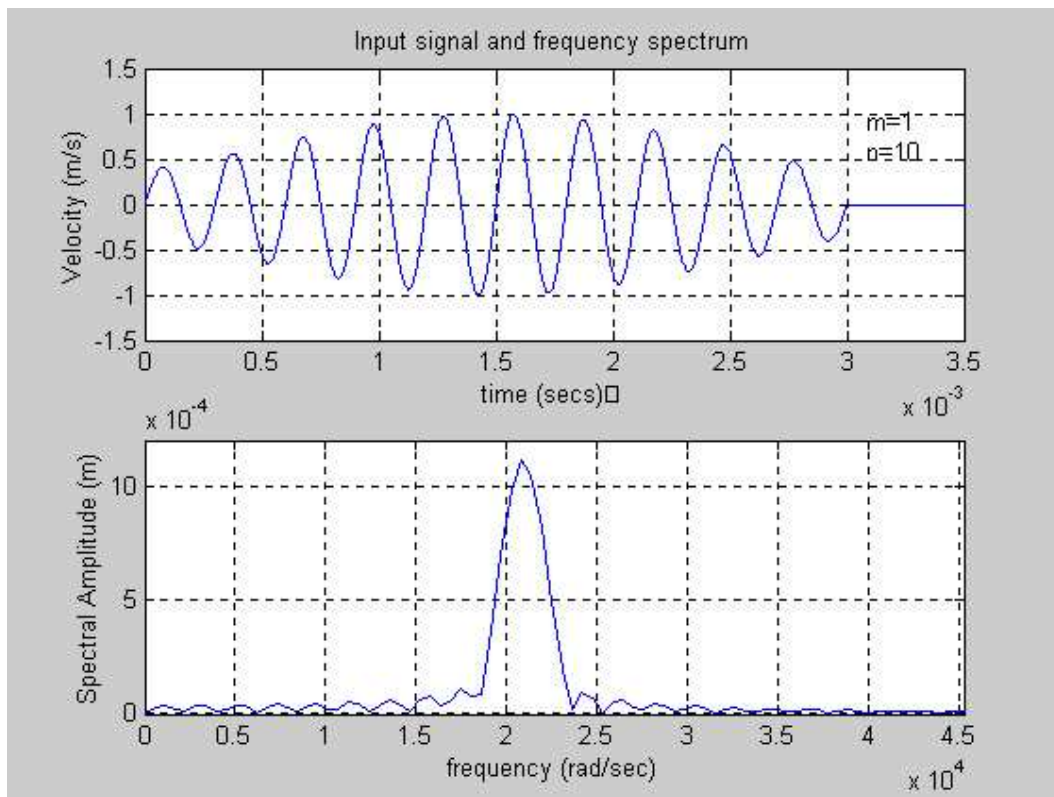


Figure 5.1: Pulse with $T = 3 \text{ ms}$, $m = 1$, $n = 1$

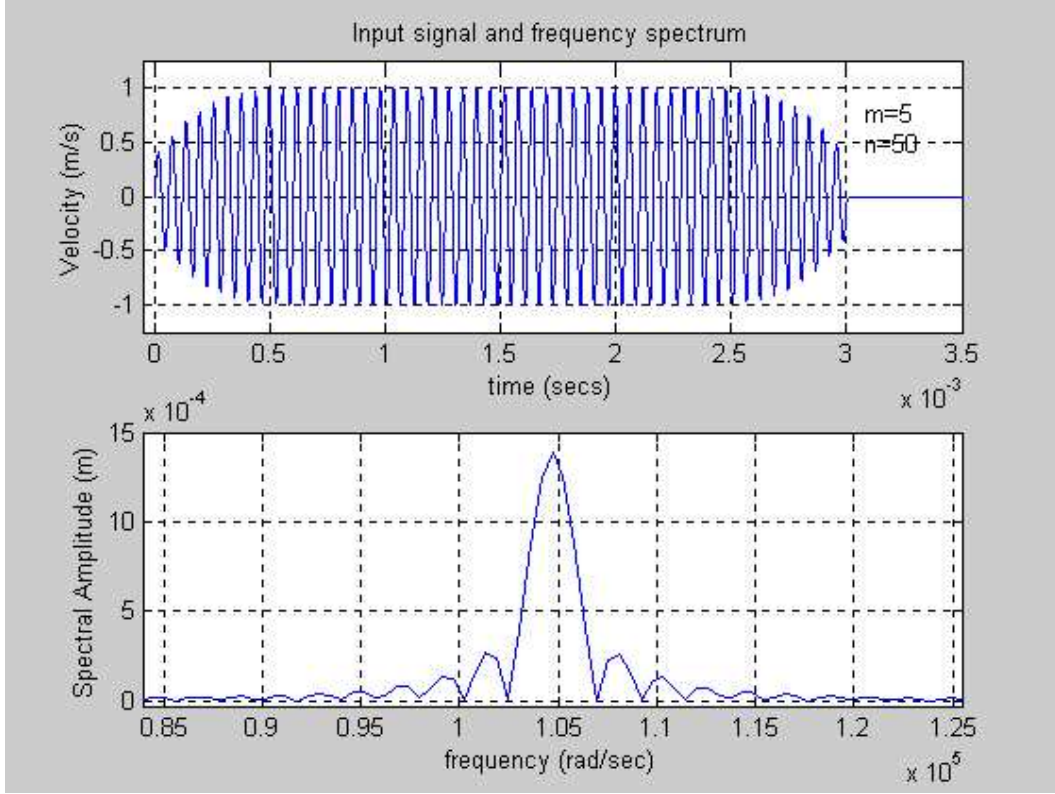


Figure 5.2: Pulse with $T = 3 \text{ ms}$, $m = 5$, $n = 50$

5.2.2 Performance Indices

The performance indices used to assess the performance of the array are:

- Signal suppression,
- Directionality.

Signal suppression will be quantified via a set of parametric curves. Directionality will be quantified via the energy content of a typical plot of the forward and backward traveling waves emerging from the directional array.

The parameters which will be varied to evaluate the performance indices of the directional array are:

- Length of the signal: T .
- The rise time of the envelope: m .
- The frequency of the signal contained within the tone: n .
- The array strength A_s .

Figure 5.3 illustrates the parameters used to evaluate the directional array.

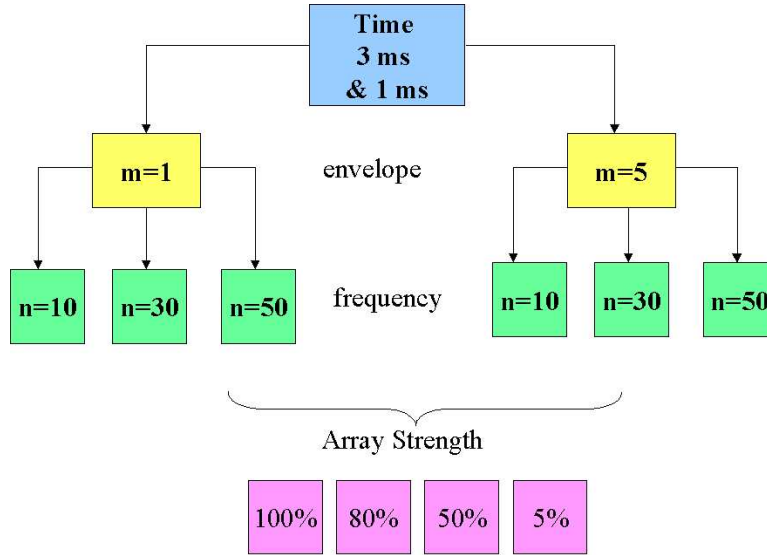


Figure 5.3: Evaluation signals for the directional array

Two time durations will be used in the evaluation: 3 ms and 1 ms, each of which will have two rise time parameters: $m = 1$ and $m = 5$. Within each envelope, three frequencies¹ will be considered $n = 10$, $n = 30$ and $n = 50$.

¹The parameter $n = 10, 30$ or 50 refers to the number of cycles in the pulse.

For each frequency, the array strength will be either 100, 80, 50 or 5 percent, for a total of 48 cases.

Array strength A_s is defined in terms of the number of dominant coefficients used to synthesize the signal, not transducer count. Array strength is a user defined parameter. The algorithm sweeps through the entire set of Fourier coefficients, finds the dominant coefficient² F_d ; and based on a user defined percentage r it discriminates against frequencies whose coefficients have an absolute value less than rF_d .

An array at 100 % strength is one in which all of the possible frequencies (and therefore all of the transducers available to the designer) are used to synthesize the transient signal. In contrast, an array at 50 % strength ignores any frequency which has a Fourier coefficient, whose magnitude is less than 50 % of F_d . The number of transducers fired therefore, is not directly proportional to the percentage used to exclude non-dominant frequencies. The relationship between array strength and number of transducers fired unique to each case. Different array strengths can use the same number of transducers (and at times the same number of harmonics) to synthesize the incoming signal. For example, if the incoming signal is such that the Fourier spectrum has one dominant coefficient of magnitude 1 and the rest of the coefficients have magnitude below 0.4 there will be no difference between an array strength of at 80 and 50 %. Both configurations will ignore frequencies with Fourier coefficients below 0.8 and 0.5, respectively, and the number of harmonics and

²The dominant coefficient F_d is defined as the Fourier coefficient with the largest absolute value.

transducers used to synthesize the wave will be identical.

This concept is illustrated by Figures 5.4 and 5.5.

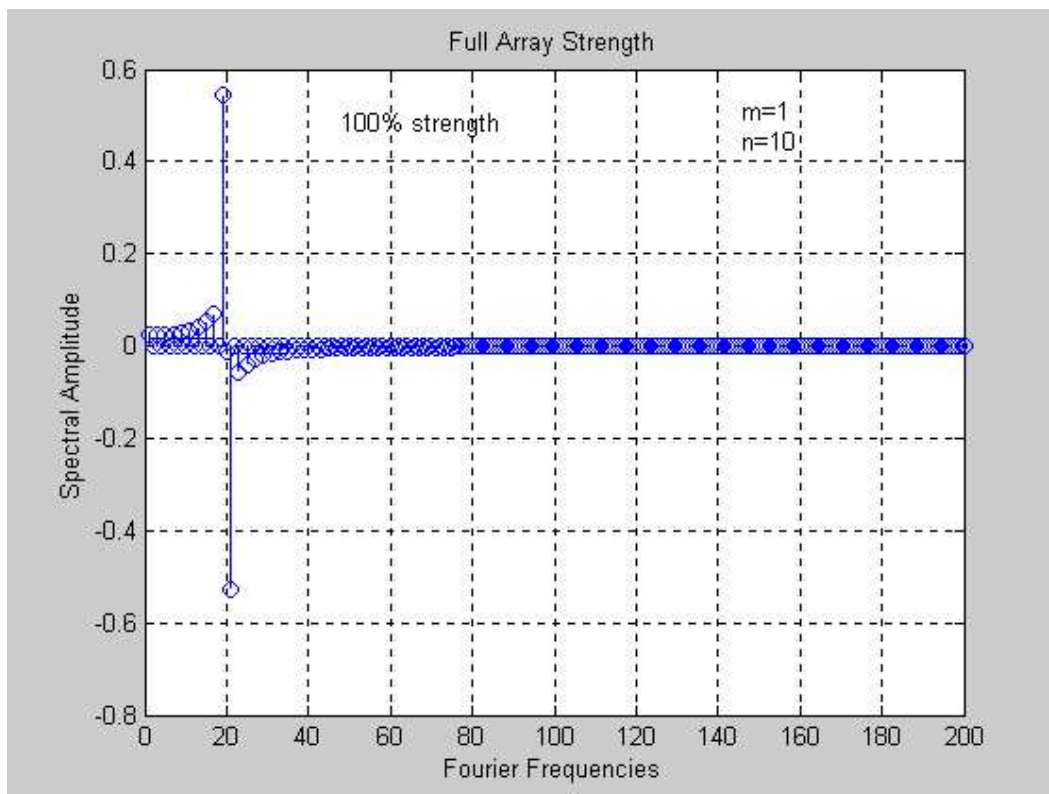


Figure 5.4: Full strength array: 200 harmonics, 48 transducers

Figure 5.4 shows the dominant coefficients of a pulse with $m = 1$ and $n = 10$. The pulse has only two dominant frequencies. The rest of the harmonics contribute very little relatively speaking. Figure 5.5 shows the dominant coefficients after the algorithm has removed coefficients with magnitudes below $0.8F_d$ and $0.5F_d$. Only two dominant coefficients remain. Note that two different array strengths use the same number of harmonics (and in this case

transducers) to synthesize the wave. The frequency content of the original signal is what ultimately defines the number of harmonics and transducers fired for each array strength.

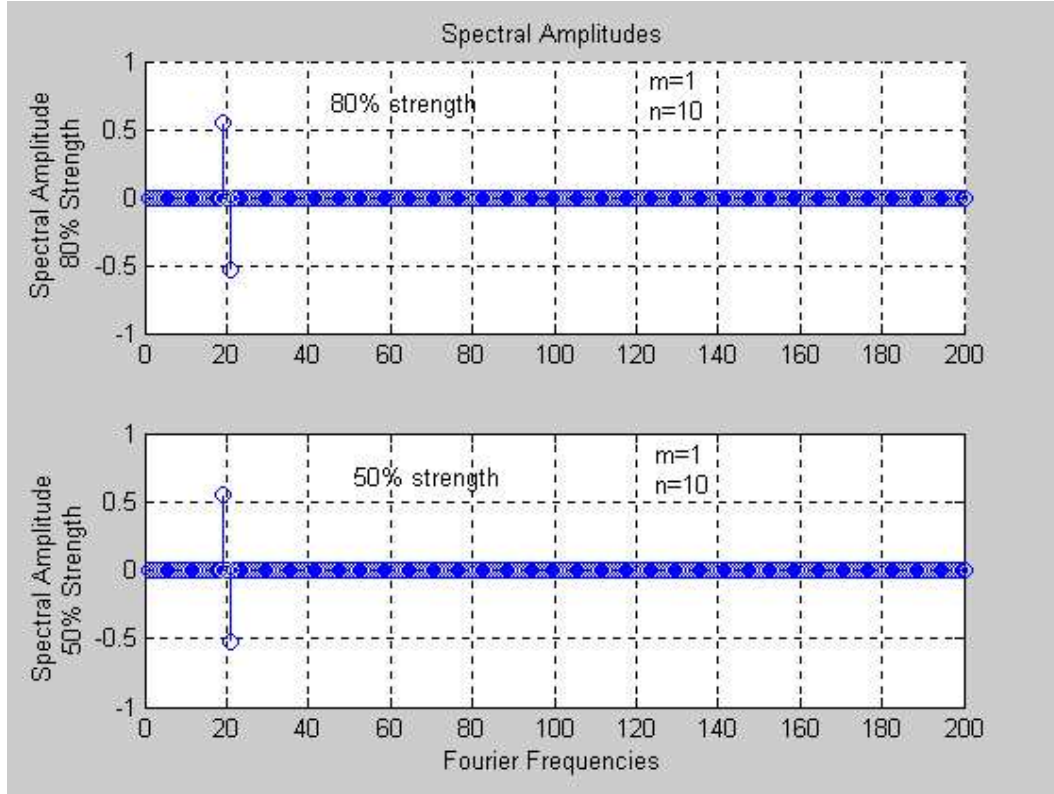


Figure 5.5: Fourier coefficients at 80% and 50%

Directionality and signal suppression are defined in terms of a Performance Index (PI):

$$PI_k = \frac{E_{out}}{E_{in}} \quad (5.2)$$

The energy of a signal³, E_i , is given by Parseval's theorem [118]:

$$E_i = \int_{-\infty}^{\infty} |F(f)|^2 df \quad (5.3)$$

Where $F(f)$ is the Fourier transform of the signal of interest.

E_{out} and E_{in} for $PI_{suppression}$ is defined as the energy of the residual signal⁴ and the original signal, respectively and E_{out} and E_{in} for $PI_{directionality}$ is defined as the energy of the backward and forward traveling waves emerging from the directional array, respectively.

5.3 Results

5.3.1 Signal Suppression - Parametric Curves

The ability of the array to cancel incoming tones is summarized in Figures 5.6 through 5.9. Each graph has three parametric curves, one for each of the number of cycles ($n = 10, 30, \text{or } 50$) contained within the envelope. The number of transducers, along with the dominant frequencies used to synthesize the cancelling wave, are shown adjacent to each data point. The results for the pulse with $T = 3 \text{ ms}$, $m = 1$ and $n = 30$ shown in Figure 5.6 are summarized below. Other parametric curves are interpreted similarly. The fundamental frequency for a pulse of 3 ms in duration is 166.67 Hz ⁵.

³The subscript i refers to the output or input signal.

⁴The residual signal is defined as: Array output minus original signal.

⁵The fundamental frequency f_0 is given by $f_0 = \frac{1}{2T}$

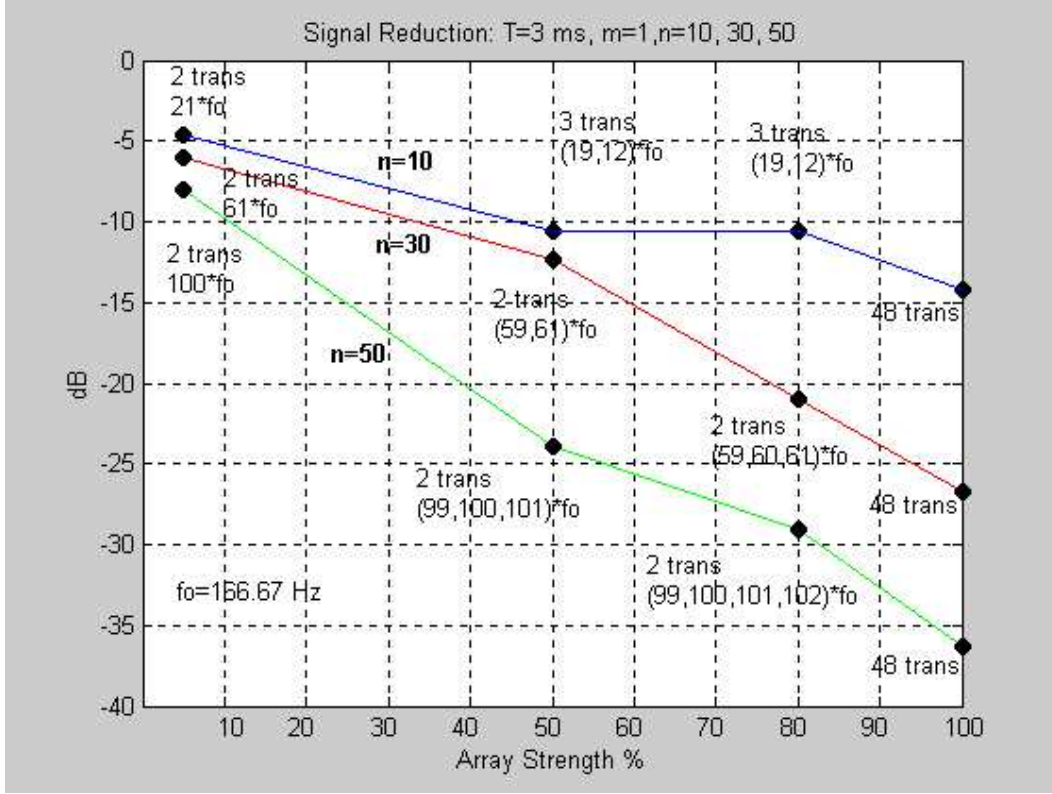


Figure 5.6: Array performance for $T = 3$ ms, $m = 1$

At full strength, 200 harmonics and 48 transducers are used to synthesize the waveform. At 80% strength, three dominant frequencies (59, 60 and 61) are fired by a single pair of transducers. The array fires a wave packet composed of the sum of three sinusoidal pulses of 9833 Hz, 10,000 Hz and 10,1667 Hz. When the array strength is reduced to 50% only two dominant frequencies remain, but the number of transducers used to synthesize the wave does not change. At 5% strength, only the 61st harmonic is fired by the single transducer pair. As expected, the performance of the directional array increases with the

number of harmonics used to synthesize the signal. The noise reduction is decreased substantially from -27 dB to -7 dB as the number of harmonics used to synthesize the wave are decreased. The performance of the array increases with frequency due to the decrease of the “non-convergent” region discussed in Chapter 4. Note that for the $n = 10$ parametric curve, there is no difference in noise reduction between an 80 and 50 strength array. This is an example of the phenomena discussed in Section 5.2.

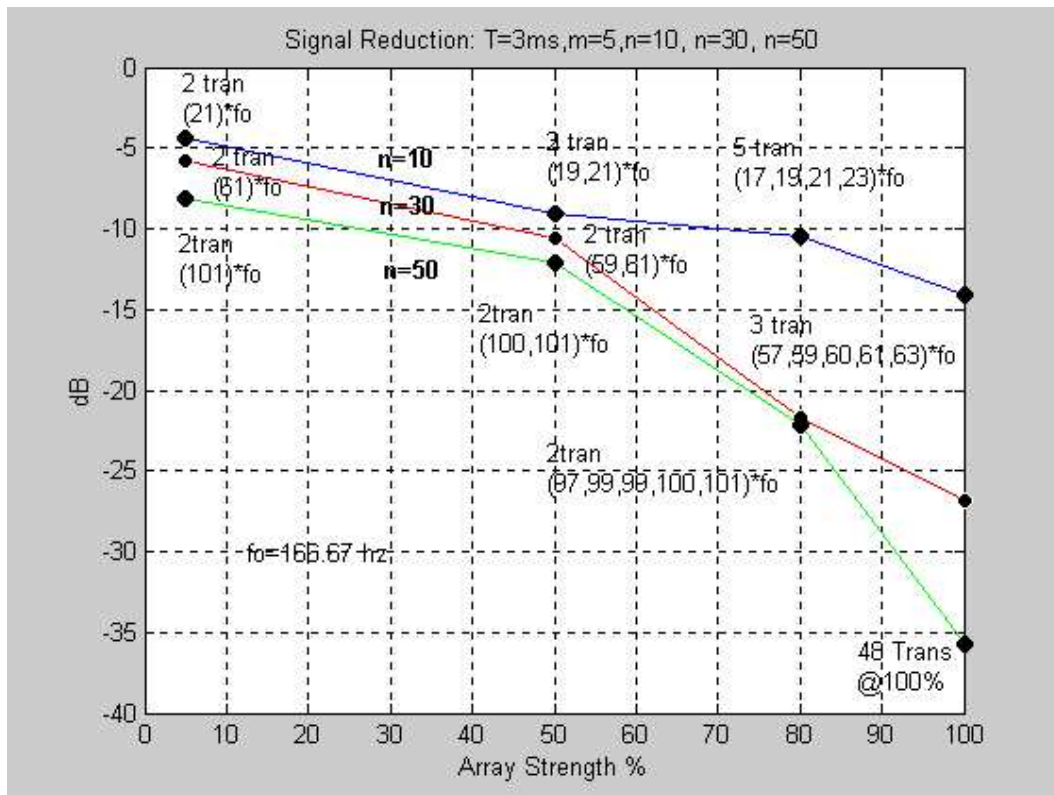


Figure 5.7: Array performance $T = 3 \text{ ms}$, $m = 5$

Figure 5.7 shows the array performance when the envelope of the pulse

is increased to $m = 5$ from $m = 1$. The performance of the array is comparable to the $m = 1$ case. The array is robust to the envelope within the $T = 3 \text{ ms}$ window.

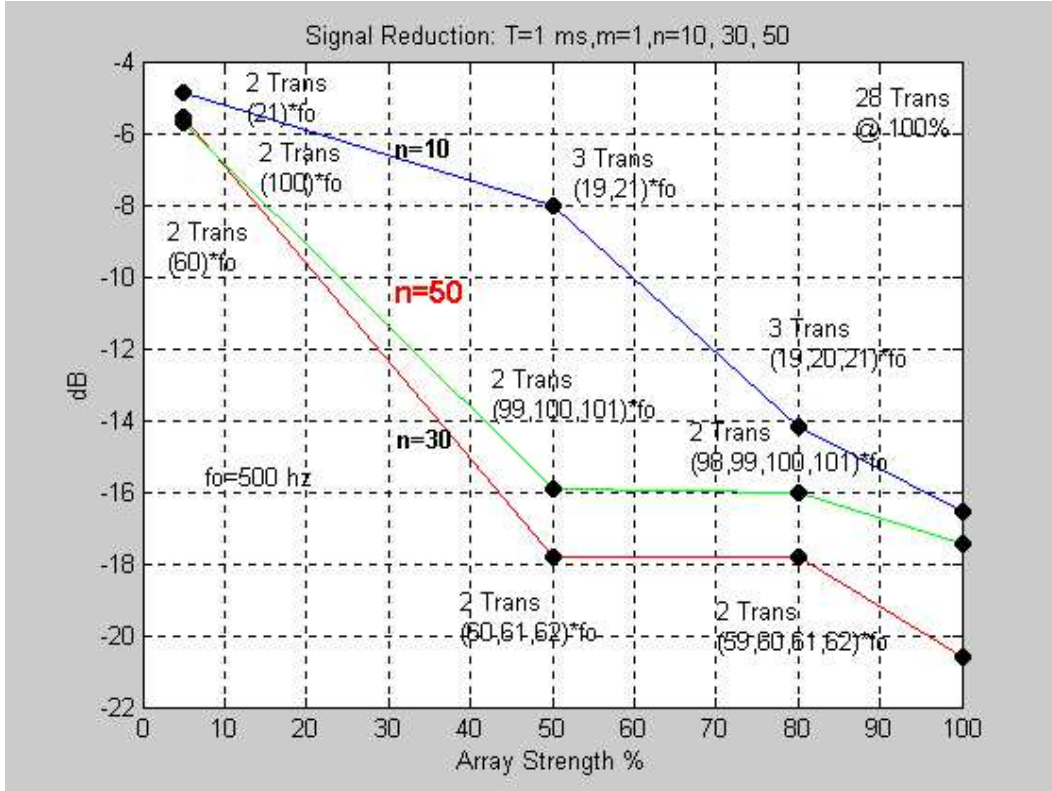


Figure 5.8: Array Performance $T = 1 \text{ ms}$, $m = 1$

Figures 5.8 and 5.9 show that the performance of the array decreases as the length of the signal is decreased. Decreasing the length of the pulse by three (from 3 ms to 1 ms) increases the carrier frequency proportionally. The directional array is faced with a faster rise time and the array is not able to keep as well as it did with larger frequencies. The combination of a faster rise

time, shorter signal length and increased frequency ($m = 5$, $T = 1 \text{ ms}$ and $n = 50$) shown in Figure 5.9 provides the biggest challenge to the directional array, as it has to generate steep, highly oscillatory signals. The performance of the array between the longer ($T = 3 \text{ ms}$) and shorter ($T = 1 \text{ ms}$) cases is clear. Within each time domain, the ability of the directional array to cancel incoming signals is a weak function of m .

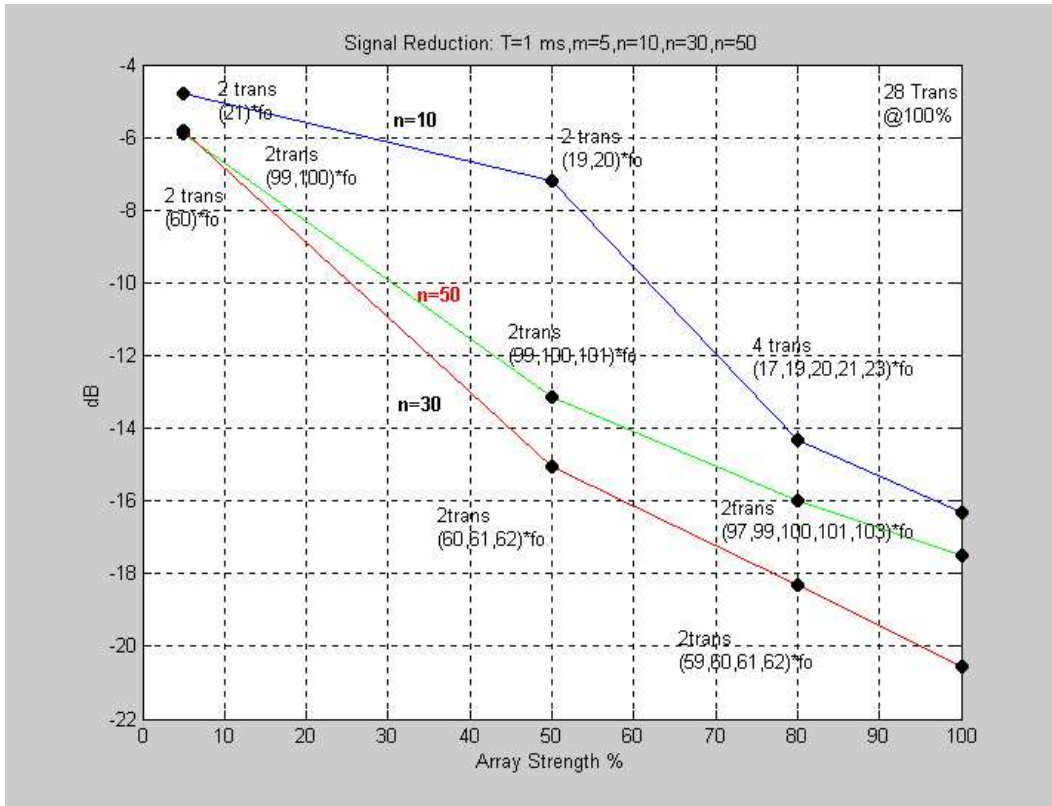


Figure 5.9: Array Performance $T = 1 \text{ ms}$, $m = 5$

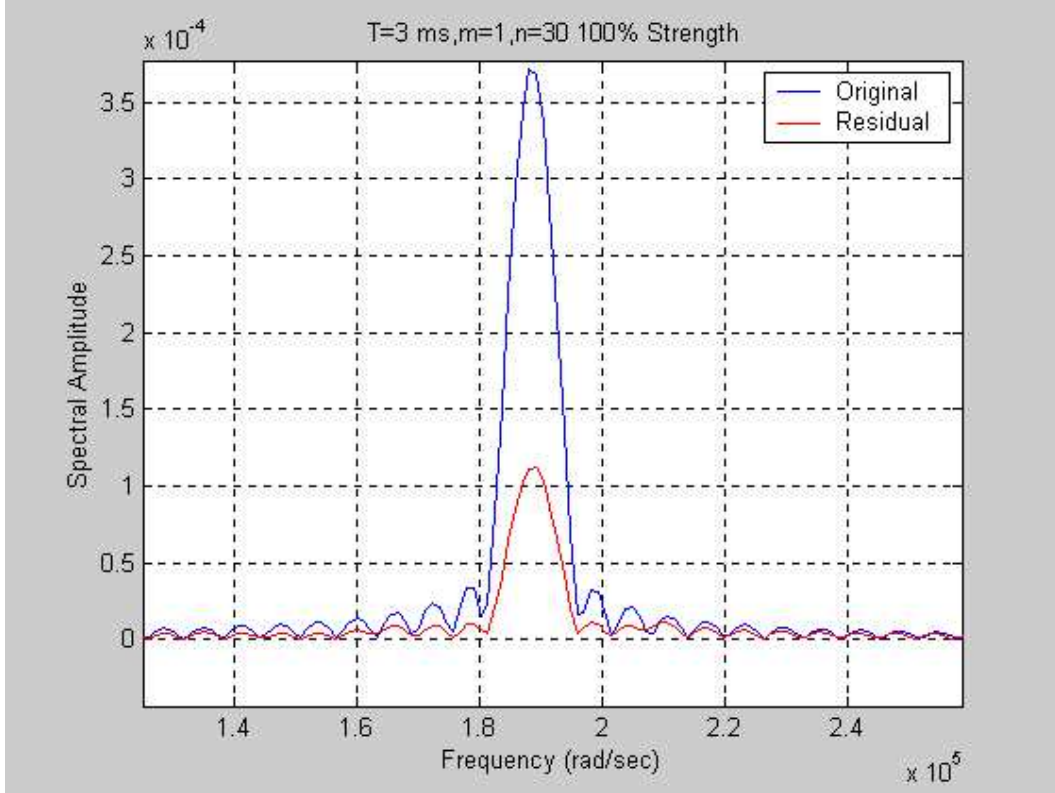


Figure 5.10: Original and residual spectra $T = 3 \text{ ms}$, $m = 1$ and $n = 30$

5.3.2 Frequency Domain

The Fourier transforms of the input and residual signals (for selected cases) are shown in Figures 5.10 through 5.13. All of the cases investigated clearly show the ability of the directional array to significantly reduce the energy of the incoming signal, not only at the dominant frequency, but also in the side lobes of the spectrum.

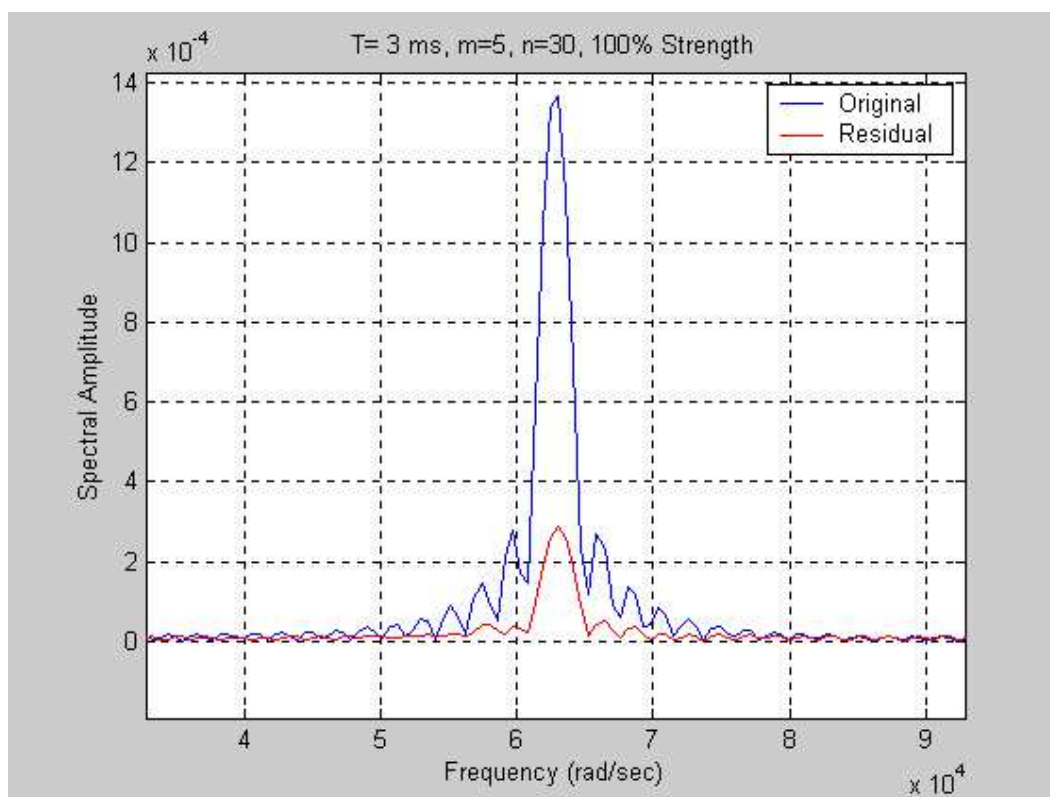


Figure 5.11: Original and residual spectra $T = 3 \text{ ms}$, $m = 5$ and $n = 30$

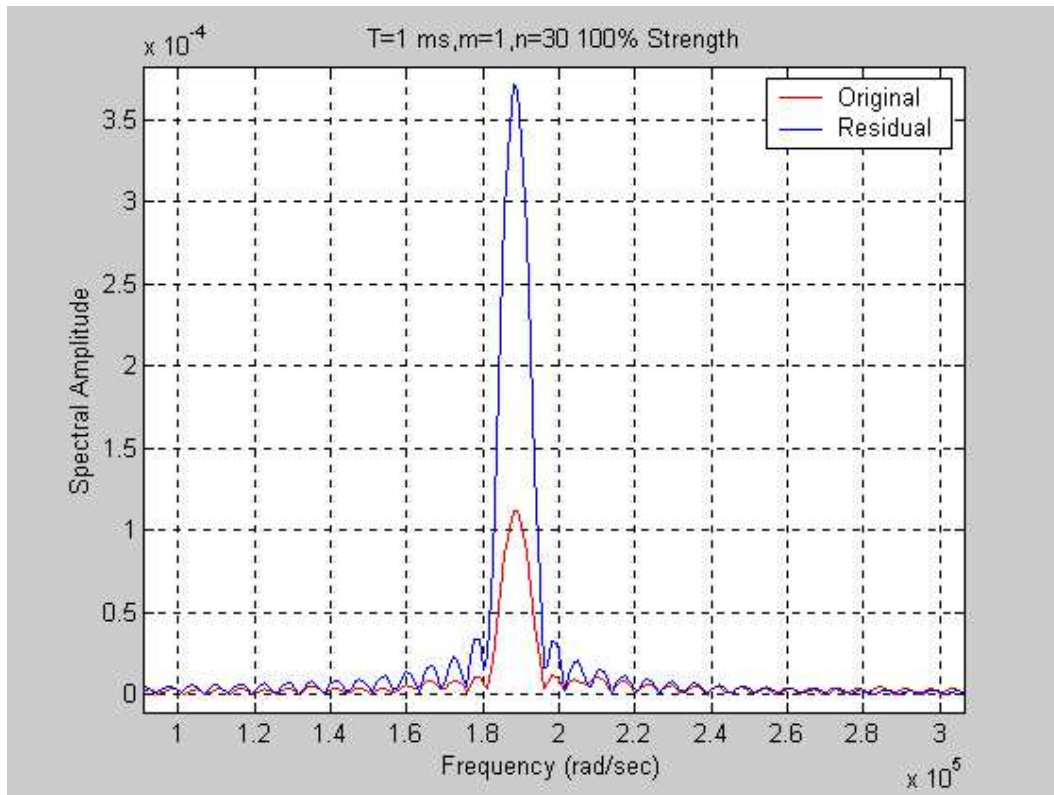


Figure 5.12: Original and residual spectra $T = 1 \text{ ms}$, $m = 1$ and $n = 30$

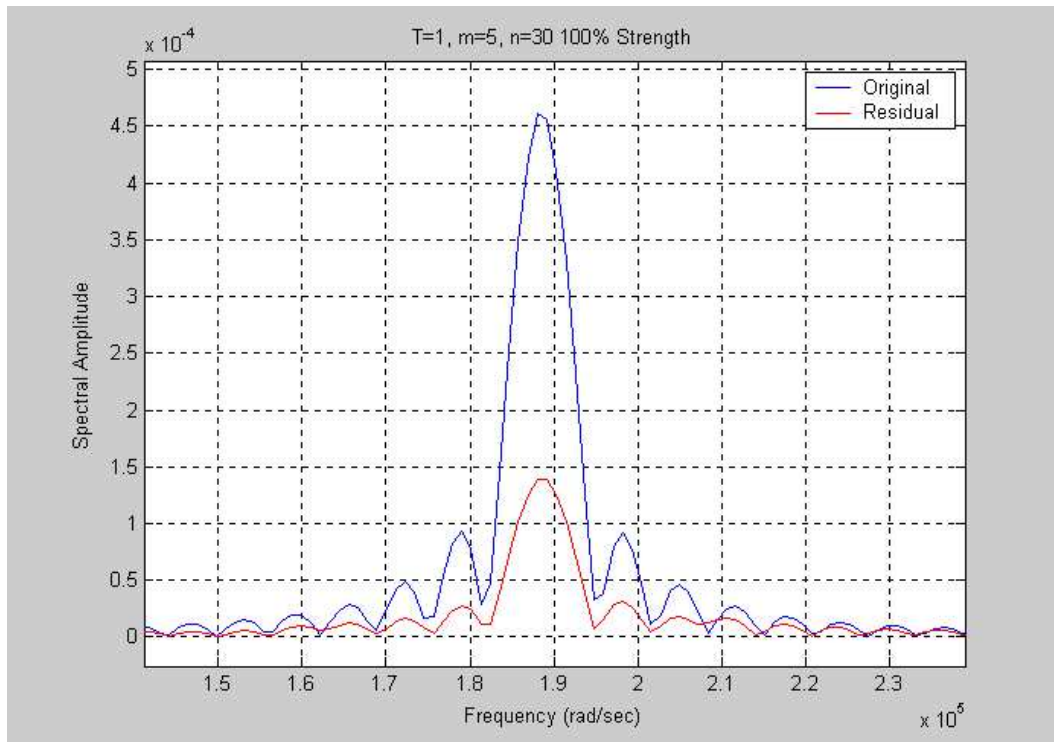


Figure 5.13: Original and residual spectra $T = 1 \text{ ms}$, $m = 5$ and $n = 30$

When the number of harmonic frequencies used to synthesize the wave is reduced to one (i.e. the dominant frequency) the directional array does a poor job in cancelling the incoming signal. Figure 5.14 shows original and the residual signal when using only the dominant frequency to synthesize the wave.

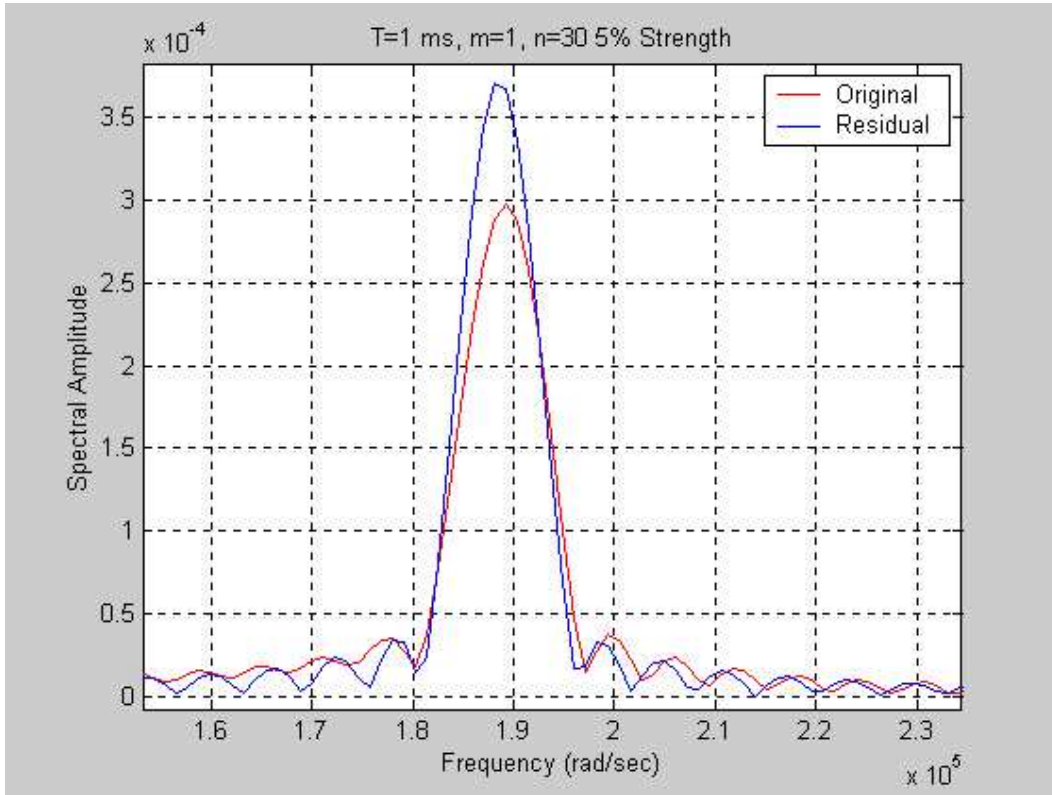


Figure 5.14: Single transducer pair $T = 1 \text{ ms}$, $m = 5$ and $n = 30$

5.3.3 Directionality

Array directionality was quantified by examining the ratio of energy in the wave traveling away from the array and the wave generated by the array to cancel the incoming signal, as well as the time domain signals. A typical result of the evaluation is shown in Figure 5.15.

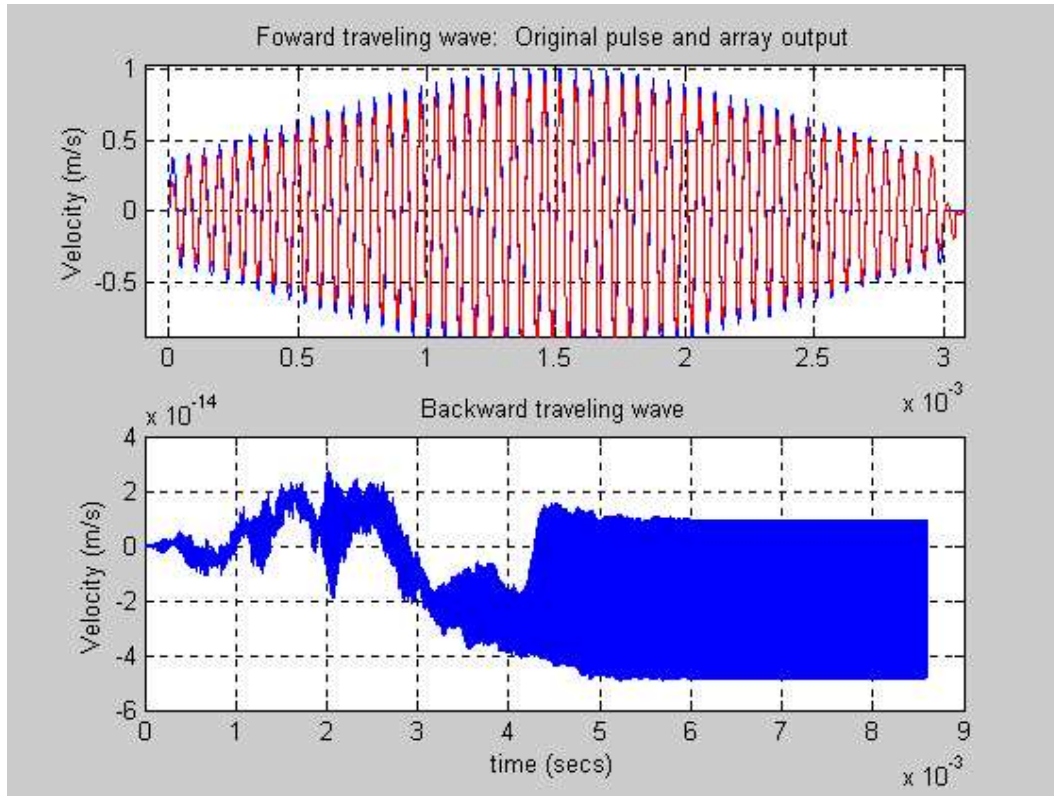


Figure 5.15: Forward and backward traveling wave

The top of Figure 5.15 is the time signal for of incident pulse ($T = 3 \text{ ms}$, $m = 1$, $n = 50$). Superimposed on the incident pulse (in red) is the signal generated by the directional array.

The signal at the bottom of Figure 5.15 is the backward traveling wave generated by the directional array. The backward traveling wave has a noise-like appearance. The time signal is bounded in magnitude by 10^{-13} . The ratio of the energy contained in the left traveling wave over the right traveling wave remained consistently less than 0.0018 for all 48 of the cases considered in this evaluation.

5.4 Closing Comments

The directional array proposed in this dissertation is capable of cancelling broadband signals of various frequency content and complexity. The array performs better with slower rise times envelopes and lower frequencies. Arrays which fire wave packets containing dominant frequencies are more successful in cancelling broadband signals than their monotone counterparts. Signal reduction using a single stage of the directional array varies from 35 dB (for $T = 3\text{ ms}$) to 22 dB (for $T = 1\text{ ms}$), depending on the rise time of the envelope pulse signal, and the number of harmonics used to synthesize the signal.

The directionality of the array is preserved by timing, phasing and delaying the backward traveling waves generated from each of the sources to destructively add at the left-most transducer interface. The forward traveling wave is several orders of magnitude larger than its backward traveling counterpart for all 48 cases examined. The array provides directionality while maintaining signal integrity of the forward traveling wave.

The simulations presented here show that better performance can be

obtained when using a Fourier synthesis decomposition in conjunction with a properly phased set of PZT transducers, rather than with a single transducer pair tuned to a the dominant frequency of the incoming broadband wave. The performance of the directional array decreases monotonically as the number of harmonics are decreased. Use of a Fourier series decomposition in conjunction with a properly spaced and phased set of transducers has the potential of improving noise reduction of broadband signals by a factor of 4.

Chapter 6

Directional Array - Numerical Simulations

6.1 Introduction

This chapter addresses the ability of the directional array to emulate acoustic signals emerging from the $\frac{1}{20}^{th}$ scaled model of the drill string described by Drumheller in [15]. The directional array is composed of a set of transducers embedded in an uniform cylindrical waveguide. The acoustical impedance of the transducers are matched to the waveguide by properly selecting their cross-sectional area. The scaled model of the drill string is twenty five unit cells long with infinite boundary conditions on the right hand side and time varying boundary conditions on the left hand side. Initially on the left hand side, the velocity field is specified. Subsequently the left hand side is changed to a stress free boundary condition. These boundary conditions are similar to

what can be expected in a laboratory test.

Four different signals are injected into one end of the drill string, and the output is examined at the other end. The frequency ranges were chosen to lie in the middle of the pass bands. This provided broadband inputs in frequency ranges in which the periodic structure passes information from one end to the other. The simulations shown are for a twenty five unit cell, scaled model of a real drill string. Four drill strings lengths were used for simulation purposes: four, nine, sixteen and twenty five. The twenty five unit cell drill string provided the most complex transient signals. The four signals used for simulation are as follows:

- Sinusoidal pulse train in the middle of the 2nd pass band.
- Sinusoidal pulse train in the middle of the 3rd pass band.
- Hammer input, used to approximate an impulse response.
- One period of a sinusoidal pulse.

The response of a scaled model of a drill string to the inputs described above are the inputs to the terminating impedance, which in turn attempts to cancel the incoming disturbance. The dimensions of the scaled model of the drill string are shown in Table 6.1.

The termination impedance is a set of PZT transducers embedded in a uniform waveguide of the same dimensions as the pipe of the drill string. The piezoelectric constants of the PZT transducers can be found in Table 4.1 in Chapter 4 of this dissertation.

Section	Length	Cross-sectional Area	Speed of Sound
Pipe	$d_1 = 17in$	$a_1 = 0.0185in^2$	$5130\frac{m}{s}$
Tool Joint	$d_2 = 1in$	$a_2 = 0.0968in^2$	$5130\frac{m}{s}$

Table 6.1: Model dimensions

As shown in Chapter 3, the drill string is a highly dispersive medium with filtering properties. Energy injected at one end of the drill string is highly dispersed. Information continues to arrive at one end of the structure without a definitive end. The array designer may be faced with a transient signal which theoretically has no end. The focus must therefore shift to the duration in time for which the bulk of the acoustic energy resides, as it becomes impossible to define a clear cut end to the incoming information. To this extent, the transient behavior of the drill string must be characterized for all possible inputs of interest. The terminating impedance designer must answer the question: Is the bulk of energy in the emerging signal contained within a *reasonable*¹ time window? This question is hard to answer for the general case, however, for simple pulse trains and hammer like pulses, several simulations reveal that the bulk of the energy is contained within the first $3ms$ of the output signal.

¹Cancelling longer transient signals require a proportionally larger design space for the terminating impedance.

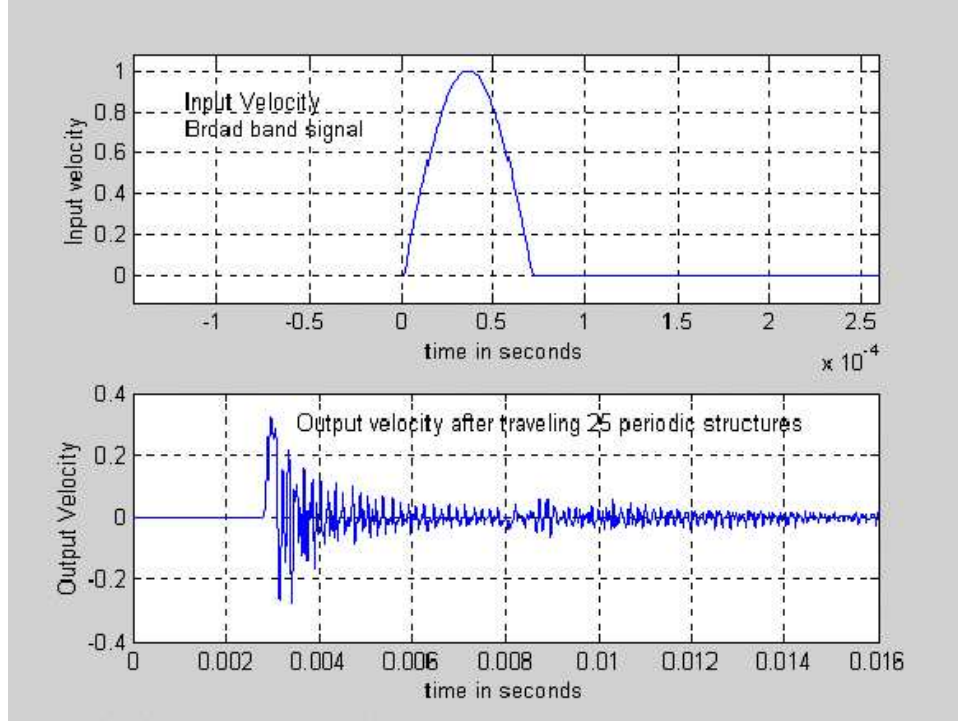


Figure 6.1: Hammer response of periodic structure

Figure 6.1 shows the response of the $\frac{1}{20}^{th}$ scale model to a hammer type blow. The bulk of the acoustic energy is contained within the first 3ms of the signal. Based on the data obtained from the various simulations², the termination impedance discussed in this dissertation was designed to cancel transient signals of 1 – 3 ms in duration. Assuming the speed of sound in steel is $5130 \frac{m}{s}$, this translates to approximately 8 to 25 feet of uniform pipe (using a scaled model drill string as the feeding structure to the terminating impedance).

²Broadband signals in the middle of the second and third pass bands, as well as a hammer like input were injected into drill of 4, 9, 16, and 25 unit cells in length. The input signals were 5 full cycles in duration

As noted in Chapter 3, it is the “comb” filtering properties of the drill strings the alternating pass bands and stop bands, that make the transmission of information across the drill string a difficult task. The dispersion relationship (i.e. the passbands and stop bands) is defined by the ratio of the acoustic impedances, the length of the drill pipe and tool joint and the periodicity of the unit cell. The dispersion relationship is partially responsible for the frequency content of the signal emerging from the drill string. The frequency content of a signal is also affected by the length of the drill string. The frequencies of the input spectrum that overlap with the stop band get trapped in the first few unit cells of the drill string. Signals emerging from a long drill string are different than those emerging from a short drill string of the same dimensions. The length of the drill string therefore has an effect on the output signal³. The directional array must therefore be robust to drill string length, input spectra, changing geometry and environmental noise. The robustness of the directional array discussed herein lies in the open-loop - feed-forward input of the (modified) Fourier coefficients, which are computed for every signal. The drawback of such a system is of course a heavy penalty in computation time; the algorithm used to synthesize the transient signals used 85 to 250 harmonics. These coefficients combined with the correct electrical input to the transducers can generate the necessary basis functions to synthesize complex directional acoustic waves.

³Incorporating structural damping into the model to account for energy losses will introduce a larger dependence on drill string length.

6.2 Terminating Impedance Design

Figure 6.2 is a schematic representation of the terminating impedance discussed in this dissertation. It consists of two cancelling stages. The incoming signal is sent to an adaptive algorithm, which defines the electrical inputs to the first-stage. First-stage cancellation happens at the boundary of the first-stage and the uniform waveguide.

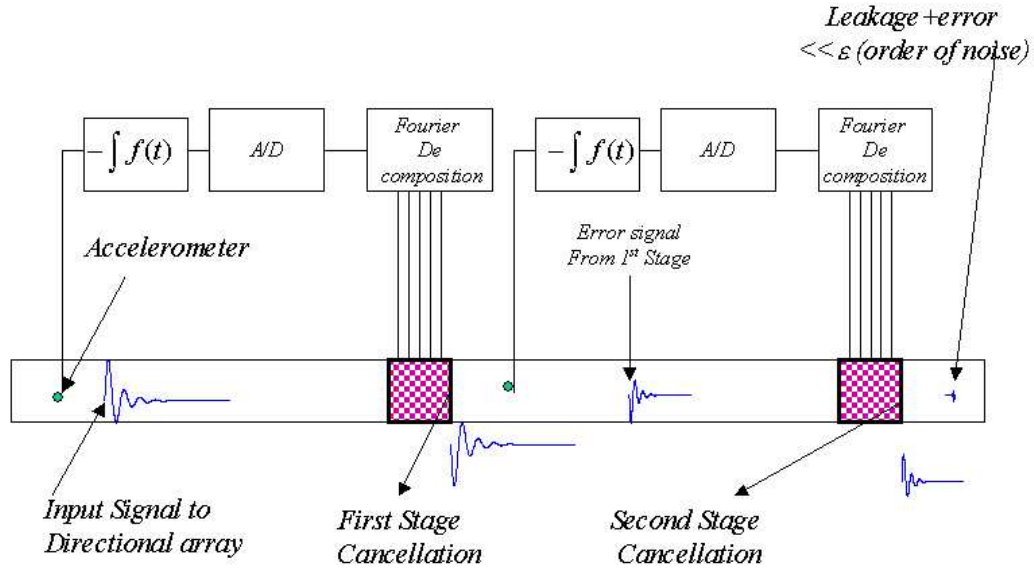


Figure 6.2: Two-stage terminating impedance

The residual from the first-stage is subsequently fed to a second identical (cancelling) stage. A directional sensing array which feeds the information to both cancelling stages is assumed to exist⁴. The objective of the two-stage cancelling device is to act as an “acoustic black body”.

⁴The simulations presented here make directly of the velocity field computed numerically.

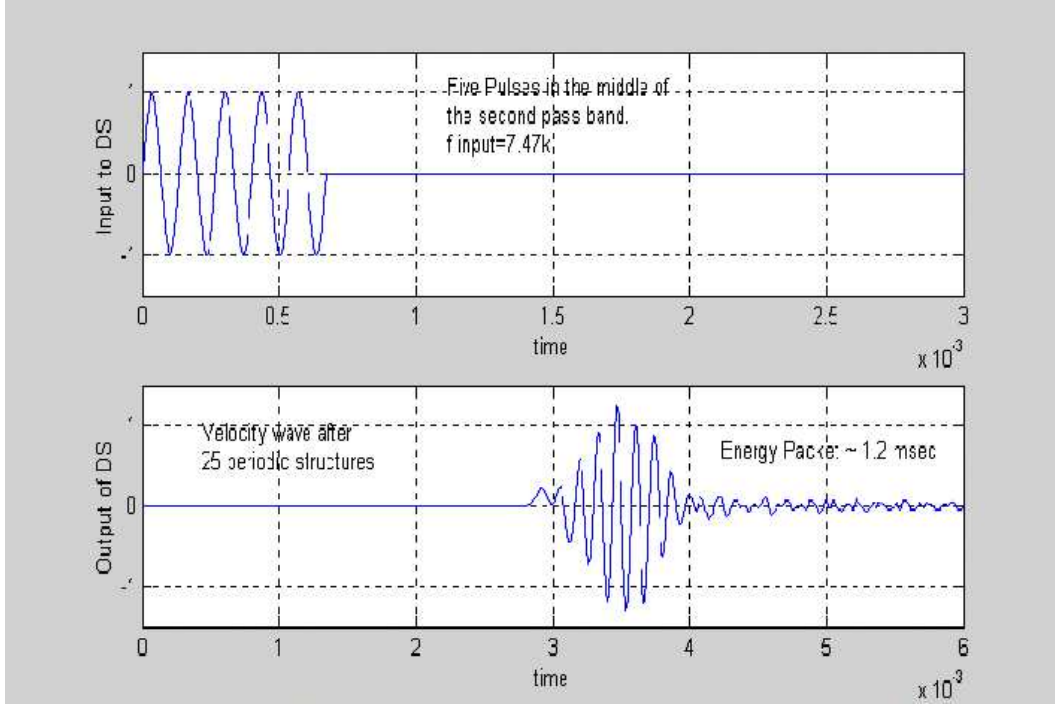


Figure 6.3: Sinusoidal pulse train - 2^{nd} pass band

6.3 Sinusoidal Pulse Train - 2^{nd} Pass band

This section quantifies the performance of the terminating impedance to a sinusoidal pulse train whose dominant frequency lies in the second pass band of scale model of the drill string. The top of Figure 6.3 shows the input to the scaled model drill string, and the bottom of the figure shows the signal emerging from a 25 unit cell drill string. The bulk of the acoustic energy emerging from the drill string is contained in a window approximately 1.2 ms long. Figure 6.4 shows the Fourier Transform of the input and output waveforms. Note that the general shape and dominant peak of Fourier Transform remains un-

changed. The output spectra is the same as the input, except “truncated” at the stop bands. Figure 6.5 shows the Fourier Coefficients for the half range expansion of the signal at the bottom half of Figure 6.3- the output signal from the drill string.

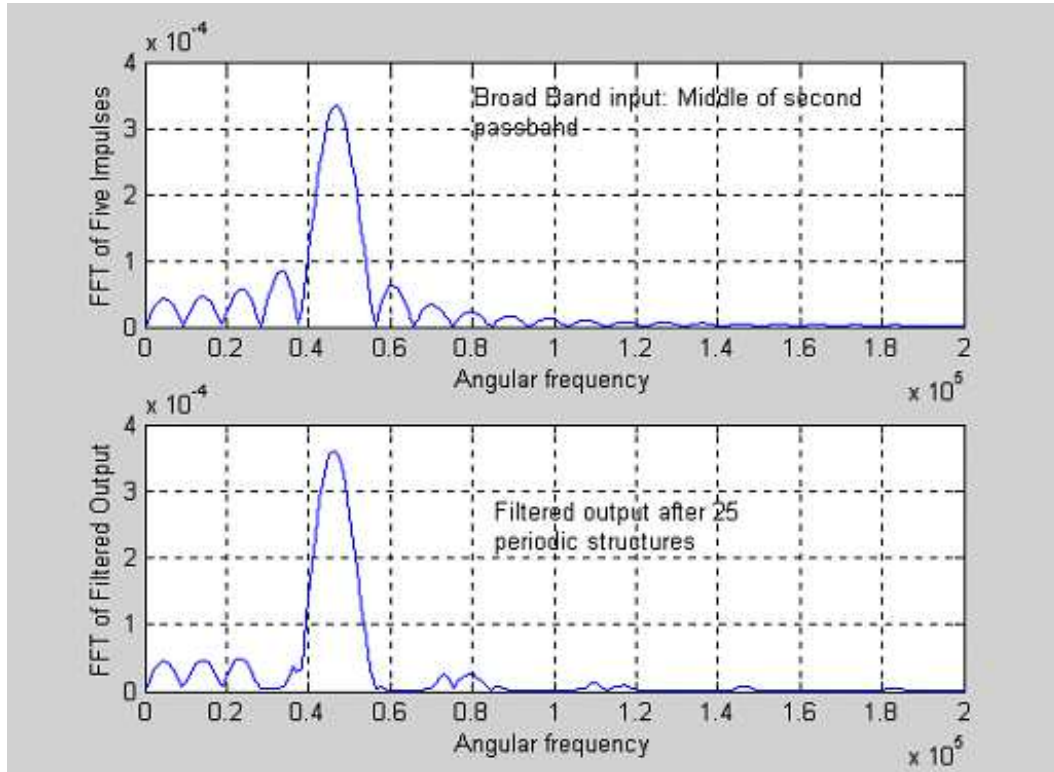


Figure 6.4: Fourier domain output signal 2nd pass band

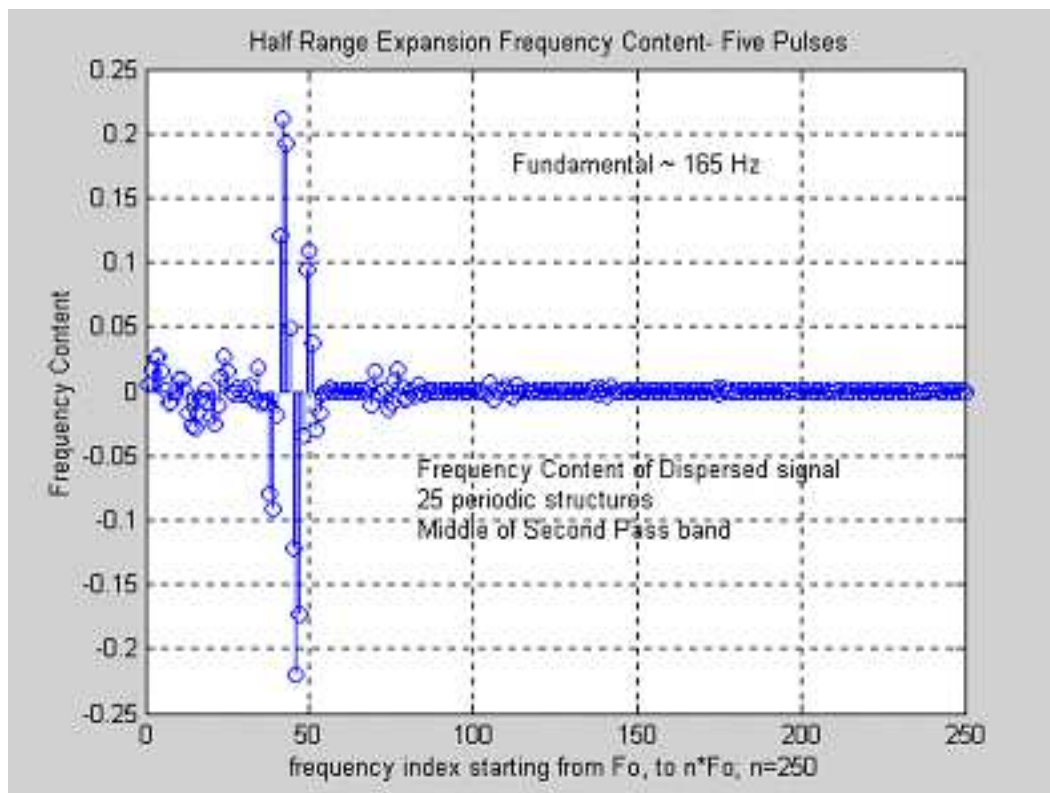


Figure 6.5: Half range expansion coefficients

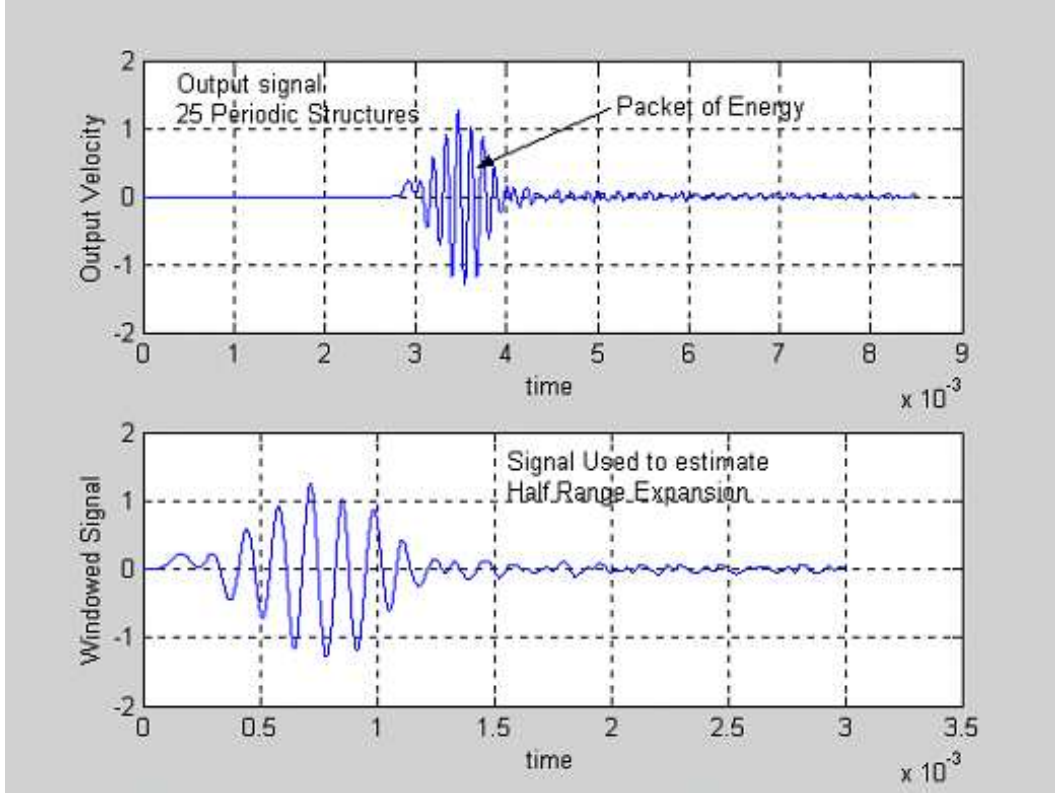


Figure 6.6: Drill string output and windowed signal 2nd pass band

The top of Figure 6.6 represents the signal which would be gathered by an accelerometer and integrated to obtain the velocity field. The algorithm must now define the bulk of the energy and ignore the leading dead zone and trailing “noise”. This is done numerically using a Heaviside window $3ms$ wide with a decaying exponential tail to minimize discontinuities. The truncated signal is fed to the algorithm, which turns around and designs the electrical inputs to the transducer array. The set of transducers generate an acoustic signal designed to cancel the incoming disturbance.

Figure 6.7 shows the incoming acoustic signal exiting the scaled model of the drill string, and the waveform produced by the first-stage of the directional array. Note the poor convergence at the beginning of the signal, and the injected noise at the tail end. Figure 6.8 shows the original signal and the residual from the first-stage cancellation. The first-stage was able to reduce the incoming signal by approximately $6dB$. The residual from the first stage is gathered, windowed, and fed into the second cancellation stage. The residual after the first stage of cancellation is shown on the top of Figure 6.9. The coefficients of the Half Range Fourier expansion as a function of harmonic index is shown at the bottom of Figure 6.9.

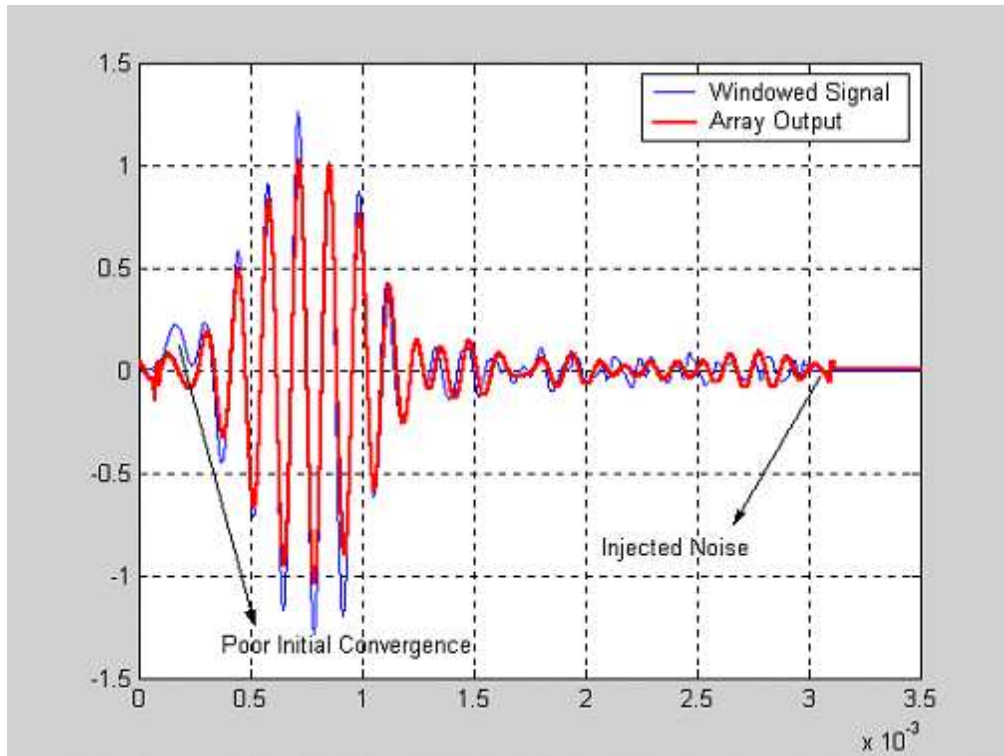


Figure 6.7: First stage array output vs. exiting signal 2^{nd} pass band

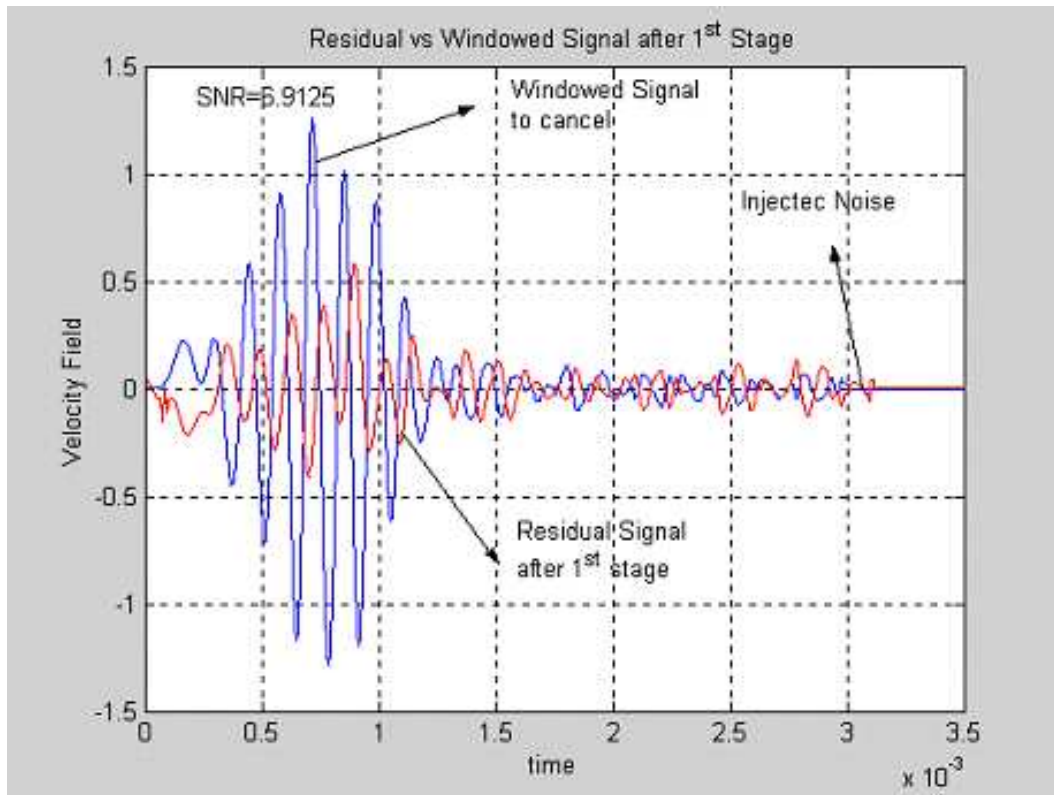


Figure 6.8: First stage cancellation of incoming transient 2nd pass band

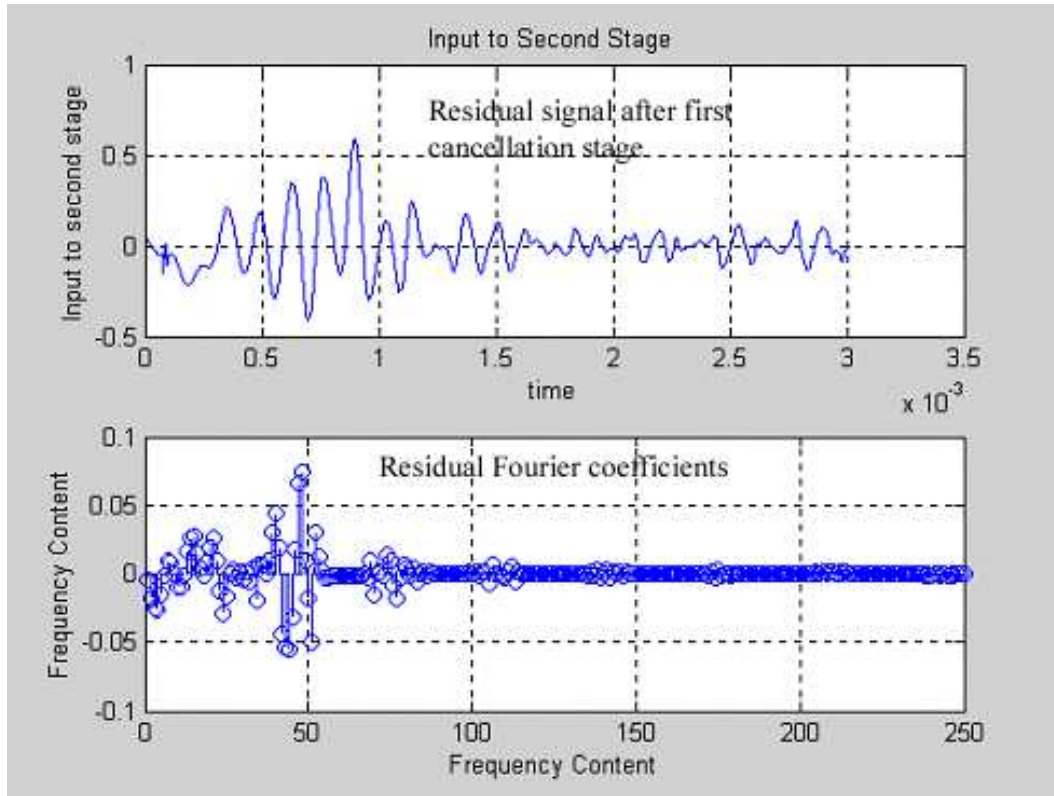


Figure 6.9: Residual from the first stage 2nd pass band

Note that the coefficients are drastically different from those generated for the first stage of cancellation. The inputs to each of the stages, as well as the firing sequence, timing and phase delays are unique for each incoming signal.

The output of the second stage of the terminating impedance is shown in Figure 6.10. Note that the directional array continues to inject noise into drill string and fails to converge to the requested signal for the first $250\mu sec$ of the original signal.

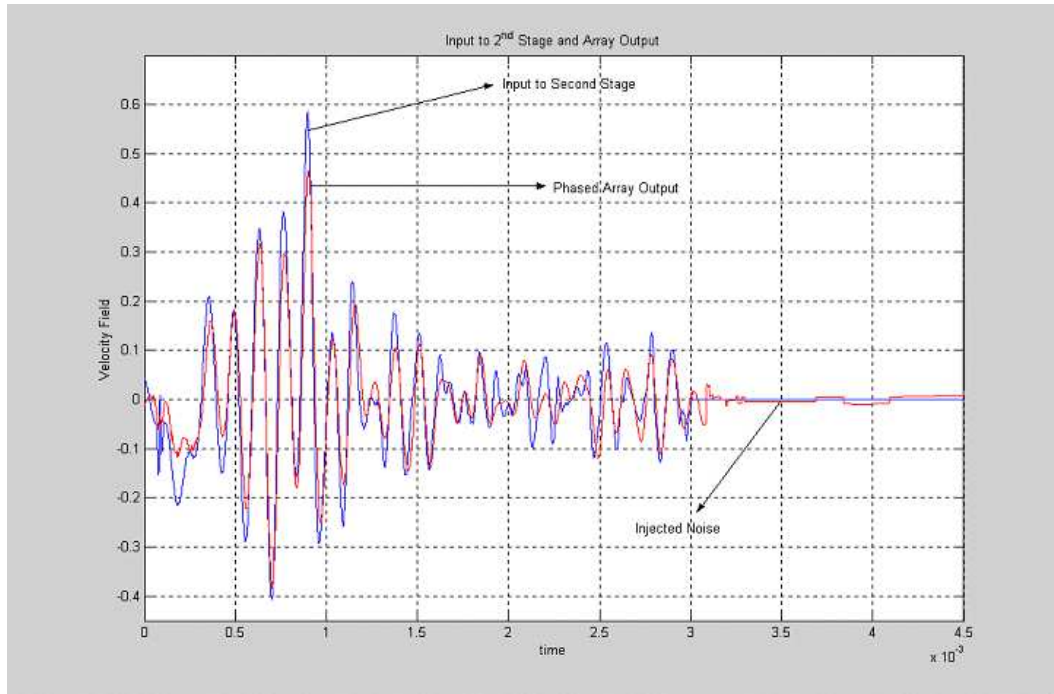


Figure 6.10: Array output vs. residual signal 2nd pass band - 2nd stage

The residual from the second stage is compared with the original windowed signal in Figure 6.11. The two-stage combination was able to provide a $13dB$ reduction. The remaining (residual) signal is brought down into the noise level of the original.

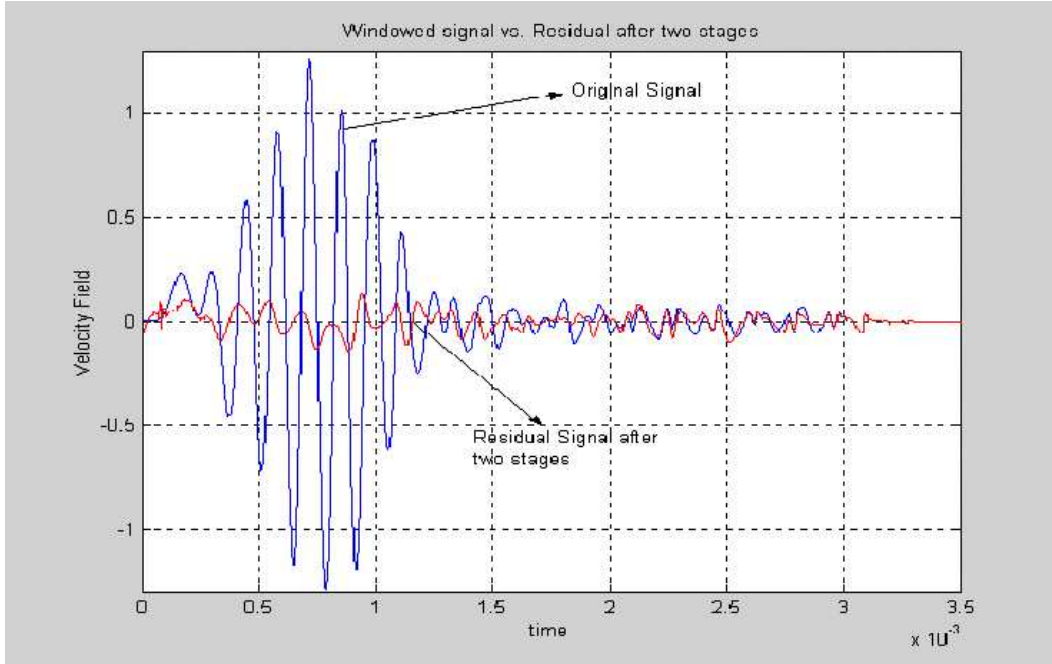


Figure 6.11: Second stage output vs. original signal 2^{nd} pass band 2^{nd} stage

6.4 Sinusoidal Train Pulse in the 3^{rd} Pass band

The second type of signal discussed is a sinusoidal train in the middle of the third pass band. The number of harmonics used to generate all of the transient signals for this particular case was reduced to 85 harmonics.

The input signal to the drill string, and the drill string response to the injected signal shown in Figure 6.12.

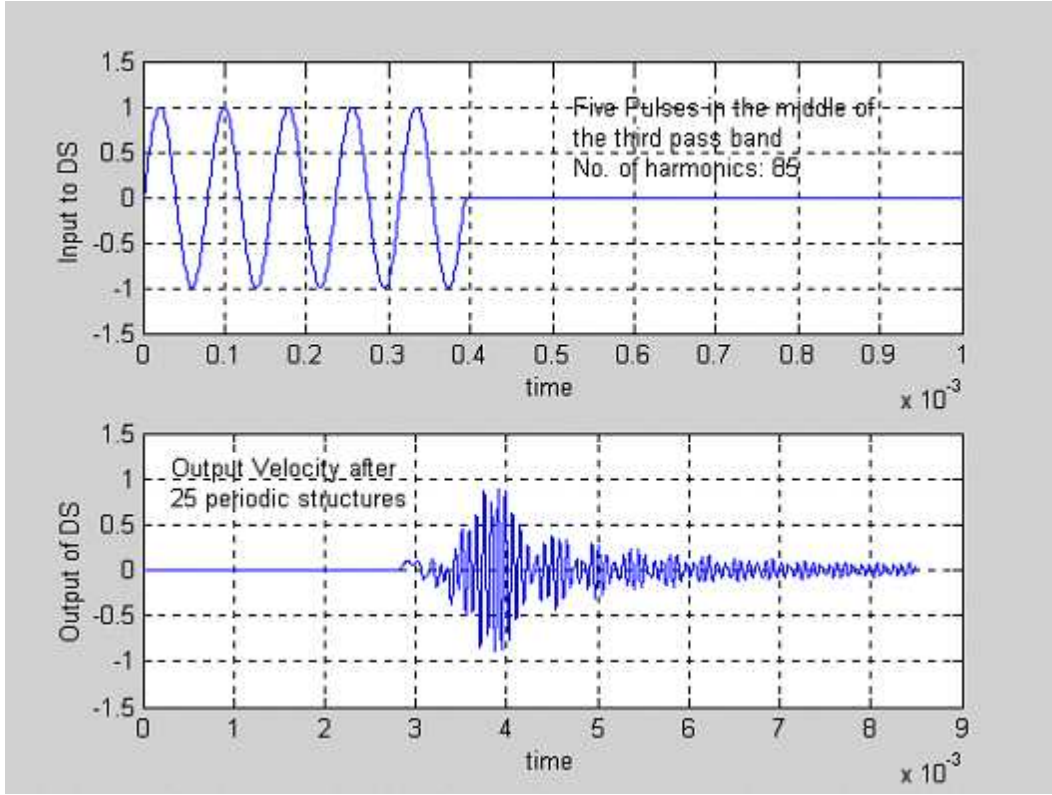


Figure 6.12: Sinusoidal pulse train - 3rd pass band

As shown in Figure 6.13, the output signal is dominated by high harmonic frequencies from the 70th to the 90th harmonic. Section 6.3 showed that the output of the drill string due to a sinusoidal input train with a dominant frequency in the middle of the second pass contained the majority of the energy within the 40th to 50th harmonics. The terminating impedance design for all of the cases presented is fixed in space. The terminating impedance is

able to cancel signals of vastly different frequency content.

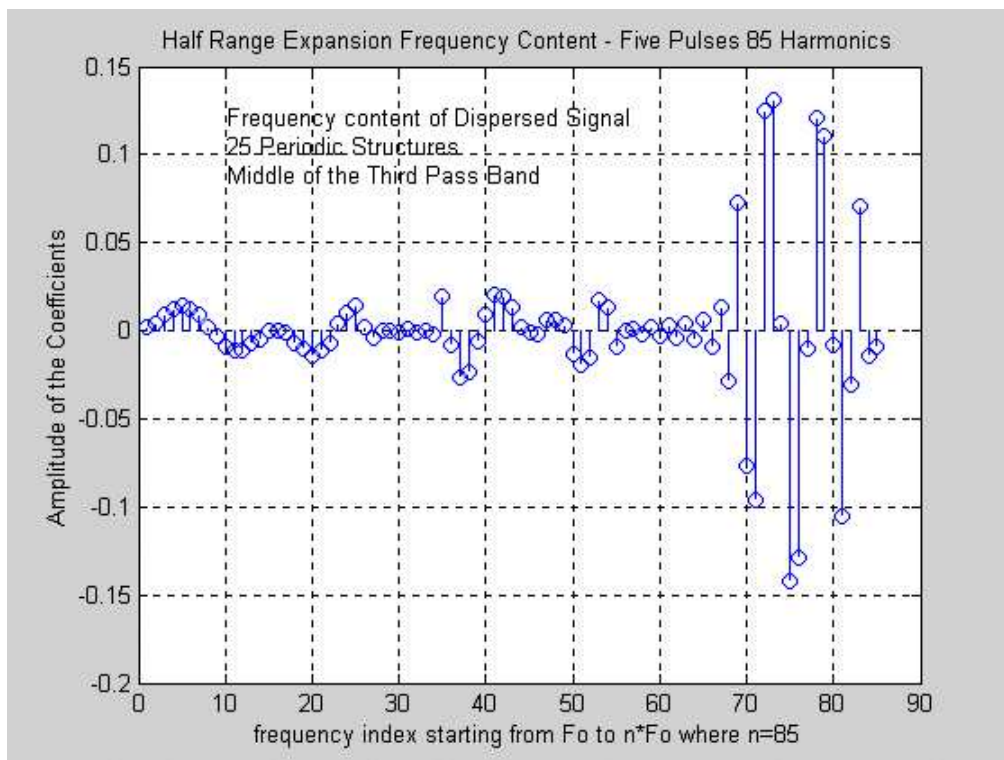


Figure 6.13: Fourier coefficients of output signal

The algorithm used to generate the electrical inputs to the geometrically spaced transducers in the directional array is capable of selecting only dominant harmonic frequencies for acoustic signal generation. The algorithm selects dominant frequencies by sorting through the amplitude of all of the coefficients relative to a fraction of the absolute value of the largest coefficient in the half range expansion. The fractional value used to determine the dominant contributions to the signal is user defined. This feature minimizes the number of electrical inputs to the transducer pairs while maintaining signal integrity. Some of the simulations in this section make use of this feature.

Any frequency with a Fourier coefficient less than thirty percent of the largest coefficient in the Fourier decomposition was not used in the synthesis process.

Using a $3ms$ Heaviside window, the incoming signal is truncated and fed into the decomposition algorithm.

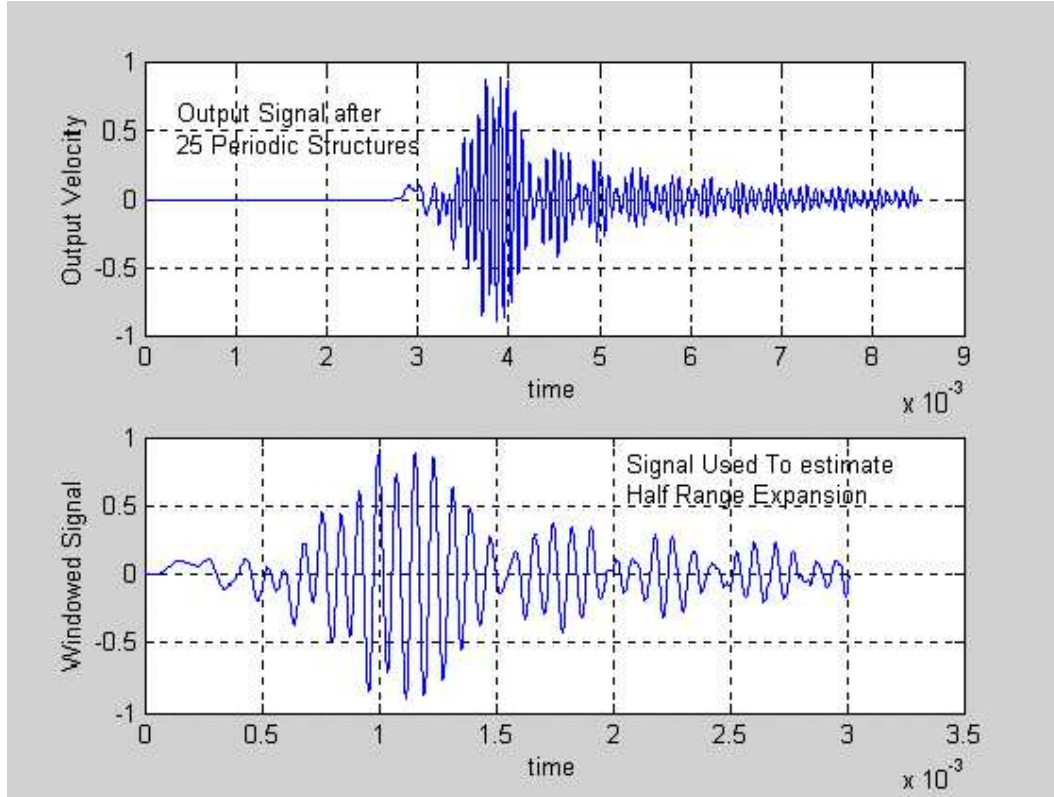


Figure 6.14: Drill string output and windowed signal 3^{rd} Pass band

Figure 6.14 shows the original and windowed signal. The output of the first stage of the terminating impedance, relative to the original windowed signal, is shown in Figure 6.15.

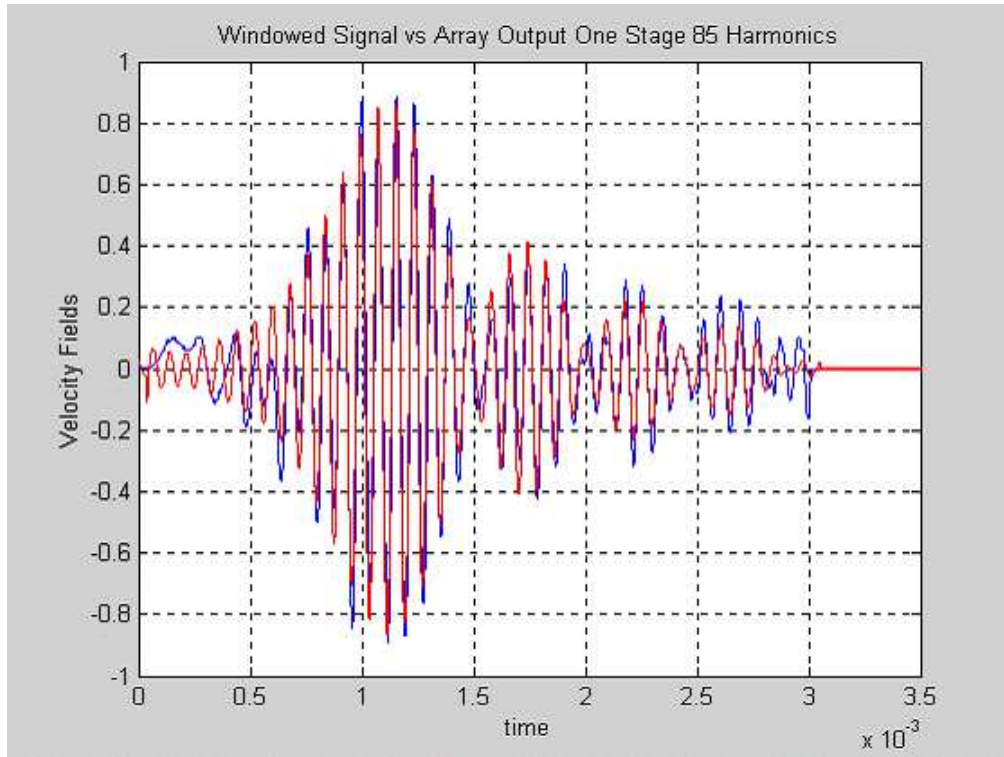


Figure 6.15: First stage array output vs. original signal

The residual after the first stage of the terminating impedance vs. the original windowed signal is shown in Figure 6.16. The original signal was reduced by $8dB$.

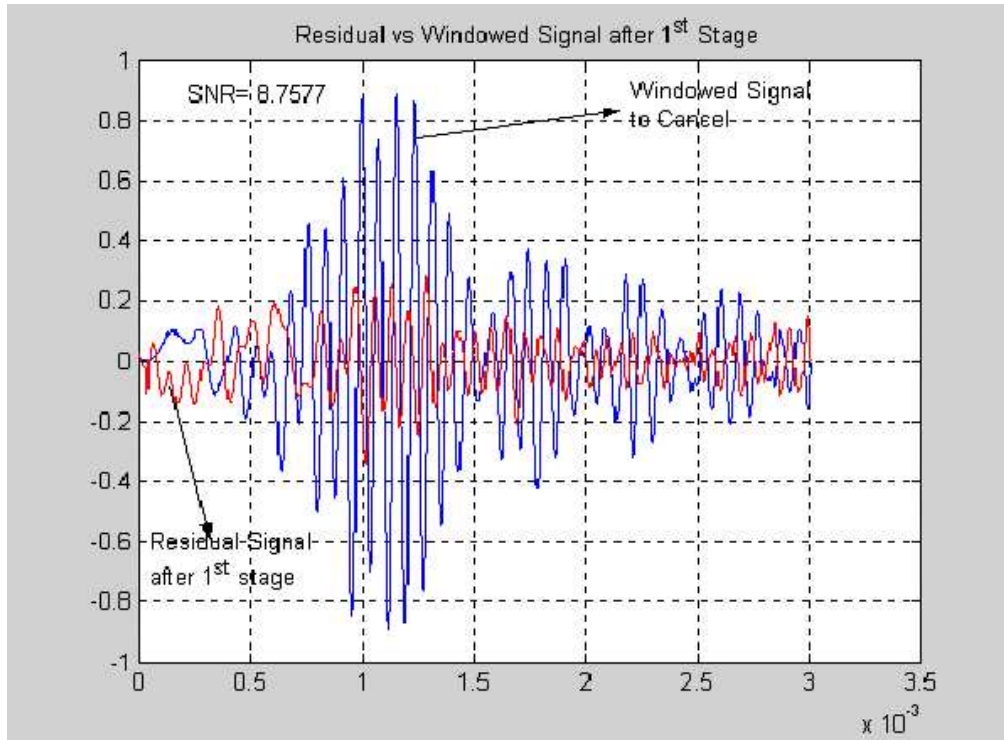


Figure 6.16: Original and residual signal

After the first stage, the residual signal is fed into the algorithm for the second directional array, which defines the electrical inputs for the second stage. The residual from the first stage along with the output of the second stage is shown in Figure 6.17.

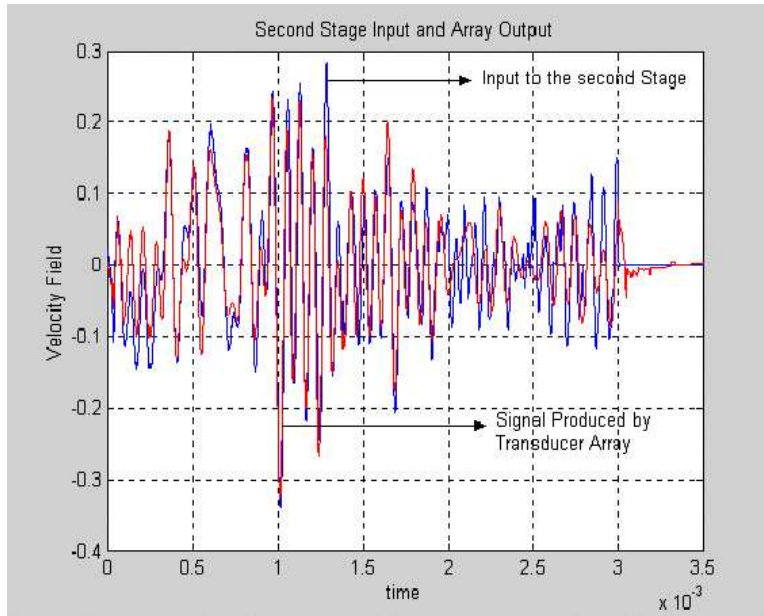


Figure 6.17: Input to second stage and array output

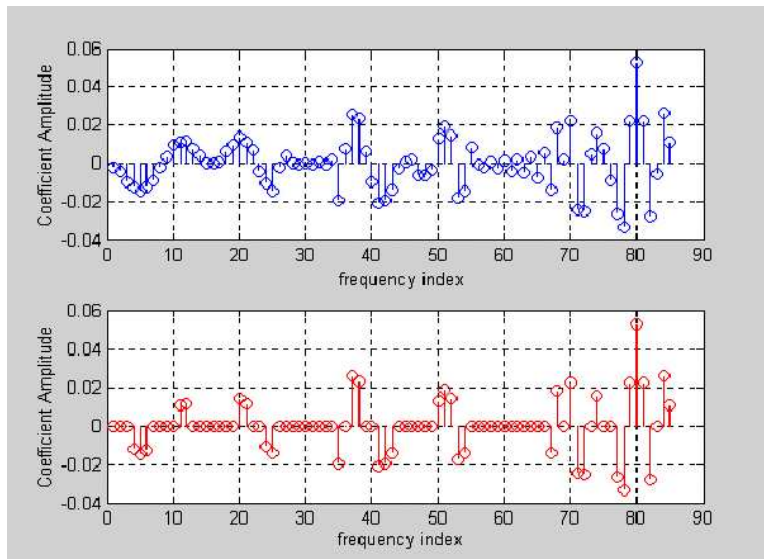


Figure 6.18: Fourier coefficients residual signal

The ability of the second stage to mimic the residual results in a $15dB$

reduction from the original windowed signal. Note the inability of the acoustic array to eliminate the double hump at the very beginning of the signal. This is because the directional array is not capable of accurately generating any portion of a signal with a strong DC components without modifications to the input signal to the directional array. The approach to get around this deficiency will be discussed in Section 6.5.

Figure 6.19 shows the original and the residual signal after two-stage of cancellation. The injected noise at the tail end of the signal generated by the acoustic array was removed for the sake of clarity.

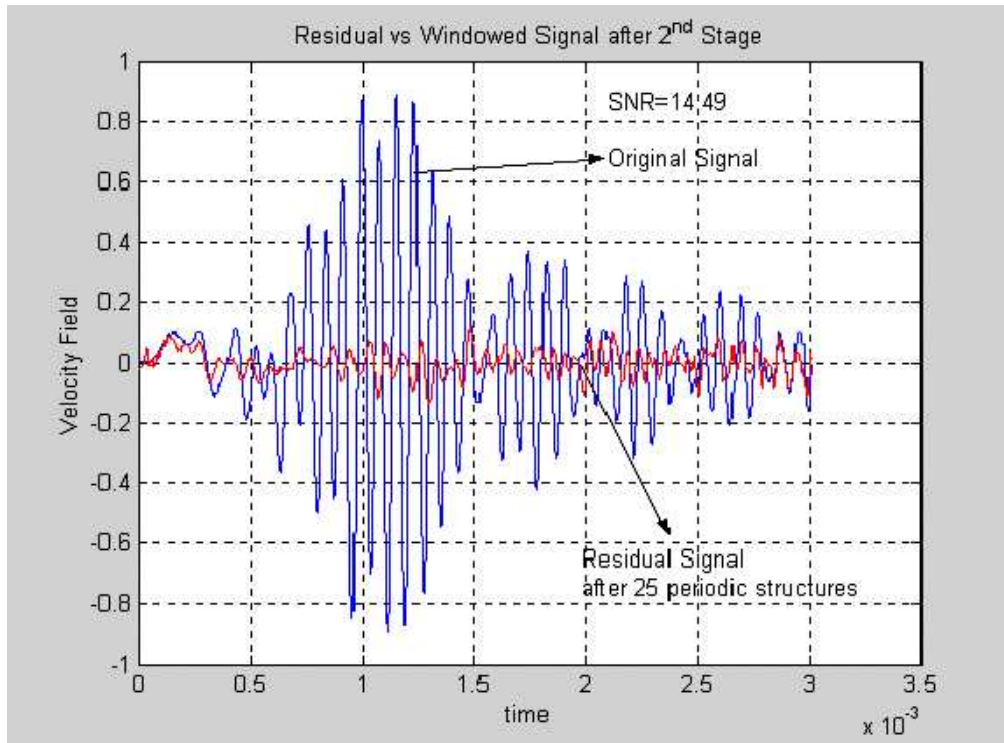


Figure 6.19: Incoming signal and directional array output after two stages

6.5 Hammer Pulse

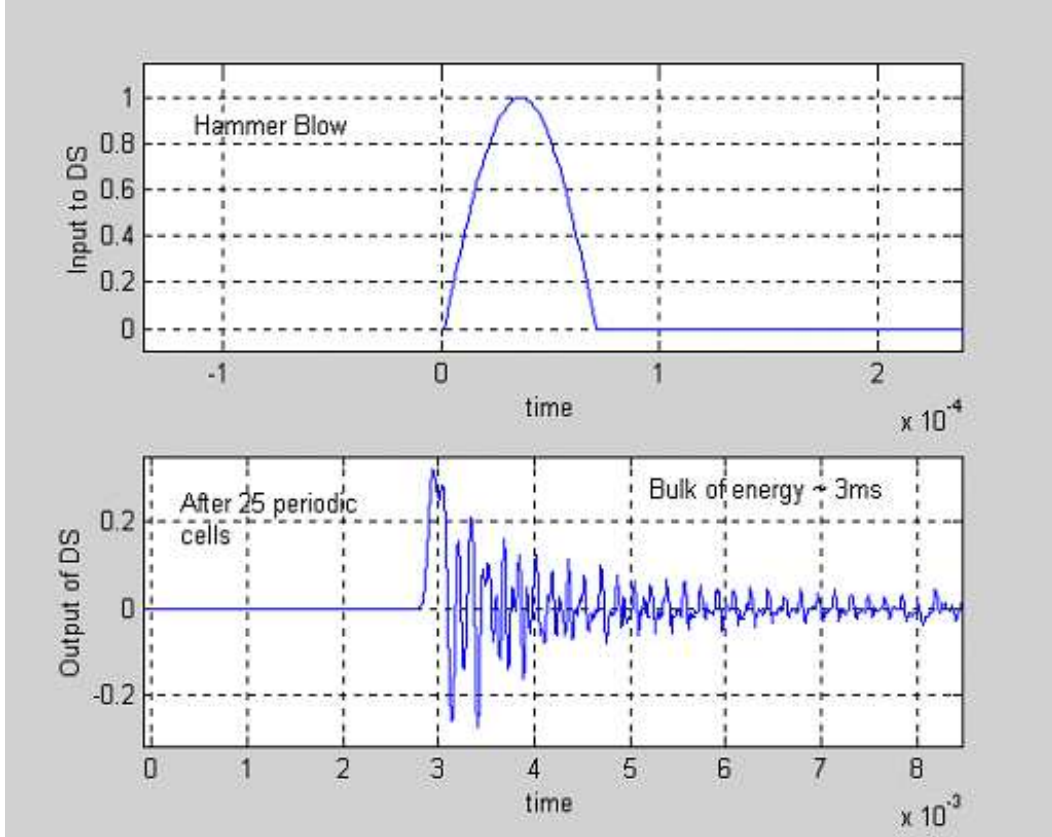


Figure 6.20: Hammer input and output of twenty five periodic structures

As mentioned in Section 6.4, the directional array presented here is incapable of generating the DC component of the even half range expansion without modifications to the input signal. The response of the drill string to a hammer blow input ⁵, is used to assess the performance of the directional array for signals that have a strong DC component. The hammer input and output

⁵A signal which has a strong DC component.

emerging out of the periodic structure after travelling twenty five unit cells is shown in Figure 6.20. The output signal and its windowed output is shown in Figure 6.21.

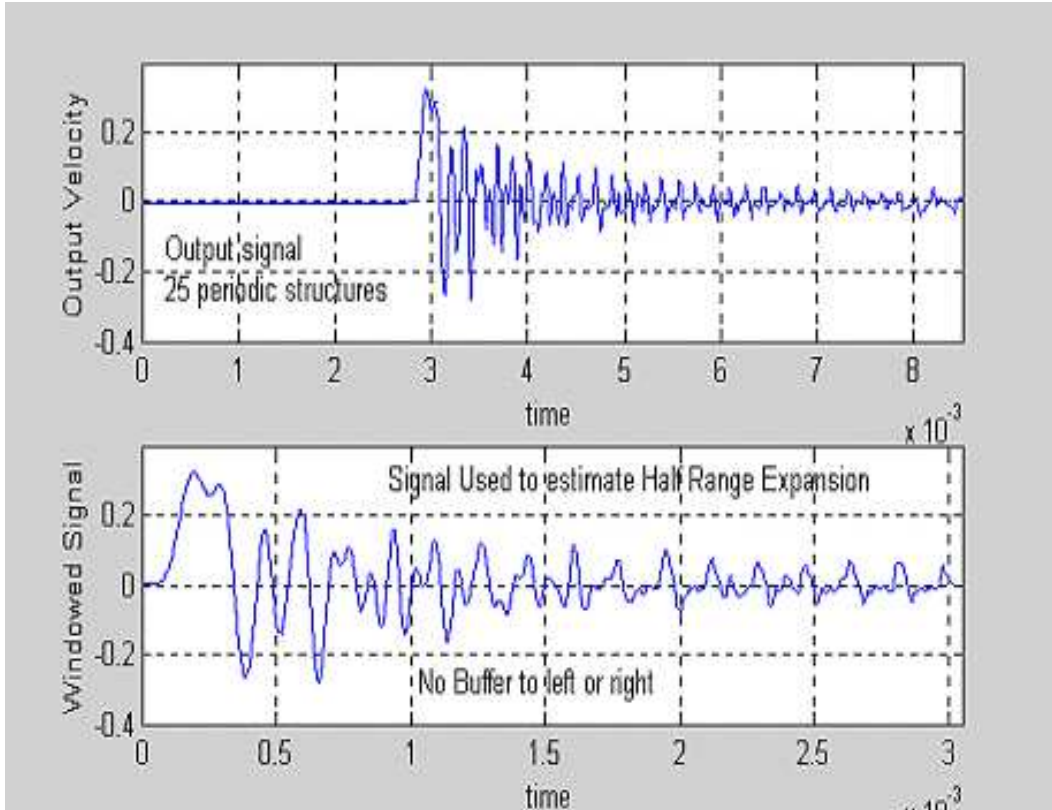


Figure 6.21: Drill String response to hammer input and windowed output

The harmonic frequency content of the drill string response to the hammer input, along with the *binary decision* map used to define the transducer firing sequence is shown in Figure 6.22. Note that the harmonic frequency content has strong components between the 1 and 75th harmonic, indicating the low frequency nature of the hammer response.

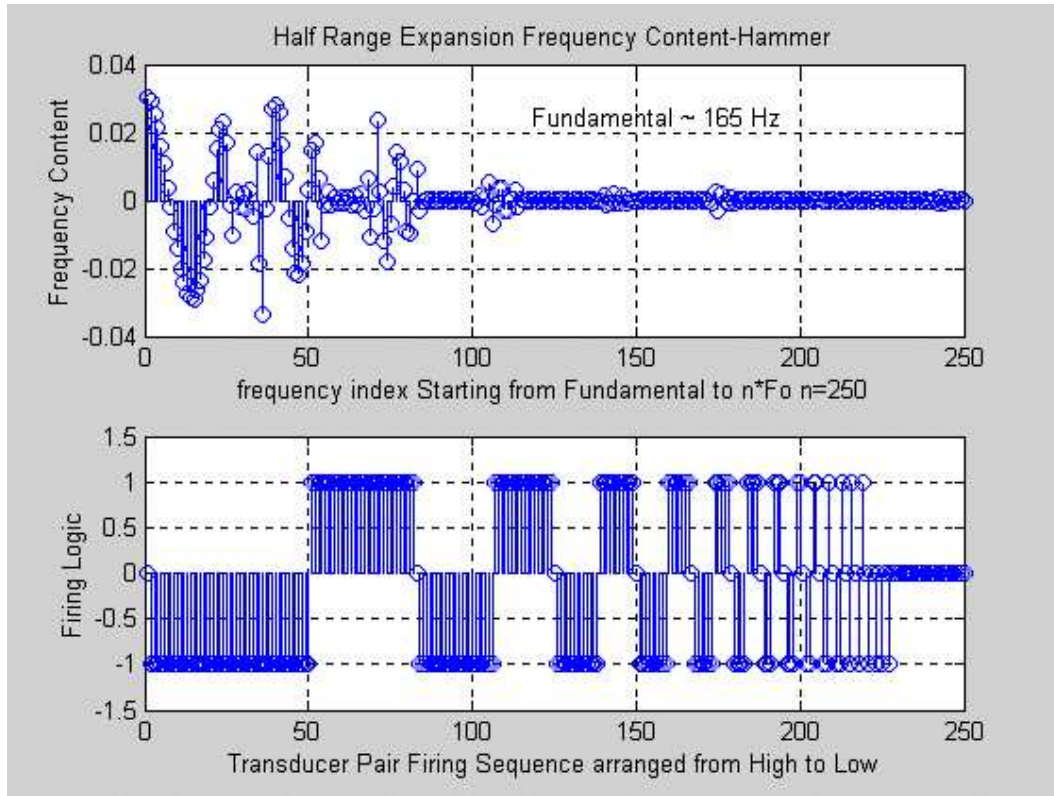


Figure 6.22: Half range expansion - coefficients and firing sequence

Figure 6.23 shows the original windowed signal and the output of the first stage of the terminating impedance. Two key features to note is the poor initial convergence at the beginning of the signal, and the duration and magnitude of the injected noise at the tail end of the signal. For the first $300\mu\text{sec}$ the directional array struggles to generate a signal that tracks the windowed input. The array output approximates the initial peak, except for its amplitude, which is roughly half of what is needed.

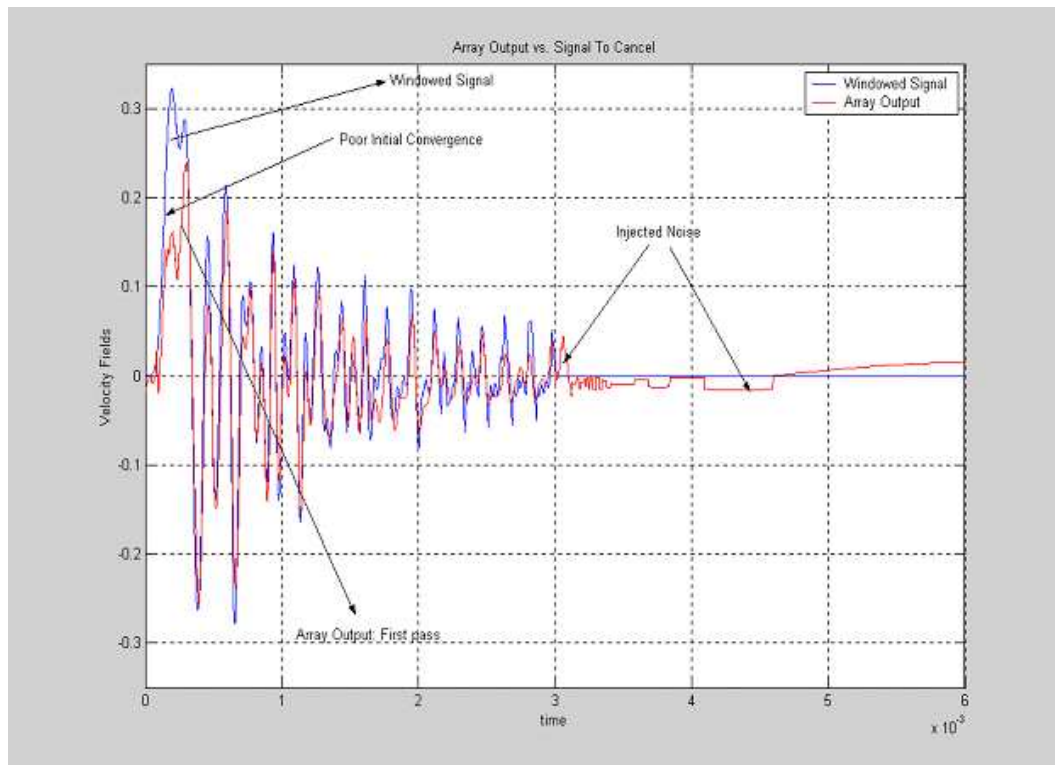


Figure 6.23: Original and generated signal - First stage

This is consistent the analysis of a transducer pair tuned to transmit a directional sinusoidal train. The first half cycle of the sinusoidal pulse is only half of the required amplitude. The injected noise is the consequence of dominant low frequencies. Note, however, that the directional array is able to track the initial sharp gradient of the signal. This capability is a function of the initial windowing of the incoming acoustic signal. The original windowing is repeated below in Figure 6.24. Note that the windowing allowed a small *Dead Zone* at the beginning of the signal - the input signal to the directional array is purposely “doctored” in order to gain better convergence.

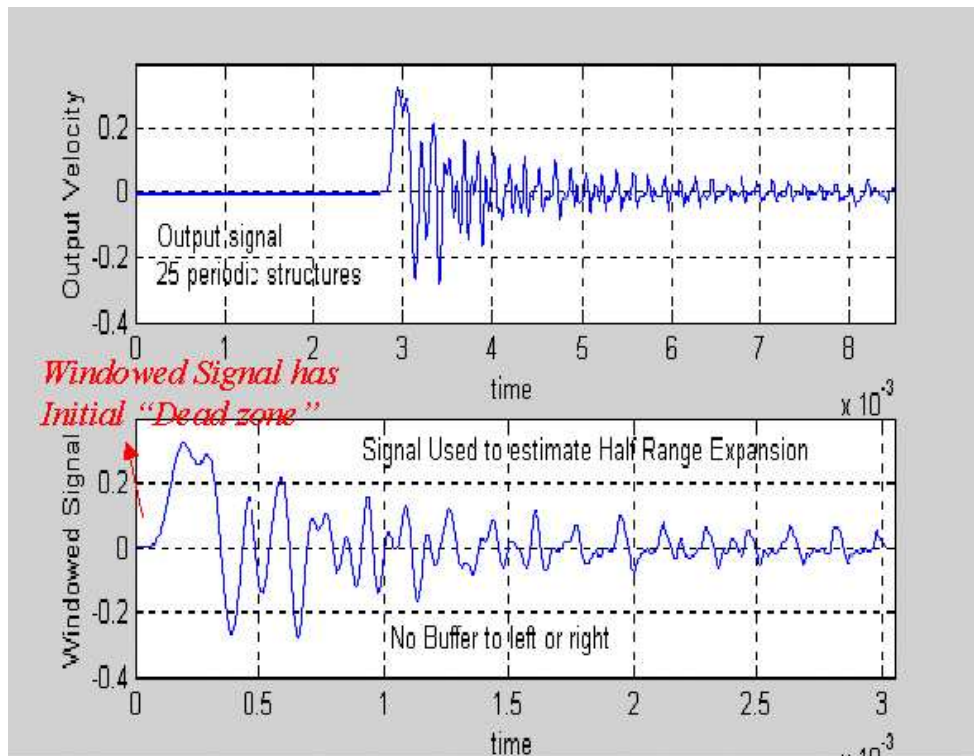


Figure 6.24: Hammer pulse with dead zone

Due to the directional array’s inability to perfectly track the (hammer

output) signal in the early stages, the dead zone submits a request to generate a half range expansion which will have poor convergence in the dead zone - a *don't care* region, while improving the convergence over the reduced convergence zone. Figure 6.25 illustrates the concept.

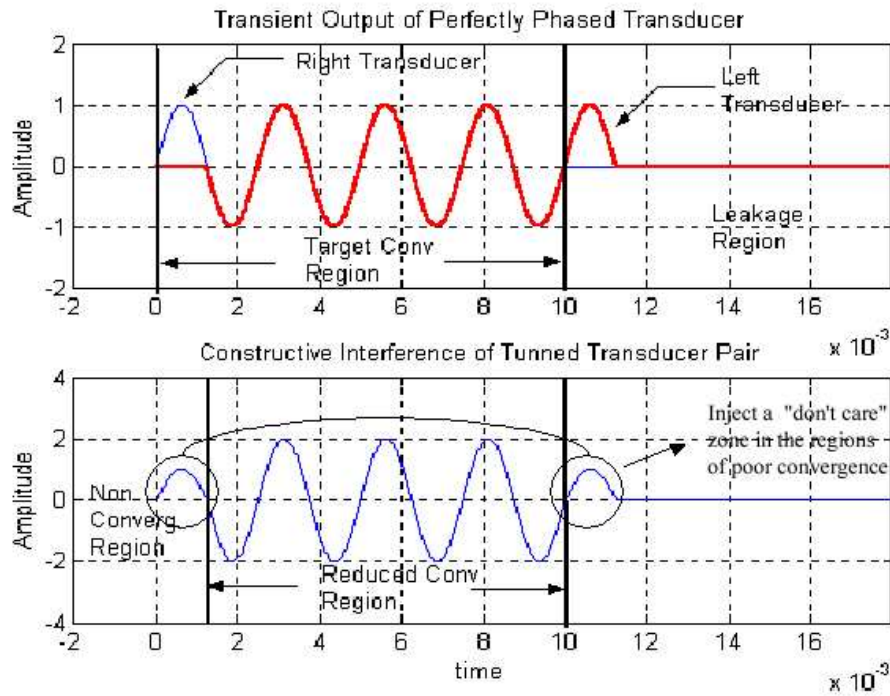


Figure 6.25: Injecting a dead zone for improved convergence

The *don't care* region allows for the bulk of the acoustic energy to be defined over an extended convergent region. This increases the performance of the directional array at the expense of computational time and increased design space. Figures 6.26 shows the synthesis of the waveform by the directional array at various transducer interfaces. The top of the figure shows the velocity

field generated at the face of the first transducer pair. The signal's accuracy is dramatically increased at the 22nd transducer pair, and by the time it reaches the final *master* transducer, it is synthesized as accurately as possible with the frequency limitations of the PZT transducers and dead zone. Note how the injected noise is largest at the beginning of the synthesis and decreases as more transducers are included in the generation of the acoustic signal. This is because the injected noise is not phased to constructively add to form any portion of the original signal.

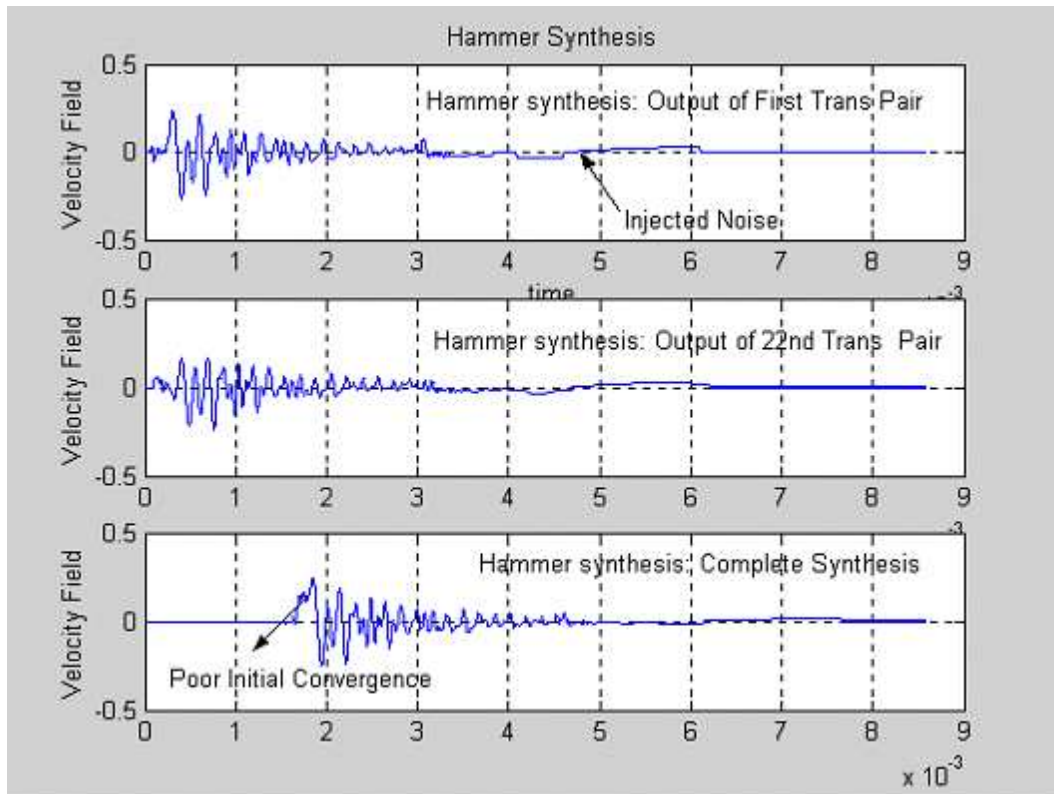


Figure 6.26: Signal synthesis as a function of distance along the array

The cancellation from the first stage of the terminating impedance using a small dead zone is shown in Figure 6.27. The first stage is capable of reducing the original signal by about $5dB$.

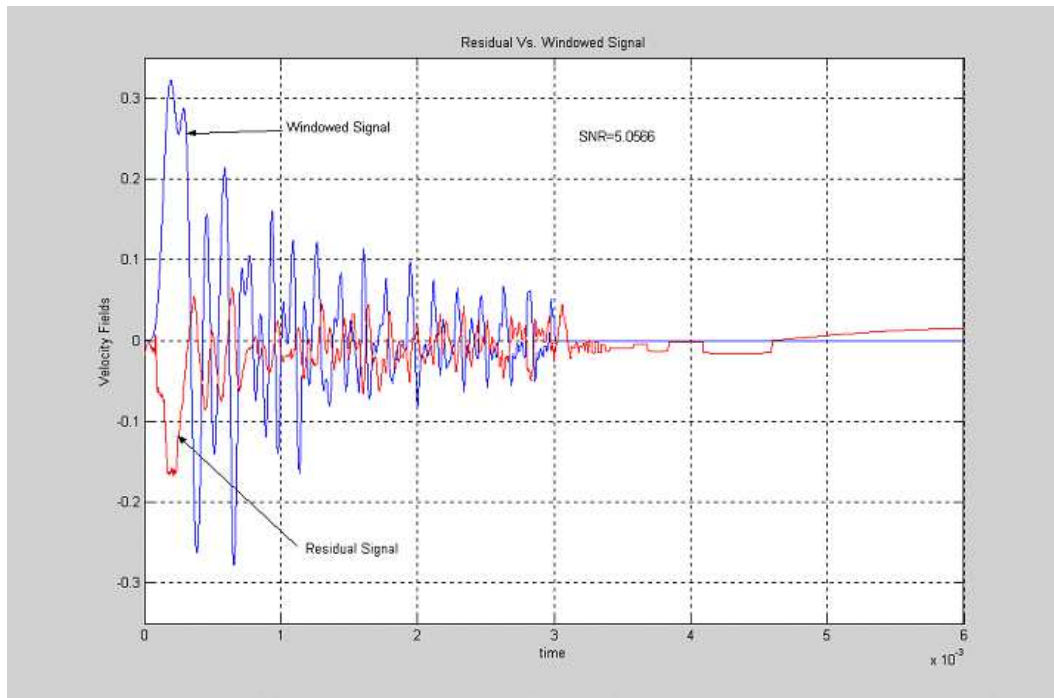


Figure 6.27: Original and reduced hammer pulse - first stage

Once the dead zone is extended both at the beginning and tail of the incoming signal, the directional array does a much better job at mimicking the extended acoustic wave. The top of Figure 6.28 shows the windowed signal and output produced by the directional array. Note how well the directional array is able to track the original at the beginning and end of the signal. The performance of the first stage of the terminating impedance is almost doubled by increasing the dead zone at the beginning and end of the signal. The

first stage suppresses the original signal by almost $10dB$. The price for this performance, is of course, an increased design space. The windowed signal is now almost $6ms$ in length - assuming a wave speed of about $5000\frac{m}{s}$ for steel, this translates into roughly 100 feet of pipe.

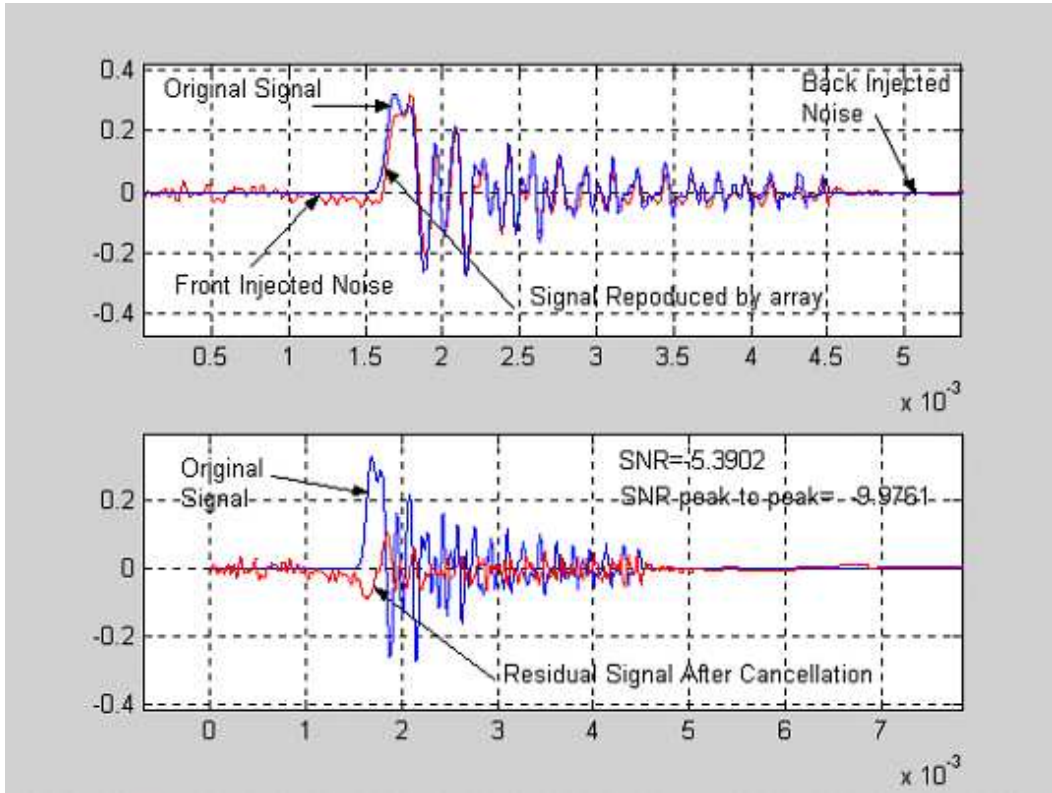


Figure 6.28: Extended dead zone into the hammer pulse

Reducing the initial dead zone to minimize design space provides an acceptable solution. Figure 6.29 shows the effect of reducing the initial dead zone to a reasonable amount. The first stage of the terminating impedance is able to reduce the original signal by about $8dB$, and the second stage brings it down to about $12dB$. For signals with strong DC component, the length of the acoustic array can not be minimized by excluding the second and third harmonics without paying a significant penalty in the accuracy of the signal produced by the directional array.

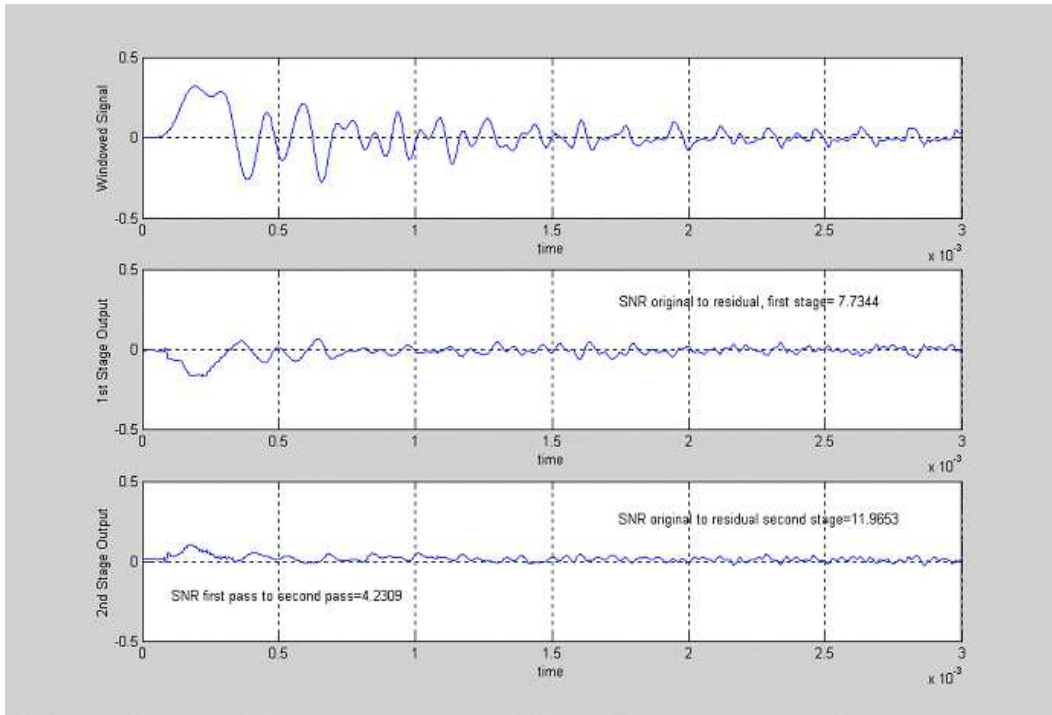


Figure 6.29: Original, first and second stage signals

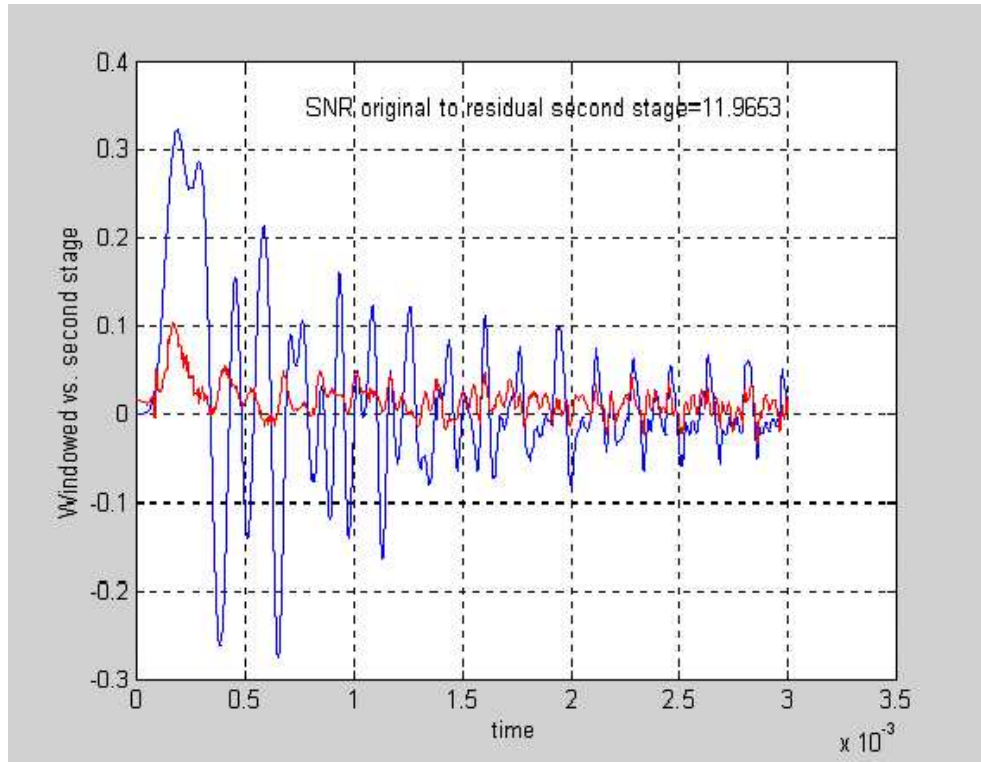


Figure 6.30: Windowed signal and residual signal after second stage dead zone used

Figure 6.30 shows the original windowed signal with a reduced dead zone and the output of the second stage of the terminating impedance.

6.6 Double Hammer pulse - One Sinusoidal Cycle in the Middle of the 3rd Pass Band

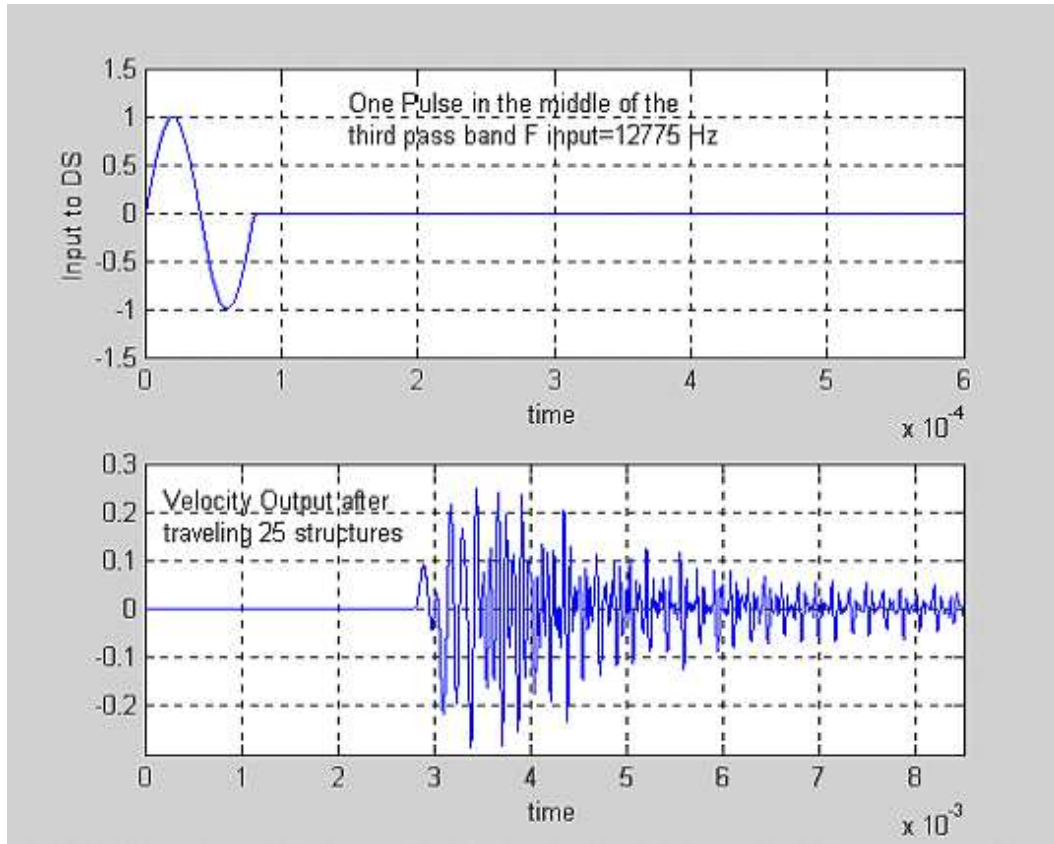


Figure 6.31: Double hammer input and drill string response

The last type of signal examined is a *Double Hammer* signal. The hammer⁶ blow used in the previous simulation is augmented by a tensile counterpart. This type of signal provides the broadest band possible, while removing the *DC*

⁶A hammer blow to the first unit cell of the drill string can be approximated by half of a sinusoidal cycle of about $60\mu\text{sec}$.

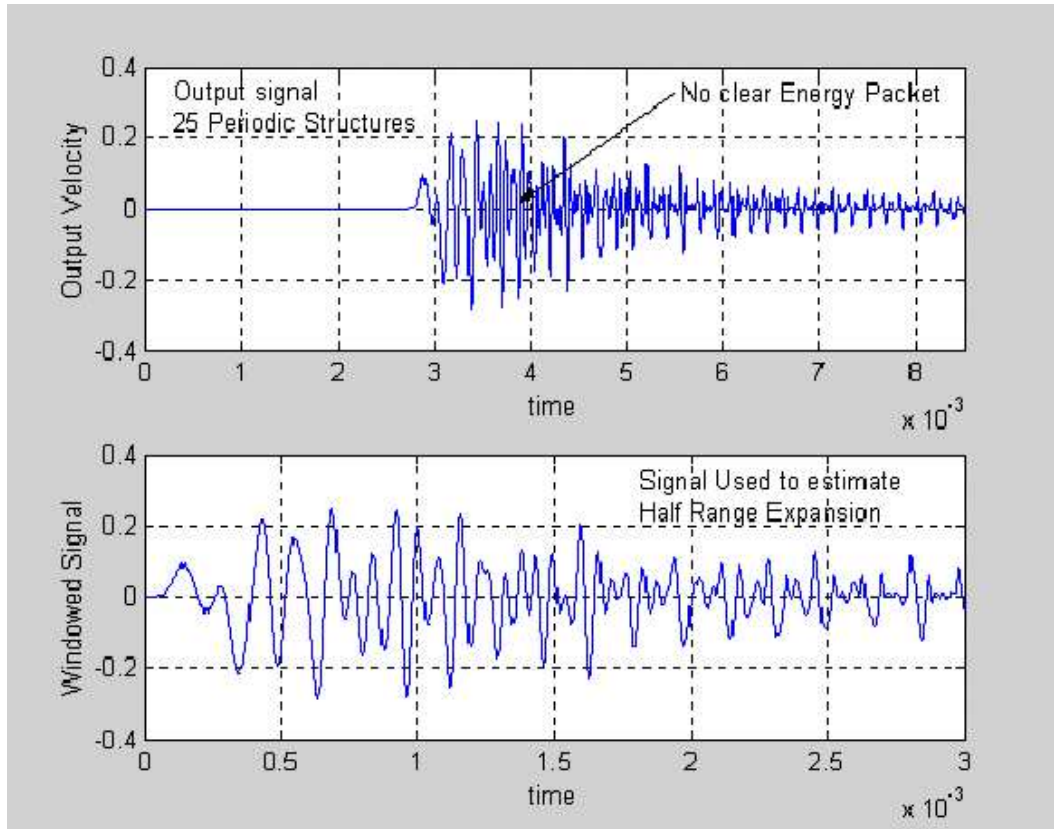


Figure 6.32: Double hammer input and windowed signal

component. The dominant frequency lies in the middle of the third pass band. Figure 6.31 shows the input signal and the drill string response. Although there is no clear energy packet, the biggest activity within the output signal happens in the first 3ms of the signal.

The bottom of Figure 6.32 shows the windowed signal with a small initial dead zone.

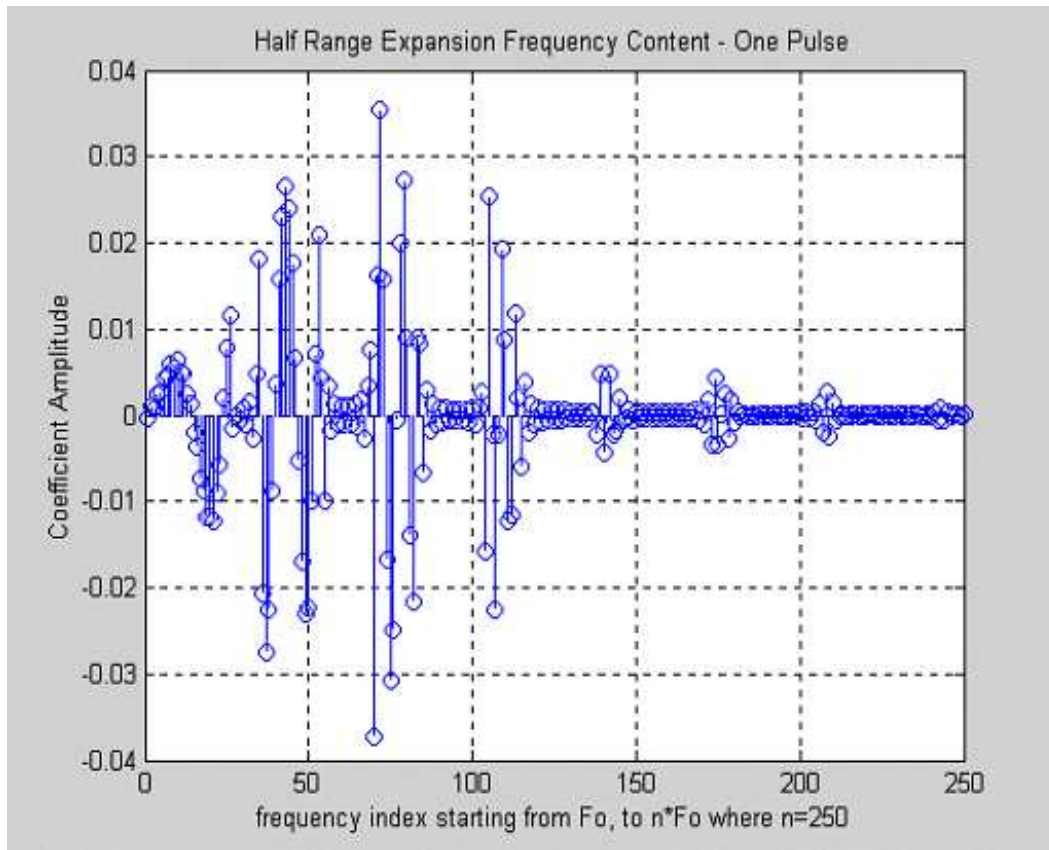


Figure 6.33: Half range expansion coefficient and harmonic frequency content

Figure 6.33 shows the frequency content of the drill string response to the double hammer input. Note that it is not dominated by low frequencies, compare to a single pulse.

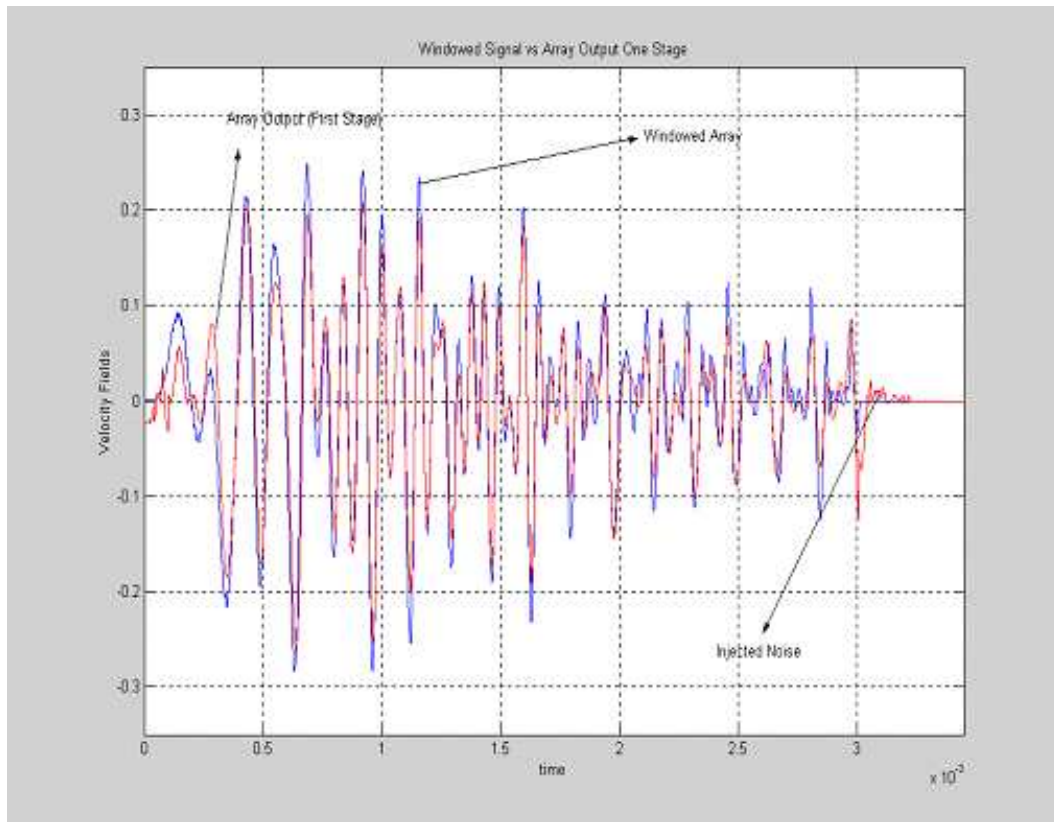


Figure 6.34: First stage output vs. windowed signal double hammer

Figure 6.34 shows the output of the directional array relative to the original windowed signal.

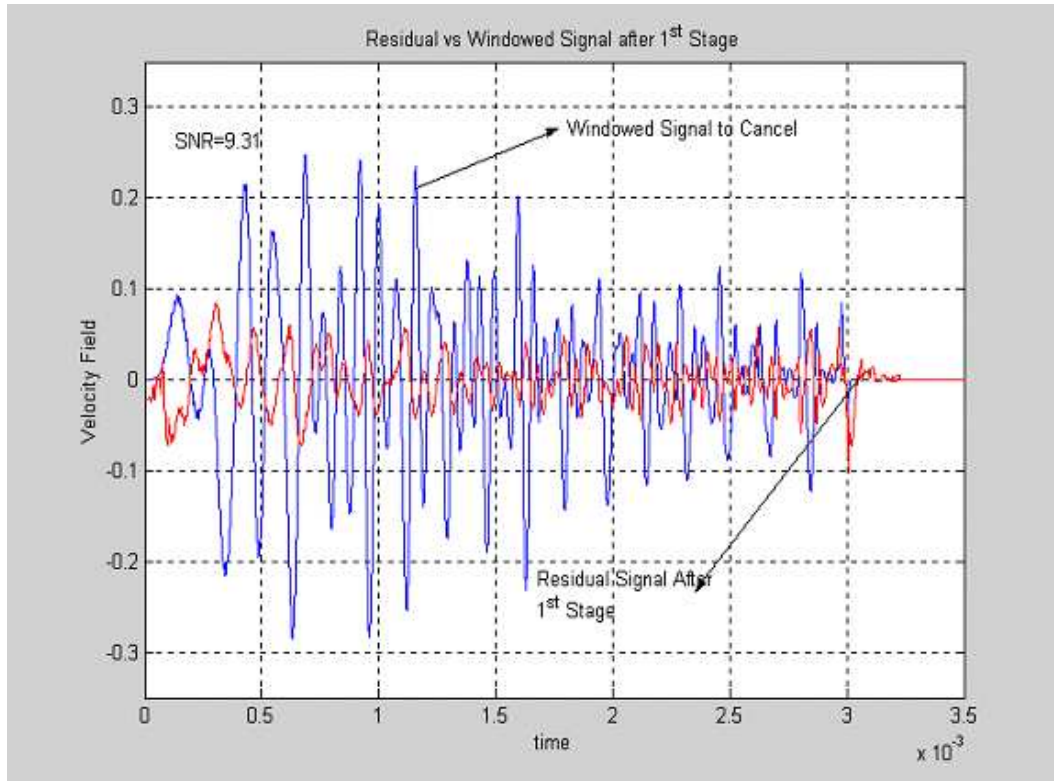


Figure 6.35: Residual after 1st stage vs. windowed Signal

The residual after the first stage of the terminating impedance relative to the original windowed signal is shown in Figure 6.35. The removal of a strong *DC* component allows for the first stage to achieve a $9.3dB$ noise reduction.

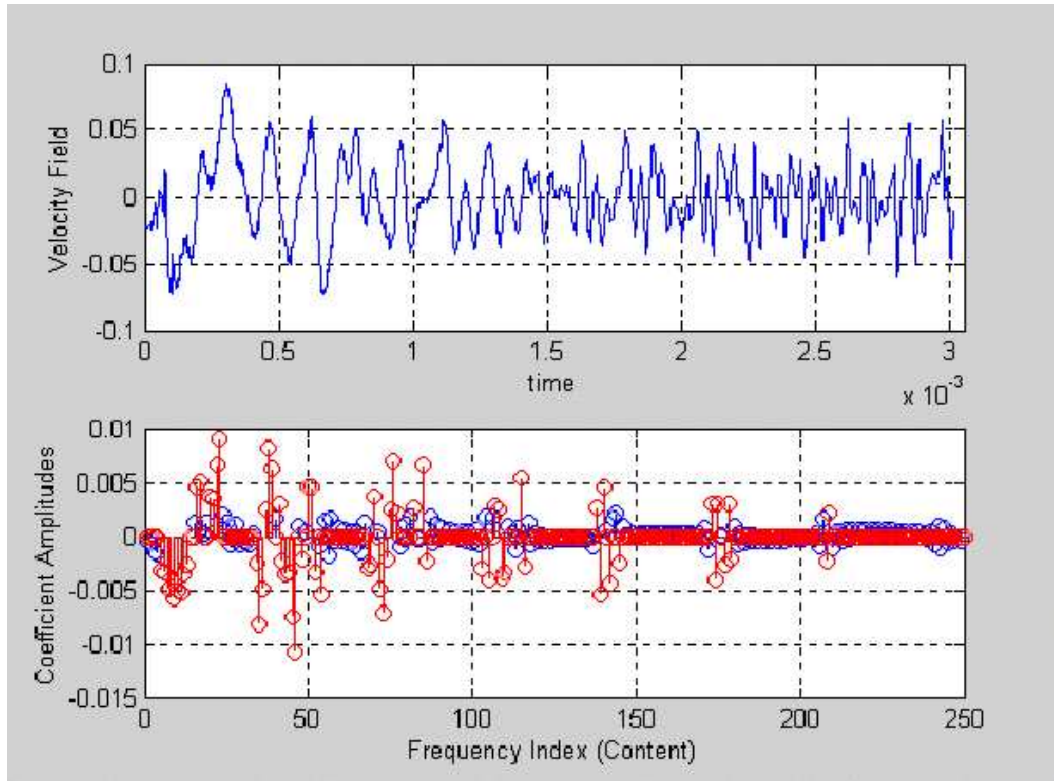


Figure 6.36: Residual fed to the second stage & HRFE frequency content

The residual is subsequently fed into the second stage of the terminating impedance for cancellation. Figure 6.36 shows the residual after the first stage and its frequency content. Again, only dominant frequencies are passed on to the algorithm for synthesis.

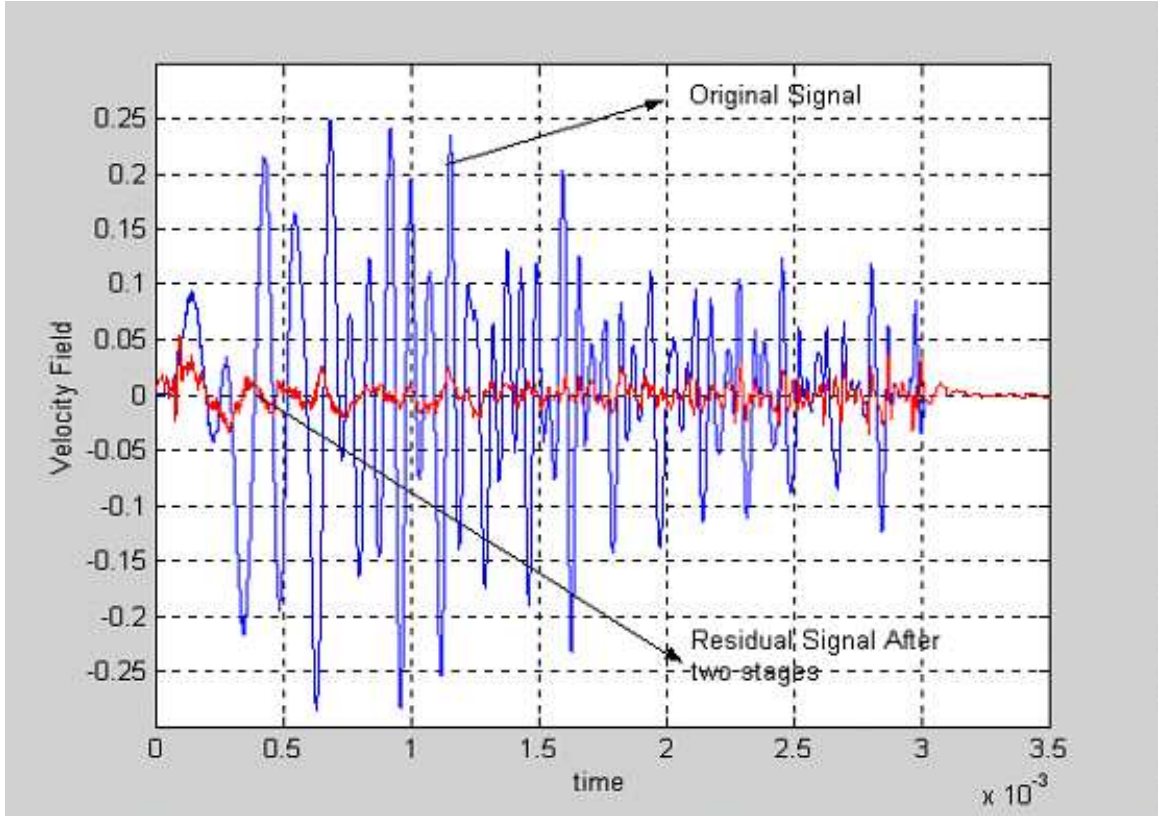


Figure 6.37: Second stage residual vs. windowed signal

The performance of the two-stage terminating impedance is best captured by Figure 6.37. The very complex original signal has been reduced significantly by $16.23dB$.

6.7 Concluding Remarks

The goal of this dissertation was to develop a method to generate directional acoustic plane waves in an isotropic solid waveguide. The remaining of this

section is devoted to describing the sequence that lead to the algorithm developed in Chapter 4.

First, it was necessary to characterize the type of signal which needed to be cancelled, as the directional array had to be capable of generating waveforms emerging from a highly dispersive and filtering structure. The work presented in Chapter 3 summarizes the characteristics of the drill string. It is a brief overview of the work done by Drumheller at Sandia National Labs.

The second step was to understand the behavior of the PZT transducers. Using field-tested, finite difference models of PZT transducers, the algorithm developed exploits the behavior of PZT's in the low frequency domain; which is that of a differentiator. This behavior can be quantified via an impulse response. Understanding the relationship between the electrical inputs to the transducers and the acoustic waves generated, lead directly to investigating the possibility of synthesizing the acoustic waveform using a Fourier Series decomposition. A decomposition of this type is usually reserved for periodic phenomena. Its continuous counterpart, the Fourier integral, is the appropriate mathematical tool for broadband signals. However, by injecting the electrical signals for a finite length of time, the Fourier Series decomposition can be used to generate transient signals in a waveguide. This technique allows the transducer to generate individual basis functions, which can be used to synthesize complex waveforms. The electrical inputs to the transducers need to be modified to compensate for the impulse response. The synthesis takes place with a finite number of terms with well defined coefficients. Thus, a

Fourier Series decomposition is almost a more “natural choice” for the problem at hand.

The decomposition technique was first used on a single transducer. It was shown that a single transducer, using 80 to 250 harmonics can accurately synthesize a broadband signal. This is for all practical purposes provides “infinite” precision.

Next, directionality had to be incorporated into the system. The well known quarter wavelength design for generating steady state signals was modified and expanded for broadband signals. It was shown that it is possible to generate directional transient waves using a finite set of properly spaced, phased transducer array using a “common” source. This requires an optimal load distribution system, which distributes the wave packets amongst the transducer pairs available. The common transducer design allows for a compact array. The directional array is defined using the length of the signal to be cancelled - L , thus it is robust to frequency and temporal variations. The possibility of reducing the design space by excluding the first two harmonics has been explored, and very good results have been obtained for the type of signals presented here. Excluding the first few harmonics reduces the design space significantly (by over half). The design is also robust to the length in the periodic structure. The algorithm presented here should be looked upon as a *design* tool to be used to down select an array configuration along with its corresponding electrical inputs. The algorithm allows the user to change the dimensions of a two cell periodic structure, the transducer type and di-

mensions, the number of cancelling stages, and the length of the incoming signal. The last is perhaps the key features of the algorithm, as the length of the signal determines the transducer layout. The length of incoming signal depends on the properties of the feeding structure tied to the cancelling array, and the original input signal to the feeding structure.

One final, but important note is that the work presented here is limited to its scale. The dimensions of a drill string are 20 times of those presented here. Assuming a full scale drill string of the same length (using 25 periodic structures), and a linear scaling factor of 20; even using the best case scenario in which both terms (sine and cosine terms) of the Fourier decomposition could be used, a signal lasting $3ms$ would translate to over 76 meters ($250ft$) of pipe. Taking it one step further, and assuming the first four harmonics will not ever be dominant in the harmonic content of the incoming frequency, this length is reduced to 15.39 meters ($50ft$). The design presented here is limited⁷

6.8 Suggestions for Further Study

The techniques presented here are not without their drawbacks. First, the low sensitivity of the PZT transducers demand large input potentials. The computational time necessary to define all of the inputs to the transducer has not been defined. It is suspected of being large. The time to perform all of the calculations proposed here in a real time DSP is of great interest, as it will

⁷The dimensions above double if only a Half Range Expansion can used to synthesize the waveform. Likewise, if the length of the signal is confined to the first $1ms$ and a full blown series representation, the dimensions above are reduced by one third.

test the convergence rate of the algorithm relative to the speed of the incoming wave. Also, there is very little room for error in the timing between transducer inputs, as all of the waveforms must constructively add at a specific point in space.

The directional array defined here introduces a “non-convergent zone” at the beginning of the signal and leakage at the tail end. This phenomena is inherent in the design but can be side stepped by including a dead zone in both regions but at the expense of computational time (which translates into a larger design space). The robustness of a physical design should be tested against the results presented here. This includes addressing all of the drawbacks discussed above.

Finally, a waveguide and transducer design with tight tolerances, and well characterized transducers is a prerequisite for testing all of open questions left behind by this dissertation.

Appendix A

Experimental Set up

A.1 Introduction

This appendix describes the experimental set up used to show proof of concept of the directional waveguide described in Chapter 4. Appendix B summarizes the numerical algorithm used to simulate a broadband directional array. The proof of concept consists of verifying the steady state directionality of the acoustic array, as well as verifying the directionality of a sensing array at a specific frequency.

A.2 Experimental Set Up

Initially the experimental set up was designed to be six PZT transducers embedded in a uniform solid brass waveguide. After several iterations of testing the transducer performance, it was determined that the amplification needed

to transmit acoustic signals of significant amplitude was not available. The experimental set up was changed to a hollow cylindrical air filled waveguide, with loud speaker mounted acting as point sources. The dimensions and geometry of the experimental set up used is shown in Figure A.1.

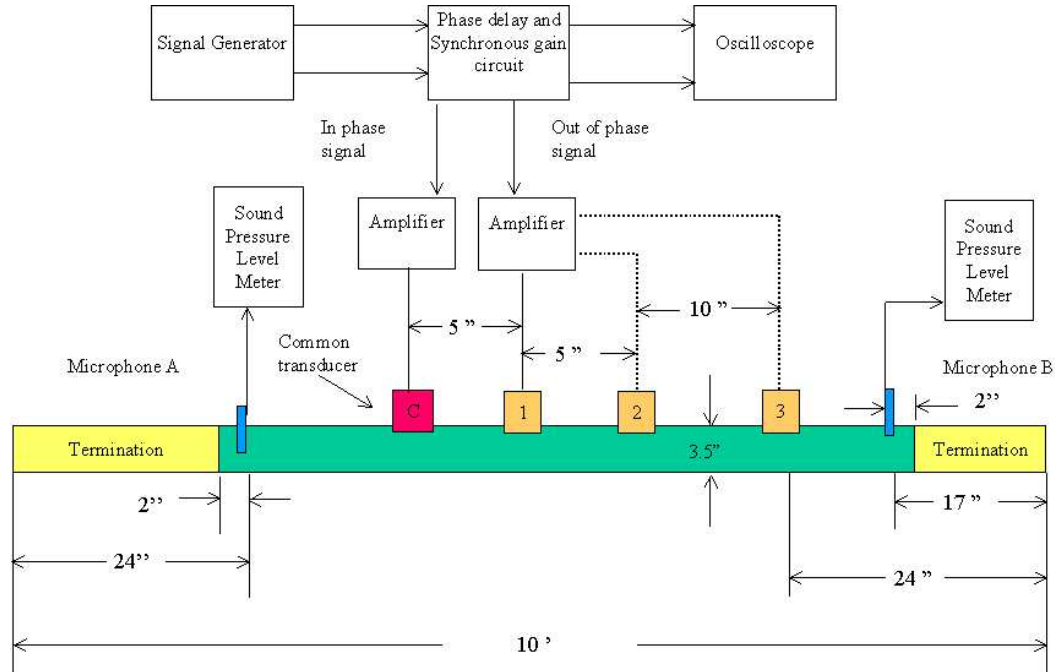


Figure A.1: N-fire directional array

The modularity of the acoustic waveguide allowed for rapid changes in the configuration to accommodate all of the experimental set ups described herein. The dimensions of the waveguide were chosen based on the available experimental space in the Electro Acoustics Laboratory - The University of Texas at Austin. This in turn determined the frequencies of the signals which could be bench marked.

The remainder of the appendix is divided in four sections:

1. Section A.3 describes the experimental setup used to show proof of concept of the directional source array discussed in this dissertation.
2. Section A.4 describes the experimental setup used to show proof of concept of a directional sensing array.
3. Section A.5 briefly discusses the conclusions of Sections A.3 and A.4.

A.3 Directional Array

To generate a directional wave we need two sources embedded in a waveguide spaced one quarter wavelength apart. The electrical inputs to the sources must be shifted by 90 degrees, of equal magnitude and opposite in phase. The sources for the experimental set up are a set of loudspeakers. The electrical inputs are generated two at a time to benchmark the directionality properties of all three transducer pairs shown in Figure A.1

Hardware and Experimental Set Up

A sinusoidal electrical input of $400mVPP$ was generated using a Hewlett Packard 33120A Arbitrary Waveform Generator and was fed into a phase delay analog circuit, which imposed the 90 degree shift on the original signal. A resistive pot was varied until the phase delay between the two signals was 90 degrees. The phase delay was verified on an oscilloscope using the $X - Y$ output of the input and phased delayed voltages. The original and the phase

shifted, inverted signal were used to drive the common (or slave) speaker and the master speaker, respectively.

The speed of sound was assumed to be $343 \frac{m}{s}$. The spacing between the speakers was selected to fit within a reasonable laboratory set up of about $14ft$. The theoretical frequencies, given the assumed speed of sound and the quarter wavelength spacing between the transducers, are $643Hz$, $350Hz$, $171Hz$ for the first through last transducer pair, respectively. However, it was found that the input signals to the first transducer pair could only be properly phased at a slightly higher frequency of $710Hz$. Speakers 2 through 4 are identical, while speaker 1 was selected to handle all of the input frequencies. The speaker selection was based on the frequencies selected to be benchmarked. The directionality of each of the speaker pairs was tested independently. The waveguide was terminated using fiberglass to minimize reflections from either end.

For all cases, the common transducer was driven by the un-phased signal generator, and the downstream acoustic signal was measured using microphone B and a sound pressure level meter. The acoustic signal generated by the common transducer was amplified to $80dB$ via a Mackie FR series *i400i* Professional Amplifier and held. The common transducer was subsequently disconnected and the master transducer was tuned to the same decibel level. This procedure assured two equal magnitudes, 180° out of phase, and properly delayed acoustic signals within the waveguide. After each of the transducer outputs had been independently tuned, both of them were fired in concert. The sound pressure level was measured using microphone B the location which the

acoustic signals added constructively and at microphone A, where no signal was expected. The procedure was duplicated reversing the role of the master and slave speakers for all of the speakers available. The results are summarized in table A.1 below.

Results

Speaker Selection	Input Frequency	dB Reduction Right	dB Reduction Left
Slave \iff Master 1	$f_1 = 710Hz$	$-29dB$	$-28dB$
Slave \iff Master 2	$f_1 = 350Hz$	$-21dB$	$-19dB$
Slave \iff Master 3	$f_1 = 171Hz$	$-1dB$	$0dB$

Table A.1: Experimental results - array Directionality

The experimental set up shows that steady state directionality for all speaker pairs is very good, except for the Slave \iff Master 3 pair at $171Hz$. The suspected reason for this is the reflections from a less than ideal termination and a wavelength in the order of $2m$ with only 2 inches separating the termination impedance and the microphone. The microphone is suspected of picking up not only the incoming signals but also those reflected by the terminating impedance.

A.4 Directional Sensing Array

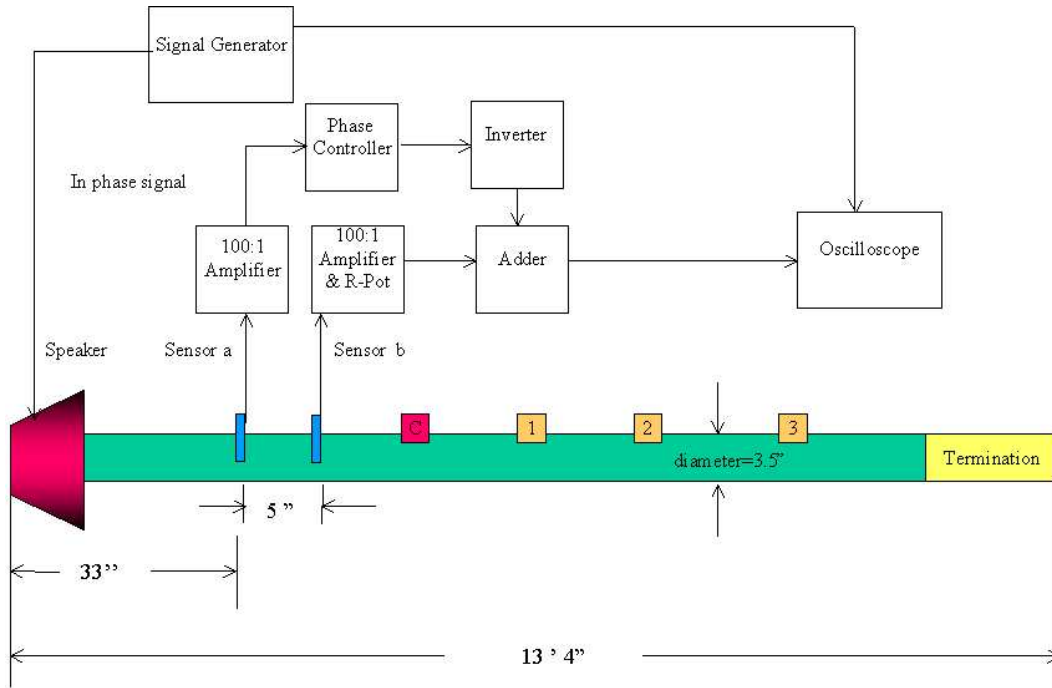


Figure A.2: Directional sensor - experimental set up

The directionality of Drumheller's [56] sensor array was verified experimentally using the set up shown in Figure A.2. The microphone pair shown is designed to pick up waves travelling in one direction and ignore those from the opposite direction. The directional sensing array is tuned to a specific frequency by the spacing between the two microphones. The loudspeaker on the far left serves as the input to the microphone array.

Hardware and Experimental Set Up

The microphones were spaced 5 inches apart corresponding to a frequency of $710Hz$. The sound source is a speaker mounted at the far left-end of the waveguide. The electrical input to the source is a $710Hz$, $1.54VP - P$ signal. Each of the microphones feeds into an analog amplifier circuit one of them continues to a phase controller circuit, followed in series by an inverting amplifier. Both of the signals from each of the microphones are added together to obtain a directional output. The amplifier for the right-most circuit has a $10k$ resistive pot to compensate for any mismatches in the gain of the operational amplifiers. The phase delay and amplitudes of the microphone array were optimized to obtain the maximum output for wave travelling from the (speaker) source towards the fiber glass termination. The order of the microphones was swapped to verify that directionality was obtained.

It was shown experimentally that the transducer array was able to differentiate between a positive travelling wave from a negative travelling wave by a $30dB$ difference.

A.5 Experimental Set Up: Conclusions

The experimental results show that by properly spacing, delaying and phasing omni-directional sources and microphones, it is possible to design a directional transmitting and receiving array. Once directionality is obtained, properly delaying each of the electrical inputs should be able to synthesize the desired

transient directional signal.

Appendix B

Algorithm Description

B.1 Algorithm Description

B.1.1 Introduction

The goal of the dissertation was to design an array capable of reproducing an acoustic signal L seconds long and of arbitrary frequency content in one direction. The feeding structure to the cancelling array was a scaled model of the drill string.

The algorithm developed to simulate a directional array contains 17 main subroutines; however it can be described in four major subsections. Each subsection described here contains one or more subroutines. A flow diagram at the end of each subsection is presented to provide a brief summary.

B.1.2 Subsection I - Defining Array Inputs

This subsection obtains the velocity field emerging from a $\frac{1}{20}^{th}$ scale model drill string for a given set of input boundary conditions. The output of the drill string is used as the inputs to the directional array.

Geometry

This subsection defines the unit cell, geometry and length of the drill string. Two short (4 and 9 unit cells) and two long (16 and 25 unit cells) drill string configurations were used. The length of the drill string is limited only by the computational power available to the user.

Scaled Model Inputs

For a given drill string geometry, the algorithm bounds the real valued Brillouin zones and defines the input boundary conditions to the drill string as a set of sinusoidal pulse trains in the middle of each pass band. An additional broadband input, $60 \mu s$ in duration using half the cycle of a sinusoidal wave is used to simulate a “hammer”-like blow.

Scaled Drill String - Array Coupling

The modular drill string is connected to the directional array. The directional array consists of PZT transducers embedded in a uniform cylindrical waveguide. The cross-sectional area of the transducers is designed to match the acoustical impedance of its surroundings. Identical type II transducers, $5mm$

thick are used throughout the directional array. The boundary conditions on the other side of the directional array are infinite.

Scaled Drill String Output

The velocity field emerging from the drill string into the directional array is defined using a $3ms$ Heaviside window¹; which in turns defines the length of the directional array (see section B.1.3). The start of the signal can be modified to include “dead zone” buffers at the beginning and the tail end of the $3ms$ window. The right hand side of the window is an exponentially decaying tail, which minimizes abrupt signal endings. Windowing the signal mimics the output of a broadband directional sensor array.

Decomposition

Once the signal to be cancelled has been defined, it is decomposed into its even and odd half range expansion. The user defines the number of harmonic signals to be used to approximate the targeted signal, and an error analysis is generated to asses the effectiveness of the choice. Good results have been obtained using 80 to 250 harmonics.

¹The length of the windowed is based upon several simulations involving different drill string lengths and inputs. It was determined that a $3ms$ window is long enough to bound most of the acoustic energy contained in the emerging signal. Outside this window, the absolute value of the signal has decreased by about 80 percent.

Flow diagram of Defining Array Inputs

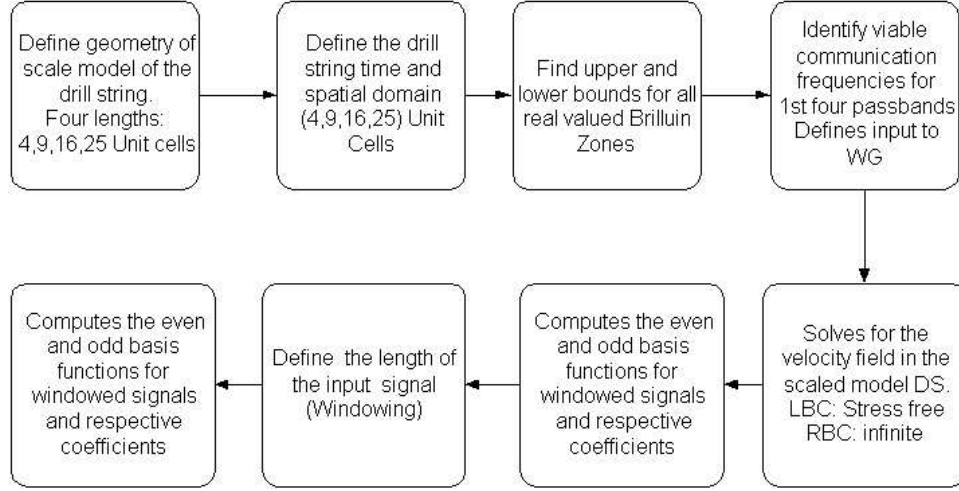


Figure B.1: Windowed drill string output incoming to directional array

B.1.3 Subsection II - Directional Array Definition

Subsection II lays out the transducers along the uniform waveguide using a geometric sequence spacing between the transducers. It defines the inputs to each transducer pair and optimizes the firing sequence to minimize the error between the generated and desired signal.

Defining the Directional Array

The duration of the signal to be cancelled, L , defines the length of the directional array. The total design space (DS) available using a common transducer configuration is given by Equation B.1 and shown in Figure B.2, where c is the speed of sound, L is the duration of the signal, δ_t is the thickness of the transducer and λ_0 is the fundamental wavelength given by Equation B.2.

$$DS = \frac{\lambda_0 + \lambda_n}{4} + \delta_t \quad (\text{B.1})$$

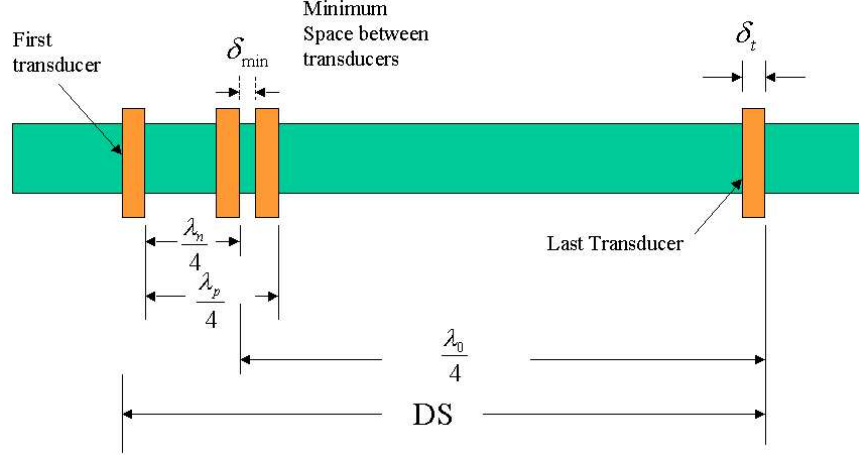


Figure B.2: Directional array design space

$$\lambda_0 = c2L \quad (\text{B.2})$$

Transducer Placement

A finite design space, transducer thickness, minimum spacing δ_{\min} and the geometric spacing between transducers limit the number of sources that can be placed along the waveguide. The bandwidth of the directional array appears to be limited by the available space. However, this issue can be side stepped by carefully designing a firing sequence between the available transducers. This subroutine places the maximum number of the transducers between the “first” and “last” transducers in the waveguide without violating any of the above constraints.

Wavepacket Load Distribution

The algorithm keeps track of the number of transducers placed, the location of the electrodes (for all transducers) relative to the origin², and the distance between them i.e. the “forbidden zones”.

Load Distribution

Finally, the subsection distributes the load (or wave packets) amongst the transducer pairs available. Some of the transducers will fire a wave packet composed of wavelengths that lie in forbidden zones to the left and right of the “master” transducer. The transducer of closest proximity to the wavelength contained within a forbidden zone is selected to fire that component of the Fourier decomposition. Figure B.3 summarizes the Wavepacket load distribution subroutine.

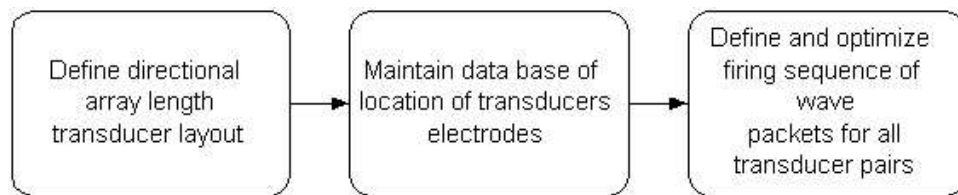


Figure B.3: Windowed drill string output incoming to directional array

Subroutine III - Transducer Gains

Once the directional array and the harmonic content of the output frequency has been defined, the algorithm must identify the transducer gains at the calculated harmonic frequencies. This is done by embedding the specific transducer

²This information is critical when deciding the transducers timing

selected into a uniform waveguide of the same dimension as the directional array and generating its impulse response. The subroutine verifies that the highest harmonic is within the frequency range in which the transducer behaves as an attenuating differentiator. The gains for each of the harmonic frequencies are obtained from the impulse response via interpolation. Once the geometry of the directional array and the gains have been identified, the force function β across the individual transducers, phase delays, delays between transducer pair and firing sequence can be defined. A database of the electrode location is kept in order to monitor the synthesis of the wave as it progresses across the array.

Flow Diagram

This Transducer Gains subroutine is summarized in Figure B.4

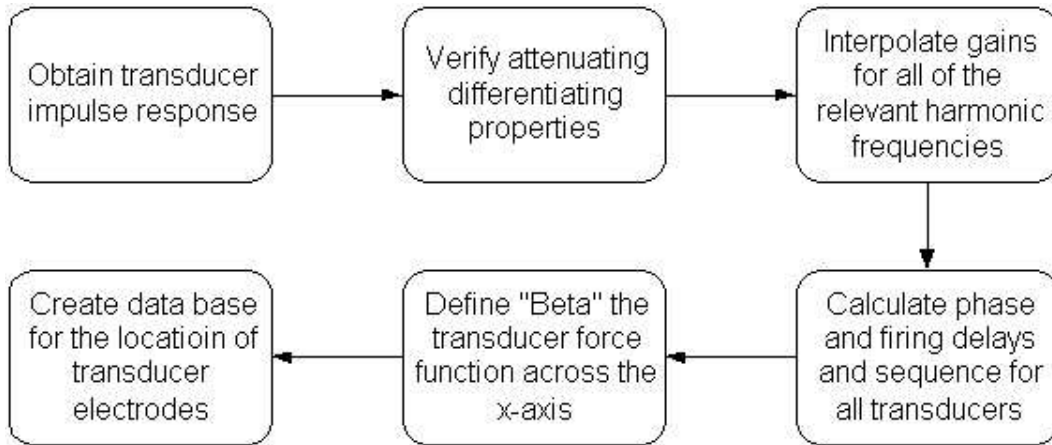


Figure B.4: Transducer gains algorithm

Subsection IV - Firing Sequence

Once the directional array has been laid out, and the inputs defined, the synthesis of the desired waveform begins. Figure B.5 shows a harmonically spaced transducer. Each transducer pair generates a directional, right travelling wave packets which are timed to constructively add at the end of each of the “master” transducers. A typical wave form is synthesized as follows: 1) transducer pair $C \iff 1$ fires a directional, right travelling wave packet. 2) transducer pair $C \iff 2$ awaits the arrival of the first wave packet and 3) when the signal from $C \iff 1$ arrives at the 2 – WG interface, the $C \iff 2$ fires its contribution to the final wave form. This process is repeated until the signal is completely synthesized at the 6 – WG interface. The signal emerging from the right-most electrode across the structure is the output of the directional array.

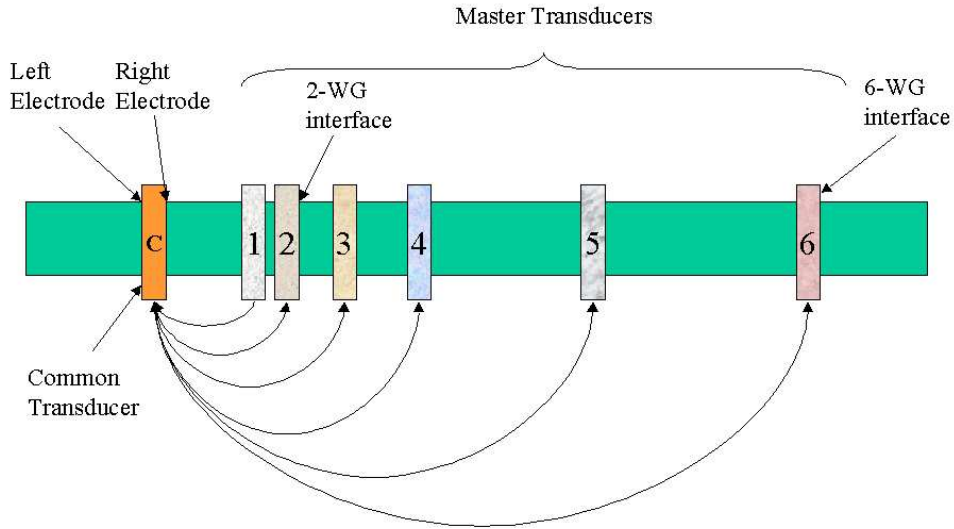


Figure B.5: Signal synthesis

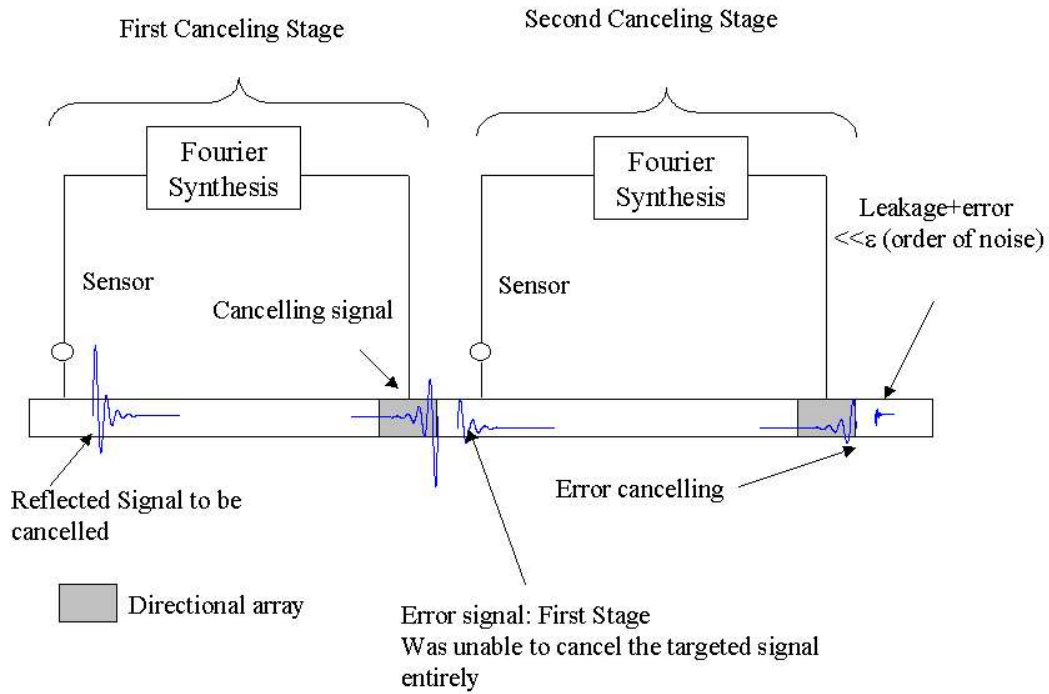


Figure B.6: Dual stage directional canceller

The output of the first stage directional array is compared with the signal incoming from the drill string. The First Stage Residual (FSR) is defined as: Drill String Output - Canceller Synthesis. The FSR now becomes the input to a second cancelling stage; identical in design as the original. The inputs to the transducers embedded on the second stage are defined using the same logistics and parameters used to define the inputs to the first stage. The output of the second stage is compared to its inputs and the original signal incoming to the first stage. Figure B.6 shows the concept of two cancelling stages acting on an incoming signal.

Flow diagram of the Firing Sequence

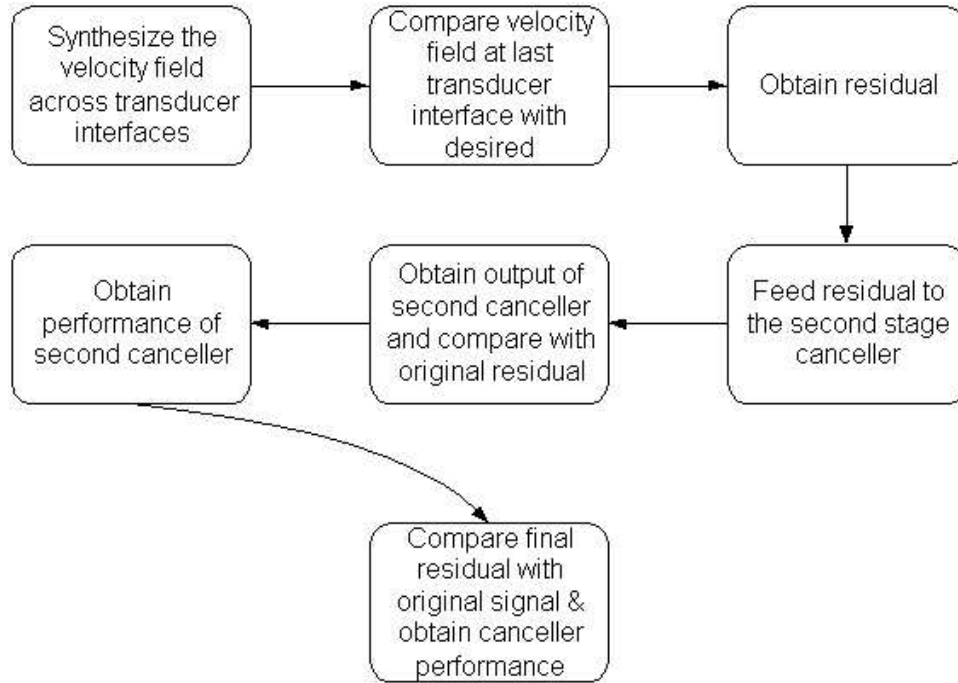


Figure B.7: Flow diagram of Subroutine IV

Figure B.3 summarizes the Wavepacket load distribution subroutine. A summary of Subroutine IV is shown in Figure B.7.

Bibliography

- [1] David T. Blackstock. *Fundamentals of Physical Acoustics*. Wiley-Interscience, 2000.
- [2] Leon Brillouin. *Wave Propagation in Periodic Structures*. Dover, 1953.
- [3] L.M. Brekhovskikh and O.A. Godin. *Waves in Layered Media*, volume 5 of *Springer Series on Wave Phenomena*. Springer-Verlag, 1989.
- [4] A. Bedford and D.S. Drumheller. *Introduction to Elastic Wave Propagation*. Wiley, 1994.
- [5] Douglas Drumheller. *Introduction to Wave Propagation in Nonlinear Fluids and Solids: Appendix A*. Cambridge Press, 1996.
- [6] Charles Elachi. Waves in active and passive periodic structures: A review. *Proceedings of the IEEE*, 64(12):1666–1698, December 1976.
- [7] E.T. Whittker and G.N. Watson. *Modern Analysis*. Cambridge University Press, 1952.

- [8] Philip M. Morse and Herman Feshbach. *Methods of Theoretical Physics Part I*. McGraw Hill Book Company, 1953.
- [9] E.L. Ince. *Ordinary Differential Equations*. Dove Books, 1926.
- [10] Fabouk Odeh and Joseph B. Keller. Partial differential equations with periodic coefficients and bloch waves in crystals. *Journal of Mathematical Physics*, 5(11):1499–1504, November 1964.
- [11] Douglas S. Drumheller. Extensional stress waves in one-dimensional elastic waveguides. *The Journal of the Acoustical Society of America*, 6:3389–3402, December 1992.
- [12] H. Kolsky. *Stress Waves in Solids*. Dover, 1952.
- [13] J.D. Achenbach. *Wave Propagation in Elastic Solids*. North-Holland, 1993.
- [14] Charles E. Bradley. Acoustic bloch wave propagation in a periodic waveguide. Master’s thesis, The University of Texas at Austin, July 1991.
- [15] Douglas Drumheller. Acoustical properties of drill strings. *The Journal of the Acoustical Society of America*, 85(3):1048–1064, October 1988.
- [16] R.B. Lindsay, C.R. Lewis, and R.D. Albright. Acoustic filtration in non-homogenous media. *Journal of the Acoustical Society of America*, 5:202–205, January 1933.

- [17] R.B. Lindsay. Filtration of oblique elastic waves in stratified media. *Journal of the Acoustical Society of America*, 11:178–183, October 1939.
- [18] William T. Thomson. Transmission of elastic waves through a stratified solid medium. *Journal of Applied Physics*, 21:89–93, February 1949.
- [19] D.L. Folds et al. Transmission and reflection of ultrasonic waves in layered media. *The Journal of the Acoustical Society of America*, 62(5):1102–1109, November 1977.
- [20] M. Rousseau. Floquet waves properties in a periodically layered medium. *The Journal of the Acoustical Society of America*, 86(6):2369–2376, December 1989.
- [21] J.S. Sastry and M.L. Munjal. A transfer matrix approach for evaluation of the response of a multi-layer infinite plate to a two-dimensional pressure excitation. *Journal of Sound and Vibration*, 182(1):109–128, 1995.
- [22] T.J. Delph et al. Harmonic wave propagation in a periodically layered, infinite elastic body: Antiplane strain. *Journal of Applied Mechanics*, 45:343–349, June 1978.
- [23] T.J. Delph et al. Harmonic wave propagation in a periodically layered, infinite elastic body: Antiplane strain: analytical results. *Journal of Applied Mechanics*, 46:113–119, March 1979.

- [24] C.T. Sun, J.D. Achenbach, and G. Herrmann. Time harmonic waves in a stratified medium propagating in the direction of the layering. *Journal of Applied Mechanics*, pages 408–411, June 1968.
- [25] E.H. Lee. Wave propagation in composites with periodic structures. *Proceedings of the Fifth Canadian Congress of Applied Mechanics*, pages 49–59, May 1975.
- [26] E.H. Lee and Wei H. Wang. On waves in composite materials with periodic structures. *SIAM Journal of Applied Mathematics*, 25(3):492–499, November 1973.
- [27] Chien-Ching Ma and Kuo-Chen Huang. Wave propagation in layered elastic media for antiplane deformation. *Int. J. Solids Structures*, 32(5):665–678, 1995.
- [28] Chien-Ching Ma and Kuo-Chen Huang. Analytical transient analysis of layered composite medium subjected to dynamic inplane impact loadings. *Int. J. Solids Structures*, 33(28):4223–4238, 1996.
- [29] A.H. Shah. Harmonic waves in a periodically laminated medium. *Int. J. Solids Structures*, 18(5):397–410, 1982.
- [30] R.C. Engels and L. Meirovitch. Response of periodic structures by modal analysis. *Journal of Sound and Vibration*, 56(4):481–491, 1978.
- [31] D.J. Mead. General theory of harmonic wave propagation in linear pe-

- riodic systems with multiple coupling. *Journal of Sound and Vibration*, 27(2):235–260, 1973.
- [32] Thomas G. Barnes. Passbands for acoustic transmission in an idealized drill string. *The Journal of the Acoustical Society of America*, 51(5):1606–1608, November 1972.
- [33] R.K. Kaul and C.S. Lee. Free torsional vibrations of a hollow cylinder with laminated periodic structure. *Int. J. of Solids Structures*, 18(4):297–314, 1982.
- [34] R.K. Kaul and G. Herrmann. Free torsional vibration of a elastic cylinder with laminated periodic structure. *J. of Solids Structures*, 12:449–466, 1976.
- [35] Manfred Heckl. Wave propagation on beam–plate systems. *The Journal of the Acoustical Society of America*, 33(5):640–651, May 1961.
- [36] Eric E. Ungar. Steady state responses of one dimensional periodic flexural systems. *The Journal of the Acoustical Society of America*, 39(5):887–894, March 1965.
- [37] D.J. Mead. Free wave propagation in periodically supported infinite beam. *Journal of Sound and Vibration*, 1(2):181–196, June 1970.
- [38] G. Sen Gupta. Natural flexural waves and the normal modes of periodically supported beams and plates. *Journal of Sound and Vibration*, 13(1):89–101, June 1970.

- [39] Seng Yung Lee, Huei Yaw Ke, and Ming Jang Kao. Flexural waves in periodic beams. *Journal of Applied Mechanics*, 57:779–783, September 1990.
- [40] Sen Yung Lee and Huei Yay Ke. Flexural wave propagation in an elastic beam with periodic structure. *Journal of Applied Mechanics*, 59:189–196, June 1992.
- [41] Ali Hasan Nayfeh. Sound waves in two dimensional ducts with sinusoidal walls. *The Journal of the Acoustical Society of America*, 56(3):768–770, September 1974.
- [42] Abdul Majid Nusayr. Propagation of waves in rectangular ducts with sinusoidal undulations. *The Journal of the Acoustical Society of America*, 67(5):1472–1476, May 1980.
- [43] Richard F. Salant. Acoustic propagation in waveguides with sinusoidal walls. *The Journal of the Acoustical Society of America*, 53(2):504–507, April 1973.
- [44] D.S. Drumheller and H.J. Sutherland. A lattice model for stress wave propagation in composite materials. *Journal of Applied Mechanics*, pages 149–154, March 1973.
- [45] C.W. Robinson and G.W. Leppelmeier. Experimental verification of dispersion relationships for layered composites. *Journal of Applied Mechanics*, March 1974.

- [46] Michael El Raheb. Transient elastic waves in finite layered media: One-dimensional analysis. *The Journal of the Acoustical Society of America*, 94(1):172–184, July 1993.
- [47] Michael El Raheb. Transient elastic waves in finite layered media: Two dimensional axisymmetric analysis. *The Journal of the Acoustical Society of America*, 99(6):3513–3527, June 1996.
- [48] Michael-El-Raheb and Reinard Tham. Transient waves in a periodic stack: Experiments and comparisons with analysis. *The Journal of the Acoustical Society of America*, 101:860–866, February 1997.
- [49] C. Gazanhes and J. Sageloli. Etude de la dispersion acoustique de celerite dans des structures periodiques. *Acustica*, 81:221–227, May 1995.
- [50] J.D. Achenbach and M. Kitahara. Harmonic waves in a solid with a periodic distribution of spherical cavities. *The Journal of the Acoustical Society of America*, 81:595–598, 1987.
- [51] Francis Bostick. Personal communication. Discussion of his previous work in the down hole telemetry problem, July 1999.
- [52] Douglas S. Drumheller and Steven D. Knudsen. The propagation of sound waves in drill string. *The Journal of the Acoustical Society of America*, 97(4):2116–2125, April 1995.
- [53] Schlumberger-Austin Telemetry Engineering Group. Acoustic seminar - schlumberger. Post Seminar Discussions, March 1999.

- [54] William H. Cox and Preston E. Channey. Telemetry system. U.S. Patent 4,293,936, 1981.
- [55] Elmer Hixson. Signal generator indicating vertical deviation. U.S. Patent 3252225, May 1966.
- [56] Douglas S. Drumheller. Wave impedance of drill strings. *To be Published in: The Journal of the Acoustical Society of America*, 2002.
- [57] Clifford W. Petersen et al. Acoustic transmitter and method to produce essentially longitudinal acoustic waves. U.S. Patent 4,314,365, 1982.
- [58] Elbert N. Shawhan. Data transmission in a drill string. U.S. Patent 4,390,975, June 1983.
- [59] H. Eugene Sharp and Miles A. Smither. Borehole acoustic telemetry system with phase shifted signal. U.S. Patent 4,562,559, 1985.
- [60] Douglas S. Drumheller. Attenuation of sound waves in drill strings. *The Journal of the Acoustical Society of America*, 94(4):2387–2396, October 1993.
- [61] Robert Bruce Lindsay. *Mechanical Radiation*. McGraw-Hill Book Company, 1960.
- [62] R. Esquivel-Sirvent and G.H. Coccoletzi. Band structure for the propagation of elastic waves in superlattices. *The Journal of the Acoustical Society of America*, 95(1):86–90, January 1994.

- [63] Evgeni L. Shenderov. Reflection of a plane sound wave from a semi-infinite periodic transversely isotropic set of layers. *The Journal of the Acoustical Society of America*.
- [64] L.M. Brekhovskikn and O.A. Godin. *Acoustics of Layered Media I*, chapter 1–4. Springer Verlag, 1989.
- [65] Michael A. Ainslie. Plane-wave reflection and transmission coefficients for a three layered elastic medium. *The Journal of the Acoustical Society of America*, 97(2):954–961, February 1995.
- [66] R.W. Hamming. *Digital Filters*. Signal Processing Series. Prentice Hall, third edition, 1989.
- [67] J.Kim Vandiver et al. Case studies of the bending vibration and whirling motion of drill collars. *SPE Drilling Engineering*, pages 282–290, 1990.
- [68] Thor Viggo Aarrestad and Age Kyllingstad. An experimental and theoretical study of a coupling mechanism between longitudinal and torsional drillstring vibrations a the bit. *SPE Drilling Engineering*, pages 12–18, March 1988.
- [69] C.M. Wu and B. Lundberg. Reflection and transmission of the energy of harmonic elastic waves in a bent bar. *Journal of Sound and Vibration*, 190(4):645–659, 1996.
- [70] Douglas S. Drumheller. Coupled extensional and bending motion in elastic waveguides. *Wave Motion*, 17:319–327, 1993.

- [71] Drumheller. Society of petroleum engineers - annual conference, houston tx. 1999. Personal communication, October 1999.
- [72] Neils J.C. Lous et al. Sound transmission through a periodic cascade with application to drill pipes. *The Journal of the Acoustical Society of America*, 103(5):2302–2311, May 1998.
- [73] Douglas Drumheller. Circuit for echo and noise suppression of acoustic signals transmitted through a drill string. U.S. Patent 5,274,606, December 1993.
- [74] Douglas Drumheller. Electromechanical transducer for acoustic telemetry system. U.S. Patent 5,222,049, June 1993.
- [75] Douglas Drumheller. Analog circuit for controlling acoustic transducer arrays. U.S. Patent 5056067, October 1991.
- [76] Douglas Drumheller. Acoustic transducer. U.S. Patent 5703836, December 1997.
- [77] Douglas Drumheller. Downhole pipe selection for acoustic telemetry. U.S. Patent 5,477,505, December 1995.
- [78] Douglas Drumheller. Acoustic data transmission through a drillstring. U.S. Patent 5,128,901, July 1992.
- [79] P. Leug. Process of silencing sound oscillations. U.S. Patent 2043416, 1936.

- [80] M. J. Jessel and G.A. Mangiante. Active sound absorbers in an air duct. *Journal of Sound and Vibration*, 23:383–390, 1972.
- [81] Dominique Laget. Active control of a sound in an air conditioner duct using an adaptive filter. Master’s thesis, The University of Texas at Austin, 1989.
- [82] M. A. Swimbanks. The active control of sound propagation in long ducts. *Journal of Sound and Vibration*, 27, 1973.
- [83] J.H. Poole and H. G. Leventhall. An experimental study of swimbanks method of active attenuation of sound in ducts. *Journal of Sound and Vibration*, 49:257–266, 1976.
- [84] K. Eghtesadi and H. G. Leventhall. Active attunuation of noise: The chelsea dipole. *Journal of Sound and Vibration*, 75, 1981.
- [85] N. Wiener. *Extrapolation, Interpolation and Smoothing of Stationary Time Series*. Wiley, 1949.
- [86] R. Kalman and R. Bucy. New results in linear filtering and prediction theory. *Trans. ASME, J. Basic Engr.*, 83:95–107, December 1961.
- [87] R. Kalman. On the general theory of control. *Proc. 1st IFAC Congress. London*, 1960.
- [88] Bernard Widrow et al. Adaptive noise cancelling: Principles and applications. *Proceedings of the IEEE*, 12(63):1692–1716, December 1975.

- [89] Bernard Widrow and Samuel D. Stearns. *Adaptive Signal Processing*. Prentice Hall, 1985.
- [90] J.C. Burgess. Active adaptive sound control in a duct: A computer simulation. *The Journal of the Acoustical Society of America*, 3(70):715–725, September 1981.
- [91] M.M. Sondhi. An adaptive echo canceller. *The Bell Technical Journal*, XLVI(3):497–511, March 1967.
- [92] Seiichi Onoda and Keniti Kido. Automatic control of stationary noise by means of stationary synthesis. *International Congress on Acoustics*, pages 185–188, August 1968.
- [93] Dennis R. Morgan. Real-time adaptive linear predictor using the least mean square gradient algorithm. *IEEE Transactions on Acoustics, Speech, and Signal Processing*, 24:494–506, December 1976.
- [94] John R. Treichler. Transient and convergent behavior of the adaptive line enhancer. *IEEE Transactions on Acoustics, Speech, and Signal Processing*, 27(1):53–62, February 1979.
- [95] Lloyd J. Griffiths. Rapid measurement of digital instantaneous frequency. *IEEE Transactions on Acoustics, Speech, and Signal Processing*, 23(2):207–221, April 1975.
- [96] Dennis R. Morgan. Steady-state response of a delay-constrained adaptive

- linear predictor filter to a sinusoid in white noise. *IEEE Transactions on Acoustics, Speech, and Signal Processing*, 4:1039–1043, August 1983.
- [97] Dennis R. Morgan. Effect of gradient noise on the adaptive cancellation of a sinusoid in white noise. *IEEE Transactions on Acoustics, Speech, and Signal Processing*, 4(ASSP-31):1043–1045, August 1983.
- [98] Fuyun Ling Guozhu Long and John Proakis. Adaptive transversal filters with delayed coefficient adaptation. *Proc. ICASSP 87*, pages 431–434, 1987.
- [99] C. F. Ross. An algorithm for designing a broadband active sound control system. *Journal of Sound and Vibration*, pages 373–380, 1982.
- [100] P. Darlington and S.J. Elliot. Stability of adaptively controlled systems - a graphical approach. *Proc. ICASSP 87*, 1:399–402, 1987.
- [101] P. Darlington and S.J. Elliott. Synchronous adaptive filters with delayed coefficient adaptation. *Proc. ICASSP 88*, 1:2586–2589, 1988.
- [102] M. Beringer and A. Roure. Radiation impedance of one or several real sources mounted in a hard-walled rectangular waveguide. *Journal of Sound and Vibration*, 71(3):389–398, 1980.
- [103] M. L. Munjal and L. J. Eriksson. An analytical, one-dimensional, standing wave model of a linear active noise control system in a duct. *The Journal of the Acoustical Society of America*, 84(3):1086–1093, 1988.

- [104] Scott D. Snyder and Colin H. Hansen. Active noise control in ducts: Some physical insights. *The Journal of the Acoustical Society of America*, 1(86):184–194, July 1989.
- [105] Philip M. Morse and K. Uno Ingard. *Theoretical Acoustics*. pg 501. Princeton University Press, 1968.
- [106] Eugene Dieulesaint Daniel Royer. *Elastic Waves in Solids I - Free and Guided Propagation*, volume I. Springer, 1996.
- [107] J.F. Nye. *Physical Properties of Crystals-Their Representation by Tensor and Matrices*. Oxford Science Publications, 1992.
- [108] Saul A. Teukolsky William T. Vetterling William H. Press, Brian P. Flannery. *Numerical Recipes in C - The Art of Scientific Computing*. Cambridge University Press, 1991.
- [109] Neil Gershenfeld. *The Nature of Mathematical Modeling*. Cambridge University Press, 1999.
- [110] R. Courant et al. On the partial difference equations of mathematical physics. *IBM Journal*, pages 23–93, 1967.
- [111] O. E. Mattiat. *Ultrasonic Transducer Materials*. Plenum Press, New York, 1971.
- [112] Warren P. Mason et al. *Physical Acoustics*, volume I. Associated Press, 1964.

- [113] Elmer L. Hixson. Sensors and actuators-class notes. EE/ME 384N The University of Texas at Austin 1992.
- [114] Leo L. Beranek. *Acoustics*. Acoustical Society of America Publications, 1993.
- [115] Elmer L. Hixson. Personal communication.
- [116] Ruel V. Churchill. *Operational Mathematics*. McGraw-Hill Book Company, third edition edition, 1972.
- [117] Georgi P. Tolstov. *Fourier Series - Translated from the Russian by Richard A. Silverman*. Dover Books, 1962.
- [118] D. Ronald Fannin Roger E. Ziemer, William H. Tranter. *Signals and Systems: continuous and discrete*. Macmillan, 1983.

Vita

Guillermo E. Aldana was born in San Salvador, the capital of El Salvador on A Tuesday afternoon at 3 p.m, 1965. He is the son of Silvia Calderon and Guillermo Antonio Aldana. He received the Bachelor of Science in Electrical Engineering, with a minor in Mathematics from Louisiana State University August, 1988 and joined Advanced Micro Devices until 1992. He entered the Graduate School of The University of Texas at Austin in Fall 1990 to pursue a Master's degree in Mechanical Engineering. He received the M.S. degree from the University of Texas at Austin in August 1992. In Fall 1996, he returned to the University of Texas at Austin to pursue a Ph.D. degree under the supervision of E. L. Hixson in the Acoustic Program at UT, while pursuing a career at Motorola.

Permanent Address: 1513 Payne Avenue

Austin, Texas 78757

USA

This dissertation was typeset with L^AT_EX 2_ε³ by the author.

³L^AT_EX 2_ε is an extension of L^AT_EX. L^AT_EX is a collection of macros for T_EX. T_EX is a trademark of the American Mathematical Society. The macros used in formatting this dissertation were written by Dinesh Das, Department of Computer Sciences.